ION EXCHANGE BEHAVIOR AMONG METAL TRISILICATES: PROBING SELECTIVITY, STRUCTURE, AND MECHANISM

A Dissertation

by

CHRISTOPHER SEAN FEWOX

Submitted to the Office of Graduate Studies of
Texas A&M University
in partial fulfillment of the requirements for the degree of

DOCTOR OF PHILOSOPHY

August 2008

Major Subject: Chemistry

ION EXCHANGE BEHAVIOR AMONG METAL TRISILICATES: PROBING SELECTIVITY, STRUCTURE, AND MECHANISM

A Dissertation

by

CHRISTOPHER SEAN FEWOX

Submitted to the Office of Graduate Studies of
Texas A&M University
in partial fulfillment of the requirements for the degree of

DOCTOR OF PHILOSOPHY

Approved by:

Chair of Committee,	Abraham Clearfield
Committee Members,	Marcetta Darensbourg
	Kim Dunbar
	Charles Glover
Head of Department,	David H. Russell

August 2008

Major Subject: Chemistry

ABSTRACT

Ion Exchange Behavior among Metal Trisilicates:
Probing Selectivity, Structure, and Mechanism. (August 2008)
Christopher Sean Fewox, B.S.,
North Carolina State University
Chair of Advisory Committee: Dr. Abraham Clearfield

One model system for the investigation of selectivity in inorganic ion exchangers is a group of synthetic analogues of the mineral umbite. Hydrothermally synthesized trisilicates with the general form $A_2BSi_3O_9 \bullet H_2O$, where A is a monovalent cation, and B = Ti^{4+}, Zr^{4+}, and Sn^{4+} have been shown to have ion exchange properties.

The extended three dimensional framework structure offers the ability to tune the selectivity based on the size of the cavities and channels. The unit cell volume, and therefore the pore size, can be altered by changing the size of the octahedral metal. The substitution of Ge for Si can also increase the pore size.

A variety of cations have been exchanged into the trisilicates including alkali and alkaline earths, lanthanides, and actinides. The reason for the selectivity rests in the pocket of framework oxygens which make up the exchange sites. Close examination of the cation environments shows that the ions with the greatest affinity are those that have the closest contacts to the framework oxygens. For example, among alkali cations, zirconium trisilicate demonstrates the greatest affinity for Rb^+ and has the most A-O contact distances approaching the sum of their ionic radii.

The origins of selectivity also rely upon the valence of the incoming cation. When cations are of similar ionic radius, a cation of higher charge is always preferred over the lower valence. Ion exchange studies in binary solutions of cations of different valence, but similar size (1.0Å) have proven the selectivity series to be $Th^{4+} > Gd^{3+} > Ca^{2+} > Na^+$.

Through structural characterization, kinetic studies, and use of in situ x-ray diffraction techniques the origins of selectivity in these inorganic ion exchangers has been further elucidated. The principles gleaned from these studies can be applied to other inorganic framework materials. The umbite system has the potential to be altered and tailored for specific separation needs. The trisilicate materials presented in this work are representative of the types of advances in inorganic materials research and prove their potential as applicable compounds useful for solving real world problems.

DEDICATION

To my wife Miriam whose dedication and dream
for me made this work complete and
to whom I pledge an eternal life of love and freedom

ACKNOWLEDGEMENTS

As contributors to my education and professional growth and enlightenment these persons hold a special place in my heart. Each one is unique, but the sum of their efforts has made me the scientist and philosopher I am today.

Ralton Harris has served as a boss, mentor, and scientific sounding board for over ten years now and has my eternal gratitude for his advice, investment in my growth, and unconditional friendship.

Dr. Forrest C. Hentz was an indispensable source of guidance and inspiration in my chemical education. A man of wit, great character, and devotion to his students, he has been blessed with the gift of teaching young minds the world of chemistry. He is the one unique person who showed me how beautiful chemistry is from a simple balanced chemical equation to the complexities of a momentum operator or Eigen function.

I would like to thank Dr. F. A. Cotton, who gave me my start here at Texas A&M. In his lab I learned the complexities of inorganic synthesis and gained the confidence to know that I can synthesize anything.

I would like to acknowledge Dr. Sharath Kirumakki. He has been a valuable colleague and advisor throughout my endeavors at A&M. Above all the friendships and relationships I have forged here in Texas, his is the one I value the most.

I gratefully thank Dr. Akhilesh Tripathi for his attention in training me as a crystallographer. There is no finer or more patient teacher that I have met. I promise him I will continue to break down communication barriers and shake the framework of an inorganic ion exchanger like a cage around a rabbit.

Dr. Daniel S. Grum has been my friend for over 17 years. It is no small miracle that we chose the same university to pursue our Ph. D. I am thankful that God chose to make us neighbors and graced us with the ability to support each other. Without him here in College Station, my experience would not have been as rich.

I would like to acknowledge my committee members, Dr. Charles Glover, Dr. Marcetta Darensbourg, and Dr. Kim Dunbar. I requested they sit on my committee

because I have the utmost respect for them as scientists, chemists, and teachers. They have taught me much, and I have always valued my time in and outside the classroom with them.

To my family, I am grateful for their support, emotionally, financially, and spiritually. I could not have done this without them. My father, Dalton Fewox, my mother, Alice Fewox, my grandparents, Julius and Irma Wiggins, and Dorothy Fewox all share in the success I have had at A&M.

Lastly, and most gratefully I acknowledge Dr. Abraham Clearfield. God truly blessed me the day I joined his research group. I could not hope for a wiser individual to steer me through my course on the way to my doctorate. He has shown patience and kindness throughout my journey over the past 5 years. He has blessed me with gifts of knowledge that I can never repay. He has guided my path, let me stumble, but has always been there for me to lean on as a scientist and a human being. There are no more words to describe appreciation and adoration I hold for him. May his dedication and all his sacrifices in my education be a mitzvah unto him.

TABLE OF CONTENTS

CHAPTER Page

LIST OF FIGURES

FIGURE Page

FIGURE Page

LIST OF TABLES

TABLE Page

CHAPTER I
INTRODUCTION

1.1. Impetus for this work

One of the significant problems facing the U.S. today is the legacy of our nuclear endeavors. Spent fuel from nuclear reactors, waste from weapons production, and medical and research waste must all be disposed of safely and effectively. Nuclear waste sites such as Hanford, Washington and Savannah River, South Carolina maintain high-level waste disposal facilities which are falling into disrepair. Approximately 2,400 million curies are spread over several sites around the country.[1] Permanent disposal of these waste streams is a national goal and a point of research important to all. Sorbents and ion exchange materials will play a significant role in the clean up process. By separating high activity isotopes and other actinides waste can be segregated and processed according to contamination threat, isotope half-life, and activity.

Cesium-137 and Strontium-90 are found in fission products and pose some of the most harmful threats to the environment. Cesium-137 ($t_{½}$ = 30.17 years) decays in a two step process, first by beta decay to Barium-137, then by x-ray emission with an energy of 662 keV. For a metal, cesium is volatile and is mistaken for potassium in living organisms making incorporation into the body facile. Strotium-90 ($t_{½}$ = 28.79 years) decays by emission of a beta particle with an energy of 550 keV. Strontium mimics calcium in the body and is readily incorporated into bone tissue.

The Savannah River site maintains several waste tanks devoted to the disposal of high-level waste. These tanks have a total capacity of approximately 1.3 million gallons. The tank waste contains three separate phases. A salt cake, composed mostly of sodium nitrates and carbonates, floats on top of the supernatant liquid which contains most of the cesium and soluble ions.

This dissertation follows the style and format of *Chemistry of Materials*.

Figure 1.1. Waste tanks are made of steel and are 30 feet in diameter. Some are buried and capped with clay leaving only important access points exposed.

The sludge phase, which resembles river bottom silt, is where most of the strontium and transuranium elements lie mixed with other insoluble hydroxides. The radiation inside is so intense that cooling coils 3 miles long are employed to maintain a temperature of approximately 90^{o}C. Though an anomaly, a tank once reached a temperature of 350^{o}C.

The supernatant liquid is extremely alkaline and contains sodium ion at concentrations of 5-6M. Organic ion exchange materials perform poorly in this environment. Indeed, they would rapidly degrade in the strong radiation field. Today the most widely used method to separate heavy metals, cesium, and strontium from the supernatant liquid is the Purex Solvent Extraction process. This process works well for plutonium and other actinides but is inefficient for the separation of strontium.

1.2. Previously studied inorganic ion exchange materials

One of the first inorganic ion exchange materials extensively studied for waste remediation was sodium nonatitanate (SNT), $Na_4Ti_9O_{20}•H_2O$.[2] SNT has been shown to be highly selective in removing strontium and plutonium ions from highly alkaline nuclear waste simulants when converted to its proton phase.[3] The nonatitanate has a layered structure but is insufficiently crystalline for complete structural analysis by

powder x-ray diffraction. Against the baseline material monosodium titanate (MST)[4] sodium nonatitanate has been shown to have a larger ion exchange capacity and higher selectivity in solutions of high ionic strength.

Titanosilicates of the ideal composition $Na_2Ti_2O_3SiO_4 \bullet 2H_2O$ are also of interest in waste remediation. The mineral form is that of sitinikite and exists in a tetragonal crystal system. Along the *c*-axis channels are formed which contain the exchangeable ions.[5] Cesium exchange studies have shown the maximum loading is given according to the formula $H_{1.5}Cs_{0.5}Ti_2O_3SiO_4 \bullet 2H_2O$.[6] Through structural characterization using powder x-ray diffraction methods, the environment of the incorporated ion can be deduced. It has been shown that the cesium ion is eight coordinate, forming strong bonds to framework oxygens which are near the sum of their atomic radii. Partial substitution of niobium for titanium (up to 25%) has improved the selectivity for cesium ion in simulants with high sodium and hydroxide ion concentration. The better selectivity is attributed to the cesium environment. Cesium is twelve coordinate in approximately 75% of its occupied sites.[7] Substitution of silicon by germanium has also been found to alter the ion exchange capabilities of titanosilicates.[8]

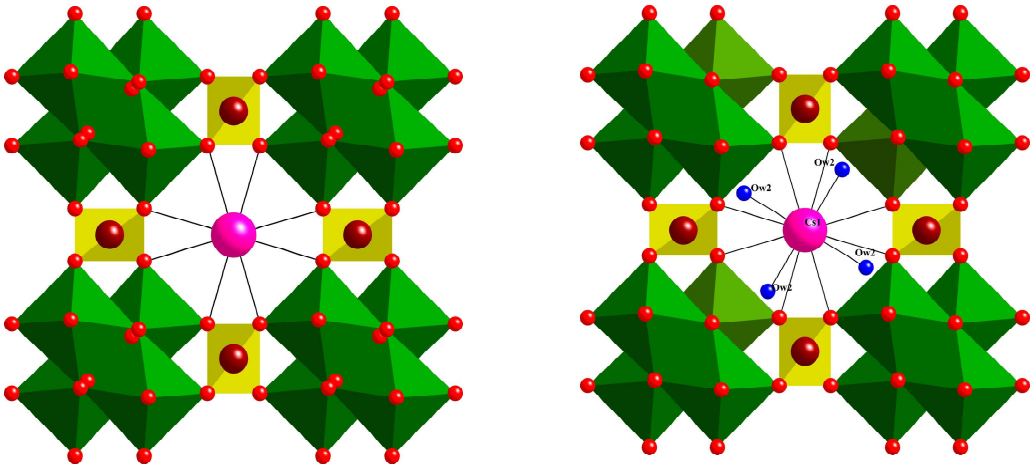

Figure 1.2. Cs^+ is 8-coordinate in the unsubstituted material but is 12-coordinate in the Nb doped material.

Another class of titanosilicates also exhibits this tunable behavior. A structural mimic of the mineral pharmacosiderite has been synthesized in the form of $HM_3Ti_4O_4(SiO_4)_3 \bullet 4H_2O$, where M = K^+ and Cs^+.[9] The crystal system is cubic giving rise to unidimensional channels. Only three cations per unit cell may be exchanged. A fourth cation would result in unfavorably close cation-cation distances. The unit cell has been altered by substitution of germanium for both silicon and titanium. The change in selectivity for cesium has been correlated with the change in the unit cell volume for compounds with various degrees of substitution.[10] Single crystals analyzed by x-ray diffraction have verified those structural results gained by powder work.[11] Again, by analysis of the coordination sphere of the cation the origins of selectivity can be elucidated.

1.3. Trisilicates

The mineral umbite is found in the northern reaches of Russia near the Kola Peninsula and has an ideal formula of $K_2ZrSi_3O_9 \bullet H_2O$. It is however, often found to contain greater than 50% Ti substituting for Zr.[12] The first thorough examination of the crystal structure of the mineral umbite was performed by Ilyushin in 1993.[13] Natural and synthetic umbite crystallizes in the orthorhombic space group $P2_12_12_1$.

The framework is composed of infinite silicate chains linked by the M^{4+} octahedral metal. No M-O-M linkages are observed. This arrangement gives rise to a three dimensional tunnel network which forms the pores through which the cations migrate to the exchange sites. Two unique tunnels run along the *c*-axis. The smaller channel is composed of a 12-atom ring containing two cations. The larger channel is marked by a 16-atom ring and contains two cations and two molecules of water. Linking these two channels is a third tunnel formed from a 14-atom ring running approximately along the *ab*-diagonal. The exchangeable cations are located in these channels and move freely through them during ion exchange.

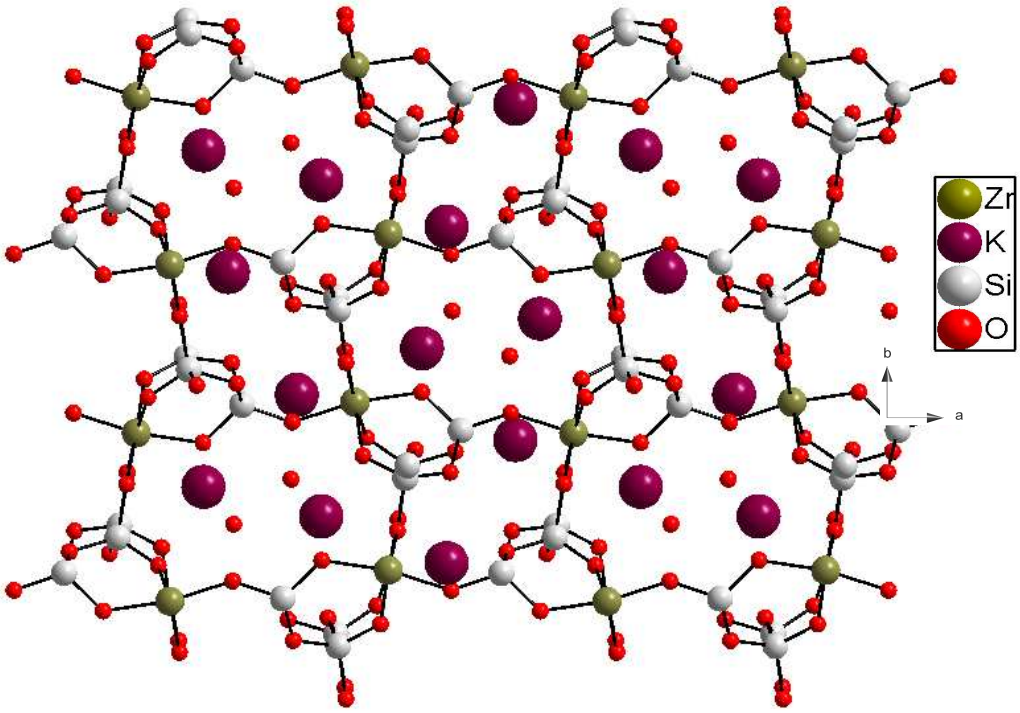

Figure 1.3. View of the trisilicate framework and exchangeable cations down the *c*-axis.

Seen in Figure 1.3, viewed down the *c*-axis, are two crystallographically identical cations, generated by the 2_1 screw axis, located in the smaller ring. Similarly, the larger tunnel contains two cations, but also two water molecules.

The unit cell volume of the pure titanium phase is approximately 915 $Å^3$ and represents the smallest cell volume of the trisilicate class. With a cell volume of 1053 $Å^3$, a germanium substituted potassium zirconium trigermanate synthesized by Yaghi and coworkers has the largest unit cell volume of the umbite mimics.[14] Figure 1.4 shows the cell volume as a function of framework substitution of the octahedral metal including Yaghi's germanium substituted compound. This demonstrates the ability to tune the size of the tunnel network for improved separations and ion exchange.

1.3.1. Titanium trisilicates

The framework structure is identical the metal substituted polymorphs, however their ion exchange properties are unique. The structure and ion exchange properties of the pure potassium titanium trisilicate and a partially protonated phase were studied by Clearfield and coworkers in 2000.[15] Crystallizing in the orthorhombic space group

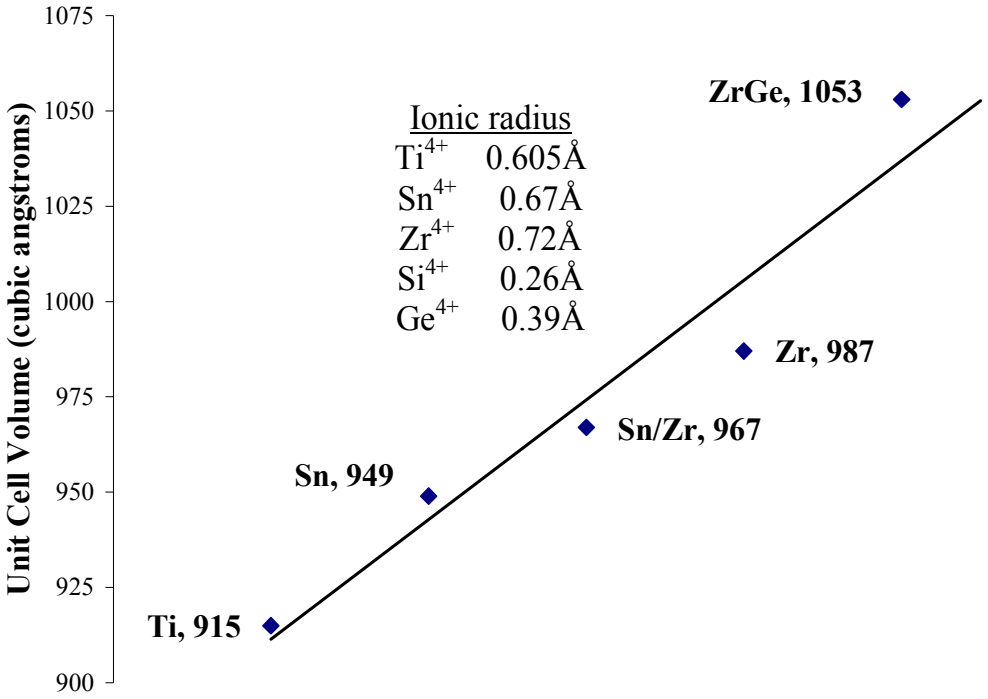

Figure 1.4. Change in unit cell volume as a function of atomic radius of the isomorphous framework substitution.

$P2_12_12_1$, the potassium titanium trisilicate is assigned the formula $K_2TiSi_3O_9 \bullet H_2O$. With unit cell dimensions of a = 9.9081(4) Å, b = 12.9445(5) Å, c = 7.1384(3) Å, the potassium titanium phase has a unit cell volume of 915.5 $Å^3$. The afore mentioned structural data on the potassium titanium trisilicate was gathered using powder x-ray diffraction techniques, however single crystals suitable for structural study were

synthesized by Zou and Dadachov and confirm the findings of Clearfield and coworkers.[16]

Upon conversion to the partially protonated phase, the crystal system changes in symmetry to the monoclinic space group $P2_1/c$. The protonated phase was assigned the molecular formula $K_{0.3}H_{1.7}TiSi_3O_9 \bullet 2H_2O$. The cell volume is slightly larger than the parent potassium phase, having cell dimensions of a = 7.2219(1) Å, b = 10.0354(2) Å, c = 12.9278(2) Å, β = 91.447(1)°.[15]

In the above study, the affinity for alkali cations was probed and the selectivity series was determined as a function of pH. Potentiometric titrations of $K_{0.3}H_{1.7}TiSi_3O_9 \bullet 2H_2O$ with MOH showed that in alkaline media the selectivity series is $K^+ > Li^+$, Na^+, Rb^+, $> Cs^+$.

Structural characterization of some group I exchange products was performed by Valchev et al.[17] Valchev and coworkers were able to show that the temperature at which the structure collapsed was dependent on the cation residing in the cavity. The thermal stability of the different exchange analogues was determined to be $K^+ > Rb^+ > Cs^+ > Na^+ > Li^+ > NH_4^+$, with temperatures ranging from 100 to 600°C.

Recently, Dobelin and Armbruster studied the structural and thermodynamic properties of potassium Ti-umbites exchanged with divalent cations.[18] Exhaustive exchange of $K_2TiSi_3O_9 \bullet H_2O$ with various cations at neutral pH gave the selectivity series Mn^{2+}, Ca^{2+}, $> Sr^{2+} > Cs^+$. The crystal structures derived from powder data showed great disorder in the cation sites of all the exchange products and their conclusions about the cation arrangement and total uptake are suspect as the suggested molecular formulas are not charge balanced. Thermal degradation studies do however confirm the cation influence on framework stability at elevated temperature as shown previously by Vlachev.

As the umbite class of trisilicates gains further attention from researchers, new uses for these microporous materials are being found. Recently, Sebastian and coworkers have demonstrated effective gas separation properties of titanium umbite membranes.[19,20]

1.3.2. Tin trisilicates

The seminal work on the tin trisilicate began almost a decade before the first detailed crystal structures of the titanium phase were published.[21-23] Although ion exchange studies were performed and x-ray diffraction data were collected, only an indexed pattern was proposed containing an orthorhombic unit cell. The crystal structure of the potassium stannic trisilicate was eventually solved by Rocha and coworkers in 1999.[24] Assigning an ideal formula of $K_2SnSi_3O_9 \bullet H_2O$, the resulting structure was shown to have the same topology as the mineral umbite crystallizing in the orthorhombic space group $P2_12_12_1$ with unit cell dimensions of a = 10.103(5), b = 13.132(6), c = 7.154(4) Å. In the framework of the potassium stannic umbite the tunnel structure is identical to the titanium phase and the cations reside in the same exchange sites.

Other stannic silicates have been prepared by Rocha and coworkers. A mixed sodium and potassium phase was synthesized and characterized. $Na_{0.5}K_{1.5}SnSi_3O_9 \bullet H_2O$ was prepared by hydrothermal methods but was found to crystallize in the monoclinic space group $P2_1/c$ with cell dimensions of a = 6.4596(1), b = 11.5523(2), c = 12.9379(2), β = 104.990°.[25] The structure however, is a mimic of the mineral Kostylevite. Increasing the level of Na substitution via hydrothermal synthesis Rocha and coworkers produced a pure sodium stannic trisilicate with the formula $Na_2SnSi_3O_9 \bullet 2H_2O$.[26] This material was found to crystallize in the space group $C222_1$ and displays cell dimensions of a = 7.9453(5), b = 10.3439(7), c =11.6252(7). Although this compound contains an open, extended three dimensional tunnel network, it does not appear to be a form of umbite.

Mixed Sn/Zr materials have also been synthesized. $K_2Sn_{0.25}Zr_{0.75}Si_3O_9 \bullet H_2O$ and $Na_2Sn_{0.25}Zr_{0.75}Si_3O_9 \bullet H_2O$ were synthesized by Garcia and coworkers.[27] The latter was synthesized by ion exchange of the potassium phase with 2M NaCl at room temperature. These two compounds do have the topology of the mineral umbite and possess the same tunnel structure and framework linkages. These two compounds demonstrate two

important advantages of the trisilicate system. First, it is possible to perform isomorphous substitutions of the M^{4+} framework metal without altering the tunnel structure. This allows definitive control over unit cell volume and therefore pore size. Secondly, that complete ion exchange substitution is possible without loss of crystallinity. Without loss of crystallinity, structural characterization of ion exchange products can be performed.

Further work on the ion exchange properties and thermal stability of the potassium stannic trisilicate was carried out by Garcia and coworkers.[28] In examinations of Cs^+ and Sr^{2+} ion exchange it was found that the affinity for Cs^+ was greater than that of Sr^{2+}. In addition, by studying the change in unit cell volume as a function of temperature, it was discovered that the framework can swell and contract depending on the amount of interstitial water while simultaneously not undergoing drastic structural collapse.

Of further interest in the realm of stannic trisilicates is the formation of single crystals of $Cs_2SnSi_3O_9$ at high temperature and pressure. Using gold reaction ampules at a temperature of 610^oC and pressures estimated to be 210MPa, Lii and Lo were able to synthesize single crystals of cesium stannic trisilicate suitable for single crystal x-ray diffraction experiments.[29] Of particular interest in this study was the lack of water in the structure and that previous attempts to synthesize single crystals of stannosilicates with umbite topology have yielded only wadite type structures.[30]

1.3.3. Zirconium trisilicates

In terms of unit cell volume, the zirconium trisilicate is the largest trisilicate with a volume of approximately 987Å^3 corresponding to the potassium phase, $K_2ZrSi_3O_9 \bullet H_2O$. A thorough study of the potassium zirconium trisilicate was undertaken by Clearfield and coworkers in 1997.[31] The structure of the potassium phase and its ion exchange phases with Na^+ and Cs^+ were examined. The structure of the framework is identical and the tunnel network is conserved in every phase. In contrast

to the sodium stannic trisilicate (space group $C222_1$), the pure sodium zirconium umbite, $Na_2ZrSi_3O_9 \bullet H_2O$, maintains the space group $P2_12_12_1$. The cation environment and site occupancies of the exchange sites were also examined closely. To model the disorder in the ion exchange sites with incomplete substitution, partial occupancies of two cations and water oxygen were placed the two unique exchange sites. This method of structural modeling suggests the two sites have different affinities for the same cation. It can be inferred from the structures that the exchange site in the smaller tunnel have greater affinity for the substituted cations as the site occupancy is almost completely full of incoming ion. Other structural information gleaned from the exchange compounds comes from examination of the cation environment. Cation-oxygen distances were tabulated and showed that the closest oxygen contacts to the cations were not always those of the water oxygen which has greater freedom to get closer to the cation.

The ion exchange properties of the zirconium trisilicate were examined in a publication by Clearfield and coworkers and compared to those of the titanium trisilicate.[31] The ion exchange experiments were carried out using a partially protonated zirconium umbite phase, $K_{0.5}H_{1.5}ZrSi_3O_9 \bullet 2H_2O$, synthesized by ion exchange using acetic acid. The crystal structure of the completely protonated form was not however solved, due to the fact that as the degree of protonation is increased the crystallinity decreases substantially.

The uptake of alkali metal cations was determined over a pH range of 2 to 12. In acidic media, the affinity of protonated zirconium umbite for group I metals was found to be $Rb^+ > Cs^+ > K^+ > Na^+ > Li^+$. As pH increases, Rb^+ remains the most favored cation, while the difference in affinities for all other alkali cations decreases. The investigators concluded that a correlation exists between the size of the ion exchange cavity, which is a function of the octahedral M^{4+} metal, and the selectivity towards different sized cations. This assertion implies that the umbite system might be tailored through isomorphous substitutions to be selective towards specific cations.

Other research groups around the world have turned their attention to zirconium silicates. Synthetic conditions of zirconium silicates were examined more closely by

Ilyushin and coworkers.[33,34] Ilyushin concluded that the crystallization of certain zirconium silicates including umbite depended greatly on the gel composition, KOH content, and the ability of the Zr^{4+} species to remain in solution.

Continuing the trend in isomorphous substitutions, Yaghi and coworkers synthesized a zirconium trigermanate, $K_2ZrGe_3O_9 \bullet H_2O$ with umbite topology.[35] Although no ion exchange data was collected, the crystal structure of the germanium umbite was solved and was shown to possess the same framework and cation arrangement as other silicate type umbites. The unit cell volume is the largest of any crystalline umbite to date, having cell dimensions of a = 13.6432(6), b = 7.4256(3), c = 10.3973(4), and a cell volume of 1053.33(8) $Å^3$.

1.4. Purpose and overview

While much structural characterization has been performed, many trisilicate exchange forms have not been characterized and the reasons for ion exchange selectivity in the umbite system remain unclear. Structural and ion exchange data for the alkali earth exchange forms of the trisilicates is incomplete, and work with polyvalent ions is almost completely unexplored. This dissertation will focus on filling gaps of knowledge in the existing trisilicate systems, while investigating new ion exchange forms of all the metal umbite systems. Through structural characterization and examination of the ion exchange environment along with kinetic measurements and use of advanced photon source technology, the structure, mechanism, and origins of selectivity in metal trisilicates with umbite topology will be elucidated.

In Chapter II, the structure of the rubidium zirconium trisilicate, $Rb_2ZrSi_3O_9 \bullet H_2O$, will be discussed along with an examination of the mechanism of ion exchange. Among alkali cations, the potassium zirconium trisilicate displays the greatest affinity for Rb^+ over the entire pH range. Until now, this compound has not been characterized and represents the last in the series of alkali metal exchange forms.

Chapter III will explore the protonated phase of the zirconium trisilicate, $H_{1.45}K_{0.55}ZrSi_3O_9 \bullet 2H_2O$, and its exchange forms with group II cations. The kinetics of exchange and structural data will show that the size of the cation is a key factor in the selectivity of the trisilicates.

Lanthanide separation is a continuing challenge in the fields of nuclear waste remediation. Chapter IV will build on the knowledge gained from ion exchange studies and makes the first steps towards application of the metal umbite system towards separations of complex mixtures. We have shown that the size of the unit cell can be controlled and in no small part determines what size cations are preferred in the particular metal umbite. The tin trisilicate has shown the best potential for separating lanthanide rare earths. The structure of the completely substituted gadolinium tin trisilicate, $Gd_{0.66}SnSi_3O_9 \bullet H_2O$, will be discussed, including details on the separation capabilities of the tin trisilicate and the reasons for its selection as the best material for lanthanide partitioning.

To further understand the impact of the valence of the incoming cation, the incorporation of Th^{4+} will be examined in Chapter V. In complex mixtures of polyvalent cations the trisilicates show preference for the ion of highest valence. The selectivity series among cations of similar ionic radius (~1.0Å) is shown to be $Th^{4+} > Gd^{3+} > Ca^{2+} > Na^{+}$. The structure of the completely substituted thorium zirconium trisilicate shows that the coordination of Th^{4+} to framework oxygens is almost identical that of the sodium phase.

To conclude, Chapter VI takes advantage of in situ x-ray diffraction ion exchange experiments to follow incoming and outgoing cations through the 3D tunnel network. Results from these studies clearly indicate that the smaller tunnel exchange site is the most stable as it is populated preferentially. As Cs^{+} ions continue to populate the partially protonated zirconium umbite the space group changes back to the original orthorhombic $P2_12_12_1$. The reasons for the change in space group along with solid state NMR studies of Cs^{+} are discussed.

CHAPTER II
STRUCTURAL AND MECHANISTIC INVESTIGATION OF RUBIDIUM ION EXCHANGE IN POTASSIUM ZIRCONIUM TRISILICATE*

2.1. Intoduction

The previous work on zirconium trisilicate ion exchange has shown the selectivity among alkali cations in basic media to be $Rb^+ > Cs^+$, K^+, Na^+, Li^+, and in acidic media, $Rb^+ > Cs^+ > K^+ > Na^+ > Li^+$.[32] The structures of some of these alkali exchange forms have been determined by powder x-ray diffraction, including mixed cation and pure exchange forms such as $K_{0.5}Cs_{1.5}ZrSi_3O_9 \bullet H_2O$, $Na_{0.6}Cs_{1.4}ZrSi_3O_9 \bullet H_2O$, $Na_2ZrSi_3O_9 \bullet H_2O$.[31] In these studies Clearfield and coworkers concluded that the smaller exchange site was more selective than the exchange site in the larger tunnel. It was also demonstrated that changing the size of the unit cell through isomorphous substitution of the octahedral M^{4+} metal altered the selectivity of the material. Those umbites with higher ratios of zirconium to titanium were selective for rubidium, while umbites containing more titanium than zirconium preferred potassium.

In this Chapter, the structure of the rubidium phase and the kinetics of ion exchange are discussed. The goal of this study is to understand the reasons for the affinity of potassium zirconium trisilicate for rubidium and to identify a possible mechanism of ion exchange in the umbite system.

---

* Part of the data reported in this Chapter is reproduced with permission from, Chemistry of Materials, C. S. Fewox, S. R. Kirumakki, A. Clearfield, *Structural and Mechanistic Investigation of Rubidium Ion Exchange in Potassium Zirconium Trisilicate*, **2007**; *19(3)*; 384-392.

2.2. Experimental methods

2.2.1. Analytical procedures and instrumentation

Phase identification and structural data sets were collected using a Rigaku computer automated diffractometer and a Bruker-AXS D8 powder diffractometer. Thermal gravimetric analysis was conducted on a TA Instruments TGA Q 500 unit. A constant temperature ramp of 5 ^{o}C/min was applied while the sample was under 9:1 nitrogen to air volume ratio. Potassium analysis was performed on a Varian AA250 atomic absorption spectrometer under an acetylene nitrous oxide flame. Samples for AA analysis were prepared by digestion of solid in hydrofluoric acid. Titrations and pH measurements were conducted on a TitraLab TIM860 Titration Manager. Measurements of ^{86}Rb uptake were performed on a Wallac 1410 liquid scintillation counter.

2.2.2. Synthesis of $K_2ZrSi_3O_9 \bullet H_2O$ and its rubidium ion exchanged phases

Potassium zirconium trisilicate was synthesized hydrothermally by modification of methods previously reported by Poojary et al.[31] 7.0 grams of silicic acid was dissolved in 45 mL of 4M KOH and 10 mL of isopropanol. 13.5 mL of a 70% solution of zirconium isopropoxide in isopropanol was diluted with 10 mL of isopropanol and added drop wise to the previous solution. The mixture was divided in two and placed in a 100 mL steel Teflon lined autoclave. The reaction was carried out at 180^{o}C. After 5 days a white precipitate was isolated by vacuum filtration and washed twice with 50 mL of distilled water. Anal. (%) Found: Zr, 21.73; Si, 20.52; K, 19.03. Calcd. for $K_2ZrSi_3O_9 \bullet H_2O$: Zr, 21.93; Si, 20.24; K, 18.80.

2.2.3. Ion exchange preparation of Rb exchange phases

Rubidium exchanged compounds were derived from $K_2ZrSi_3O_9 \cdot H_2O$. Particles of ion exchanger were ground to a sieved size of 150 μm or less. At room temperature, compound **1,** $Rb_2ZrSi_3O_9 \cdot H_2O$, was prepared by shaking 1.0g of $K_2ZrSi_3O_9 \cdot H_2O$ with 0.1M RbCl at a volume to mass ratio of 500:1 (mL/g) for 24 hours. The product was captured by vacuum filtration and rinsed lightly with distilled water. The dried powder was then shaken with a 0.1M solution of RbCl containing 0.01M RbOH for 48 hours. The product was filtered and washed thoroughly with boiling methanol. Anal. Found: Zr, 17.67; Si, 16.88; Rb, 32.81. Calcd. for $Rb_2ZrSi_3O_9 \cdot H_2O$: Zr, 17.96; Si, 16.59; Rb, 33.65.

Compound **2** was produced by shaking 0.1 grams of ion exchanger ($K_2ZrSi_3O_9 \cdot H_2O$) in 50 mL of 0.01M RbCl for 48 hours. The product was filtered, washed lightly with water, and dried at 60°C. Compounds **3** and **4** were obtained by shaking the potassium umbite for 24 hours with stoichiometric amounts of a 0.01M RbCl solution to give the desired levels of substitution.

2.2.4. X-ray data collection and structural refinement

For structural characterization of the rubidium exchanged phases a Rigaku automated powder diffractometer was used to collect data sets. A flat stainless steel sample holder was used in a Bragg-Brentano geometry. Data for compound **1** were collected at room temperature while 2θ ranged from 5 to 90°. The X-ray source consisted of a rotating anode with a copper target and graphite monochromator. Operating voltage and current were 40 kV and 150 mA, respectively. A step size of 0.03 degrees was employed with a scan rate of 7 seconds per step.

For compound **2** data were collected from 5 to 90 degrees 2θ using the same count time, step size, and operating power. Compounds **3** and **4** were collected on a Bruker-AXS D8 powder diffractometer using a quartz sample holder. Data were

collected between 9 and 90 degrees 2θ. Copper Kα radiation with an average wavelength 1.542Å was employed. Operating voltage and current were 40 kV and 40 mA. Step size and scan rate were 0.02^{o} and 10 seconds, respectively.

Powder patterns were indexed using the PowderX program suite.[36] Profile function fitting and Reitveld refinement were accomplished using the GSAS program suite. The LeBail method was used for extraction of structure factor amplitudes.[37,38] No corrections were made for absorption and neutral atom scattering factors were used as stored in GSAS. No attempt was made to model preferred orientation.

Structural refinement was initiated by utilizing the coordinates of the framework atoms, as given by the original potassium zirconium trisilicate, as a starting model.[31] Contact distance constraints were applied for Si-O, Zr-O and O-O contacts. The zirconium position was first refined and subsequently each trisilicate group. After initial refinement of atomic positions, Fourier difference maps were constructed to reveal the positions of the cations and water oxygen. These parameters were entered and the framework positions were again refined without including the positions of the cations or water. Subsequently the cation and water positions were refined while holding the framework atom positions constant. This back and forth approach was continued until the shift in atomic position was minimal and the least squares refinement converged rapidly. Together, cation, water oxygen, and framework positions were then refined.

During refinement of the atomic positions the weight applied to soft constraints was slowly reduced to a minimum where bond geometry was consistent and chemically meaningful. Isotropic thermal factors for zirconium, each cation position, and water oxygen were then refined keeping silicon and oxygen factors fixed. No attempt was made to describe the water hydrogen positions.

For compound **1,** 1021 independent reflections were found in the 2θ range of 5 to 90^{o}. Final refinement statistics show an R_{wp} of 0.0944 and an R_p of 0.0694. Systematic absences were consistent with the orthorhombic space group $P2_12_12_1$. Compound **1** displays unit cell dimensions of a = 10.4821(6) Å, b = 13.3869(5) Å, and c = 7.2974(3) Å. The final refinement difference plot is shown in Figure 2.1.

Crystallographic data are given in Table 2.1 and atomic coordinates and isotropic thermal factors for **1** are summarized in Table 2.2.

Table 2.1. Crystallographic data for the zirconium trisilicate phases.[a]

	1	**2**	**3**	**4**
fw	508.43	486.38	457.30	432.67
space group	$P2_12_12_1$	$P2_12_12_1$	$P2_12_12_1$	$P2_12_12_1$
a (Å)	10.4782(7)	10.4575(5)	10.4029(7)	10.3591(6)
b (Å)	13.3831(7)	13.3712(5)	13.3484(8)	13.3296(7)
c (Å)	7.2940(5)	7.2861(3)	7.2591(5)	7.2315(4)
V (Å^3)	1022.84(14)	1018.81(8)	1008.01(14)	998.54(12)
Z	4	4	4	4
D_{calc} (g/cm^3)	3.288	3.258	2.995	2.860
No. of reflections	1021	1017	1008	1000
R_{wp}	0.0944	0.0976	0.1328	0.116
R_p	0.0694	0.0720	0.1052	0.0914

[a] Formulas: (**1**) $Rb_2ZrSi_3O_9 \cdot H_2O$; (**2**) $K_{0.29}H_{0.1}Rb_{1.61}ZrSi_3O_9 \cdot H_2O$; (**3**)$K_{0.9}H_{0.1}RbZrSi_3O_9 \cdot H_2O$; (**4**) $K_{1.45}H_{0.1}Rb_{0.45}ZrSi_3O_9 \cdot H_2O$

Table 2.2. Positional and thermal parameters for $Rb_2ZrSi_3O_9 \cdot H_2O$.

	x	y	z	U_{iso}
Zr1	0.4432(7)	0.2117(5)	0.2558(13)	0.0315(29)
Si2	0.1656(13)	0.1772(12)	0.0184(19)	0.0800
Si3	0.0377(12)	0.0484(8)	0.7366(24)	0.0800
Si4	0.6448(13)	0.3291(12)	0.5641(20)	0.0800
O5	0.4237(16)	0.3657(8)	0.251(5)	0.0400
O6	0.3196(14)	0.2006(21)	0.0438(24)	0.0400
O7	0.5092(16)	0.0684(7)	0.252(4)	0.0400
O8	0.5643(19)	0.2368(17)	0.4665(28)	0.0400
O9	0.5899(16)	0.2278(17)	0.0796(29)	0.0400
O10	0.3001(14)	0.1924(21)	0.4374(25)	0.0400
O11	0.0962(16)	0.1598(15)	0.2206(20)	0.0400
O12	0.1152(22)	0.0636(15)	0.5406(25)	0.0400
O13	0.1455(21)	0.0729(16)	0.8985(27)	0.0400
Rb14	0.2044(10)	0.6294(7)	0.1906(18)	0.118(6)
Rb15	0.4316(7)	0.0813(5)	0.7311(15)	0.026(4)
Ow16	0.195(4)	0.4354(31)	0.105(5)	0.0150

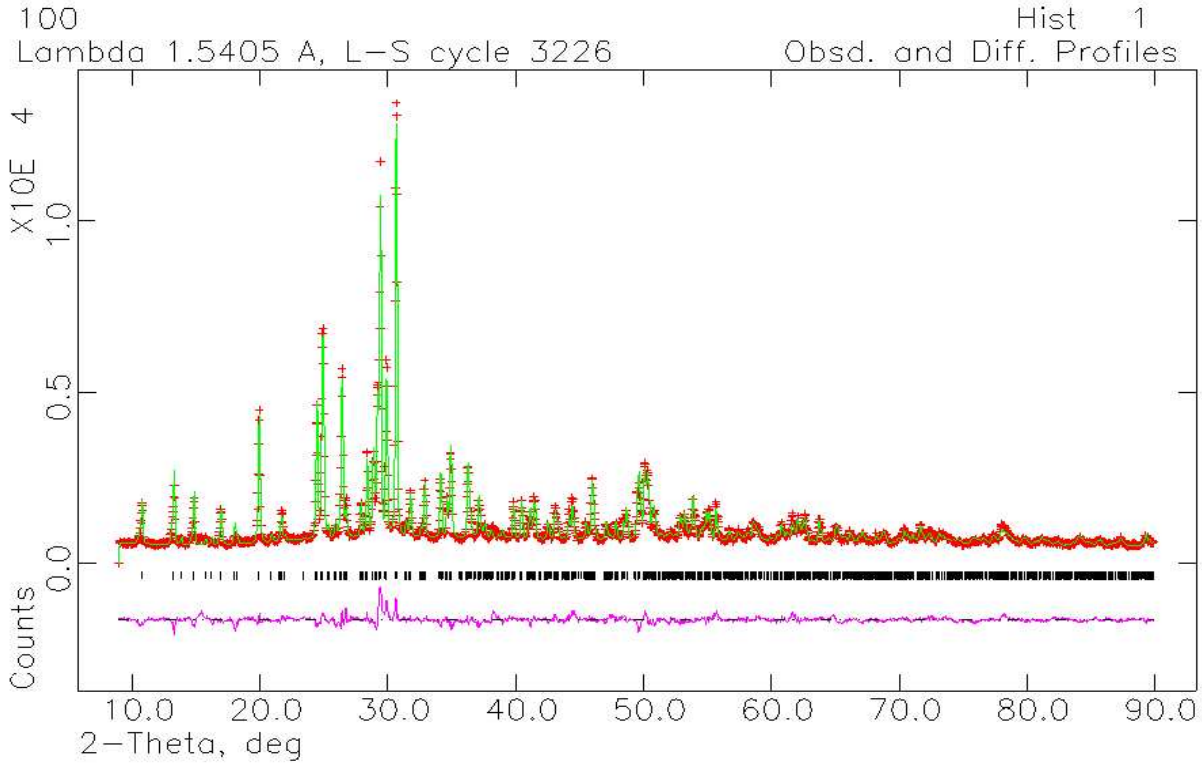

Figure 2.1. Observed (+) and calculated (-) profiles for final Reitveld refinement of $Rb_2ZrSi_3O_9 \cdot H_2O$. Difference plot is shown in the bottom as the pink line. Individual reflections are marked by the black bars.

2.2.5. Ion exchange kinetics

Experiments were carried out under infinite solution volume conditions as specified by Helfferich.[39] Vigorous stirring was employed to ensure particle diffusion controlled kinetics and not film diffusion. The rate of Rb^+ uptake was measured by tracing a 0.01M RbCl solution with enough ^{86}Rb to yield a count rate of ~50,000 counts per minute. 0.4 grams of ion exchanger was added to 200 mL of this solution under vigorous stirring. 1.0 mL aliquots were taken at designated times and filtered through a Millipore 0.22 μm syringe filter tip. The solution was then shaken with 18 mL of scintillation cocktail and the amount of ^{86}Rb was measured on a Wallac 1410 liquid scintillation counter. Diffusion coefficients were for the hydrolysis steps for $K_2ZrSi_3O_9 \cdot H_2O$ and $Rb_2ZrSi_3O_9 \cdot H_2O$ were measured on a TitraLab TIM860 Titration Manager. To 50 mL of distilled water adjusted to a pH of 7.0, 0.1g of ion exchanger was added under stirring. Values of pH versus time were recorded and related to the Vermeulen approximation as seen in the results section.

2.3. Results

2.3.1. Structure of $Rb_2ZrSi_3O_9 \cdot H_2O$ (1)

The structure of the fully exchanged rubidium phase is analogous to the parent K^+ compound.[31] The zirconium atom links the infinite polymeric silicate chains to form the framework. Uptake of Rb results in expansion of the unit cell, increasing the cell volume by approximately 36 $Å^3$. The unit cell expansion takes place mainly along the *a*-axis, with an increase of approximately 0.2 Å. Further expansion of the unit cell is not as drastic along the *b* and *c*-axes. The umbite type structure contains a three dimensional tunnel network similar to those found in zeolites. There are two independent cation exchange sites most easily defined by channels along the *c*-axis. As seen in Figure 2.2,

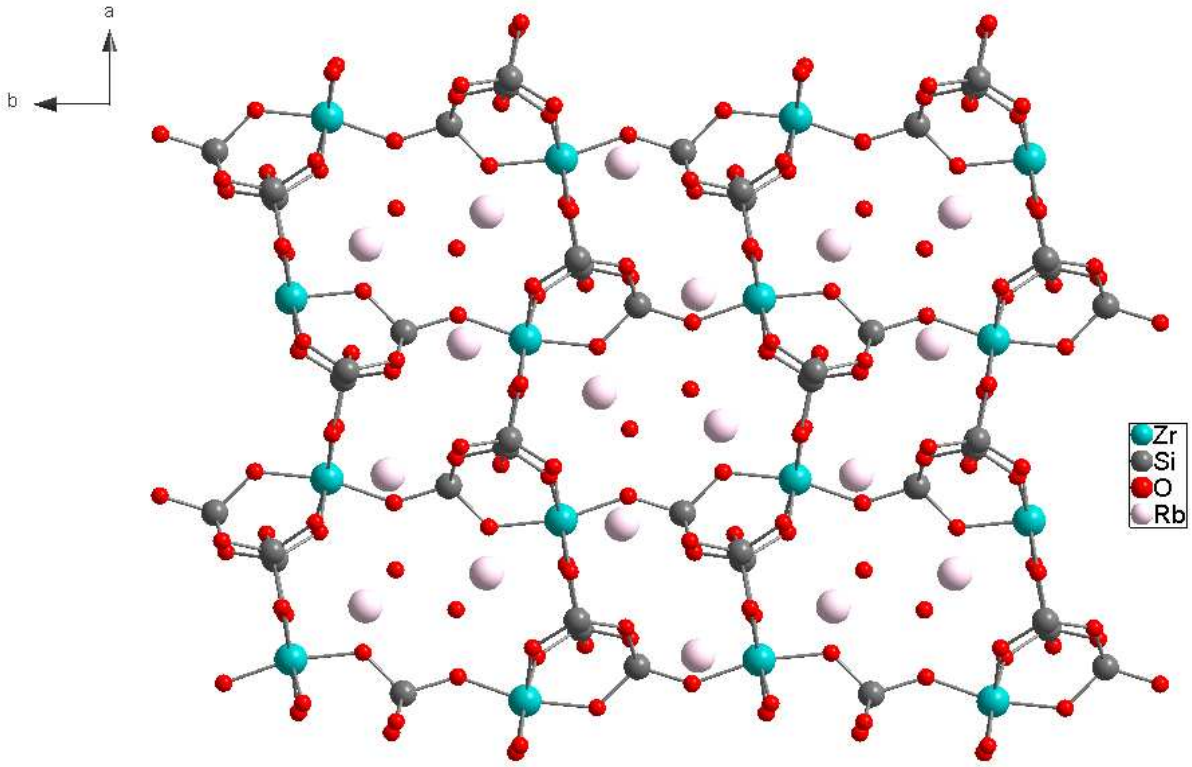

Figure 2.2. Ball and stick cartoon of compound **1** viewed down the *c*-axis. Rb14 is located in the 16-atom channel along with a water oxygen. Rb15 is seen in the 12-atom channel which is unoccupied by water.

Site 1 is marked by a 16-atom ring formed by alternating silicate tetrahedra and zirconium-oxygen octahedra. Dimensions of this zeolite type pore are 5.7 Å x 7.2 Å. The site is occupied by two exchangeable cations and two water molecules. Site 2 is described by a 12-atom ring including two zirconium octahedra and four silicate tetrahedra. This site also contains two exchangeable cations, but no water. Site 2 is significantly smaller with dimensions of 3.2 Å x 6.4 Å. Sites 1 and 2 are connected by perpendicular tunnels approximately along the $[\bar{1}10]$ diagonal. This connecting passageway between the two sites, depicted in Figure 2.3, is composed of a 14-atom ring connected by zirconium octahedra builds the framework.

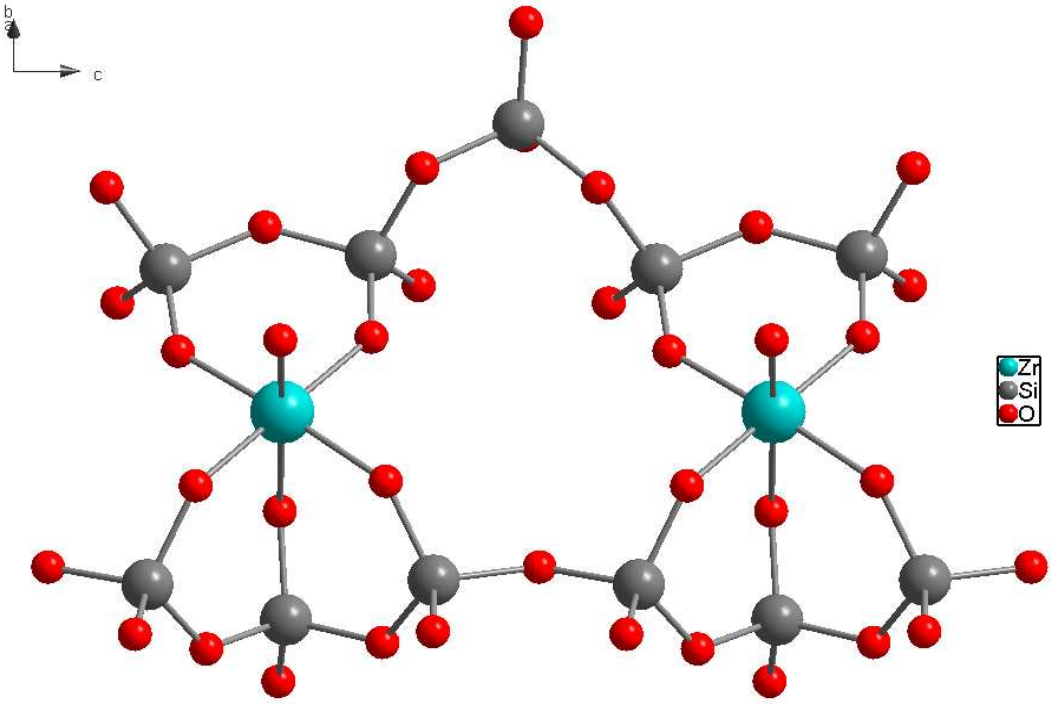

Figure 2.3. Ball and stick cartoon of the 14-atom channel linking Sites 1 and 2. The view is approximately along the [-110] plane.

Selected bond distances for framework atoms for compounds **1-4** are shown in Table 2.3. Cation-oxygen distances for compounds **1-4** are summarized in Table 2.4. For compound **1** (Rb^+ content 100%)**,** the rubidium environment in ion exchange Sites 1 and 2 shows Rb-O contact distances between 2.6 Å and 3.7 Å. In the large cavity (Site 1) Rb14 is 10-coordinate, bonding to 8 framework oxygens (O5, O6, O7, O8, O8′, O9, O10, O11) and 2 water oxygens (Ow16, Ow16′). The closest cation-oxygen contact is with

Table 2.3. Selected framework bond distances (Å) for compounds **1-4**.

Bond	1	2	3	4
Zr1-O5	2.071(8)	2.059(8)	2.093(10)	2.097(9)
Zr1-O6	2.022(8)	2.030(10)	2.000(10)	2.015(10)
Zr1-O7	2.039(8)	2.039(8)	2.077(9)	2.045(8)
Zr1-O8	2.021(8)	2.023(10)	2.012(10)	2.007(9)
Zr1-O9	2.015(8)	2.017(10)	2.008(10)	1.993(10)
Zr1-O10	2.018(8)	2.011(10)	2.018(10)	2.022(10)
Si2-O6	1.654(8)	1.643(10)	1.651(6)	1.656(5)
Si2-O9	1.661(8)	1.660(11)	1.652(6)	1.662(5)
Si2-O11	1.661(8)	1.657(10)	1.647(6)	1.651(5)
Si2-O13	1.661(8)	1.660(11)	1.655(6)	1.658(5)
Si3-O5	1.660(8)	1.670(10)	1.653(6)	1.655(5)
Si3-O7	1.643(8)	1.647(9)	1.646(6)	1.650(5)
Si3-O12	1.657(8)	1.668(11)	1.656(6)	1.658(5)
Si3-O13	1.667(8)	1.677(11)	1.666(6)	1.664(5)
Si4-O8	1.657(8)	1.653(11)	1.656(6)	1.655(5)
Si4-O10	1.652(8)	1.641(9)	1.652(6)	1.655(5)
Si4-O11	1.658(8)	1.634(10)	1.649(6)	1.650(5)
Si4-O12	1.655(8)	1.641(10)	1.659(6)	1.656(5)

Ow16 at 2.67 Å. Rb15, located in the smaller cavity (Site 2), is 11-coordinate and is bonded to 10 framework oxygens (O6, O7, O8, O9, O10, O11, O12, O12′, O13, O13′) and 1 water oxygen (Ow16). The close contact of Rb15 to a water oxygen is not seen in the parent compound where K^+ in the small tunnel shares no bond with water. While this contact is not as strong as the interaction of Rb14 with Ow16, it is still significant and its distance, 3.016(42) Å, is within the sum of the ionic radii.

Table 2.4. Cation-oxygen bond distances (Å) for compounds **1-4**.

Compound	M14-O	Distance	M15-O	Distance
	Rb14—O5	3.477(37)	Rb15—O6	3.021(26)
	Rb14—O6	3.446(26)	Rb15—O7	3.592(31)
	Rb14—O7	3.138(20)	Rb15—O8	3.161(23)
	Rb14—O8	3.042(23)	Rb15—O9	3.613(23)
(**1**) $Rb_2ZrSi_3O_9 \bullet H_2O$	Rb14—O8′	3.716(23)	Rb15—O10	2.949(23)
	Rb14—O9	3.031(22)	Rb15—O11	3.241(21)
	Rb14—O10	3.017(27)	Rb15—O12	3.603(24)
	Rb14—O11	3.241(20)	Rb15—O12′	3.016(21)
	Rb14—Ow16	2.672(42)	Rb15—O13	3.239(23)
	Rb14—Ow16′	3.317(39)	Rb15—O13′	3.286(23)
			Rb15—Ow16	3.016(42)
	M14—O5	3.426(23)	Rb15—O6	2.999(17)
	M14—O6	3.543(20)	Rb15—O7	3.664(25)
	M14—O7	3.145(16)	Rb15—O8	3.151(12)
	M14—O8	2.909(13)	Rb15—O9	3.474(12)
(**2**)$K_{0.29}H_{0.1}Rb_{1.61}ZrSi_3O_9 \bullet H_2O$	M14—O8′	3.768(13)	Rb15—O10	2.991(16)
	M14—O9	3.137(13)	Rb15—O11	3.128(14)
	M14—O10	2.918(19)	Rb15—O12	3.701(12)
	M14—O11	3.191(14)	Rb15—O12′	2.954(12)
	M14—O12	3.720(14)	Rb15—O13	3.190(12)
	M14—Ow16	2.640(36)	Rb15—O13′	3.376(12)
	M14—Ow16′	3.162(38)	Rb15—Ow16	3.311(42)
	M14—O5	3.369(31)	M15—O6	3.055(21)
	M14—O6	3.499(23)	M15—O7	3.376(22)
	M14—O7	3.121(20)	M15—O8	3.121(21)
	M14—O8	2.942(21)	M15—O9	3.67(2)
	M14—O8′	3.678(21)	M15—O10	2.847(20)
(**3**)$K_{0.9}H_{0.1}RbZrSi_3O_9 \bullet H_2O$	M14—O9	3.005(20)	M15—O11	3.264(17)
	M14—O10	2.960(23)	M15—O12	3.675(19)
	M14—O11	3.312(19)	M15—O12′	2.953(19)
	M14—O12	3.660(21)	M15—O13	3.095(19)
	M14—Ow16	3.224(39)	M15—O13′	3.374(20)
	M14—Ow16′	2.566(38)	M15—Ow16	3.308(42)
	K14—O5	3.285(31)	M15—O6	3.018(22)
	K14—O6	3.501(23)	M15—O7	3.431(25)
	K14—O7	3.089(22)	M15—O8	3.111(21)
	K14—O8	2.983(21)	M15—O10	2.832(21)
(**4**)$K_{1.45}H_{0.1}Rb_{0.45}ZrSi_3O_9 \bullet H_2O$	K14—O8′	3.577(22)	M15—O11	3.231(19)
	K14—O9	2.935(21)	M15—O12	2.861(20)
	K14—O10	2.953(23)	M15—O13	3.069(19)
	K14—O11	3.320(21)	M15—O13′	3.354(21)
	K14—O12	3.603(22)	M15—Ow16	3.201(38)
	K14—Ow16	2.462(35)		
	K14—Ow16′	3.364(39)		

2.3.2. Structure of partially substituted Rb phases

Structure solutions for the partially substituted phases were carried out in the same fashion as for compound **1**. Compounds **2**, **3**, and **4** have identical framework compositions. The expansion of their unit cell volumes express the level of substitution, 1018, 1008, and 998 $Å^3$ for Rb^+ contents of 1.61, 1, and 0.45 moles, respectively, increasing from 987 $Å^3$ in the potassium phase. In all compounds where substitution was incomplete, hydrogen cations were observed in the structure. At equilibrium the ion exchange solution displayed a pH of 10.65 indicating that, by charge balance, approximately 0.1 moles of H^+ must have remained in the exchanger. The largest difference in structure between compounds **2**, **3**, and **4** is the cation occupancy. For **2**, an excess of Rb^+ was allowed to come to exchange equilibrium with the K phase. This resulted in complete substitution of Site 2 for Rb^+. In Site 1 the occupancy was shown to be 0.29 K^+, 0.61 Rb^+, and 0.1 H^+. The coordination of Rb^+ cations in Site 2 is the same as that of compound **1**. Average Rb-O contact distances are approximately 3.23 Å. An additional contact with O6 is shown at 2.999(17) Å. The Rb-Ow16 distance has increased from 3.016(42) to 3.311(42) Å.

To obtain the desired levels of substitution in compounds **3** and **4**, stoichiometric amounts of Rb^+ were exchanged in at the same volume to mass ratio. Compound **4** shows an exchange of approximately 25% of Rb^+ for K^+ and has the formula $K_{.45}H_{0.1}Rb_{0.45}ZrSi_3O_9•H_2O$. The distribution of Rb^+ is uneven and uptake is observed only in Site 2. Final Reitveld refinement arrived at an occupancy in Site 2 of 0.45 K^+, 0.45 Rb^+, and 0.1 H^+ while Site 1 remains filled with K^+. K-O contacts in Site 1 are between 2.5 and 3.6 Å. Four more K-O contacts are described here than in the original parent compound.[31] The average K-O distance has grown from 3.05 Å in the parent compound to 3.18 Å here in compound **4**. This can be attributed to the increase in the size of the unit cell, produced by the presence of Rb^+.

Compound **3** is assigned the formula $K_{0.9}H_{0.1}RbZrSi_3O_9•H_2O$ as approximately 50% of K has been exchanged for Rb. Again there is unequal distribution of Rb among

the two exchange sites. Site 2 contains mostly Rb and has occupancy factors of 0.06 K^+, 0.84 Rb^+, and 0.1 H^+. Site 1 is now being populated by Rb cations either by direct exchange or through migration of the Rb ions in Site 2 through the 14-atom channel. Site 1 occupancy factors are 0.86 K and 0.14 Rb. M-O contacts are similar to compound **4**. There are 11 M-O contacts in both sites. As in all other compounds reported here, there are two water contacts to the cation in Site 1 and one M-Ow16 contact in Site 2. The average contact distance is 3.21 Å in Site 1 and 3.25 Å in Site 2.

2.3.3. Kinetics

The kinetics of ion exchange reactions are limited by either diffusion through a film, or particle diffusion through pores or cavities of the exchanger. For particle diffusion control, derivations of the mathematical models that govern these processes begin with isotopic exchange. A variety of mathematical models can be employed but all begin fundamentally with the description of ion flux. The flux of ion A in the ion exchanger is given by Equation 1, where J_A is the flux, D is the coefficient of diffusion, C_A is the concentration of ion *A*. The dependence of this flux, J_A, on time and concentration is given by Fick's second law (Equation 2). Combination of Equations 1 and 2 yields Equation 3. The solution to Equation 3 yields C_A as a function of particle radius *r* and time, *t*. Integration of this function yields Equation 3a where fractional attainment of equilibrium, U, is a function of time *t*, particle radius r_o, and mass diffusion coefficient D_i.

$$J_A = -\,D \text{ grad } C_A \qquad [1]$$

$$\frac{\partial C_A}{\partial t} = -\text{ div } J_A \qquad [2]$$

$$\frac{\partial C_A}{\partial t} = D\left(\frac{\partial^2 C_A}{\partial r^2} + \frac{2}{r}\frac{\partial C_A}{\partial r}\right) \qquad [3]$$

$$U(t) = 1 - \frac{6}{\pi^2} \sum_{n=1}^{\infty} \frac{1}{n^2} \exp\left(\frac{D_i t \pi^2 n^2}{r_o^2}\right) \qquad [3a]$$

An important difference in mathematical modeling of ion exchange processes is the consideration of what Helfferich[39] refers to as electric coupling of ionic fluxes. It is this distinction that separates isotopic exchange from ion exchange. Distilled, this postulate states that as the faster ion diffuses an electric potential is set up which accelerates diffusion of the slower ion while slowing diffusion of the faster ion. Thus, ion flux becomes dependent on the valence of the species in solution and Equation 1 is transformed into Equation 4. Where J_i is the transference of species i, φ is the electric potential, u_i is the electrochemical mobility, z_i is the valence of the ion, and C_i is the concentration.

$$J_{i\ electric} = -u_i\, z_i\, C_i\, \text{grad}\, \varphi \qquad [4]$$

The electrochemical mobility u_i is defined as $\frac{D_i F}{RT}$, where D_i is the diffusion coefficient, F is the Faraday constant, R is the gas constant, and T is temperature in degrees Kelvin. Incorporation of a flux term due purely to thermal diffusion, $J_{i\ diff}$, gives the Nerst-Planck equation (Equation 5).

$$J_i = J_{i\ diff} + J_{i\ electric} = -D_i \left(\text{grad}\, C_i + z_i \frac{C_i F}{RT} \text{grad}\, \varphi\right) \qquad [5]$$

Under the assumption of electroneutrality and the absence of applied voltage to the system, the Nerst-Planck equation may be approximated in terms of D_i and r_o, which are the mass diffusion coefficient and the spherical radius of the ion exchange particle, respectively. A general form is shown in Equation 6 and is expressed as a function of fractional attainment of exchange equilibrium $U(\tau)$ where τ is $D_A t/r_o^2$.

$$U(\tau) = \{1 - \exp[\pi^2\, f(\alpha_1)\, \tau + f(\alpha_2)\, \tau^2 + f(\alpha_3)\, \tau^3]\}^{1/2} \qquad [6]$$

Values of α are dependent on the valence ratios of the two exchanged ions z_A/z_B and are found tabulated by Helfferich.[39] An analysis of the practical application of mathematical models for isotopic exchange and ion exchange kinetics by Inglezakis and Grigoropoulou[40] shows that a simplified model known as Vermeulen's approximation, given in Equation 7 may be used under a variety of conditions. In Equation 7, U(t) is the given fractional attainment of equilibrium, r_o is the size of the ion exchange particle in μm, t is time in seconds, and D_i is the mass particle diffusion coefficient and has units of $r_o^2 \cdot t^{-1}$.

$$U(t) = \left[1 - \exp\left(-\frac{D_i t \pi^2}{r_o^2}\right)\right]^{1/2} \qquad [7]$$

According to Helfferich, application of the Vermeulen approximation gives less accurate results than that of the solution to Equation 3a. However, in the domain of $F(t) \geq 0.8$, as is the case with ion exchange data presented here, Helfferich suggests ignoring terms higher than first order, in which case Equation 3a looks very similar to the Vermeulen approximation. Equations 3a, 7, and Paterson's approximation were fit to kinetic data. In all cases regression statistics favored the use of Vermeulen's approximation.

Mass diffusion coefficients are summarized in Table 2.5. Experiments were carried out under infinite volume solution conditions where the concentration of K^+ in solution had no effect on attainment of equilibrium and no swelling of the exchanger occurred.

A mass diffusion coefficient, D_i, of 3.4 $\mu m^2 \cdot s^{-1}$ was observed for the ion exchange process of Rb exchange in $K_2ZrSi_3O_9 \bullet H_2O$. Figure 2.4 shows the fractional attainment of equilibrium which is proportional to uptake of ^{86}Rb as a function of time. Diffusion coefficients for the hydrolysis steps of both $K_2ZrSi_3O_9 \bullet H_2O$ and $Rb_2ZrSi_3O_9 \bullet H_2O$ were also measured as a function of fractional attainment of equilibrium.

Table 2.5. Diffusion coefficients derived from data treatment with Vermeulen's approximation.

Process	Diffusion Coefficient, D ($\mu m^2 \cdot s^{-1}$)	Vermeulen Regression Statisics (R^2, χ^2/DoF)
$K \leftrightarrow H$	D_{KH} 102.4	0.976, 0.0018
$Rb \leftrightarrow H$	D_{RbH} 25.5	0.991, 0.00075
$K \leftrightarrow H \leftrightarrow Rb$	D_i 3.4	0.994, 0.00052

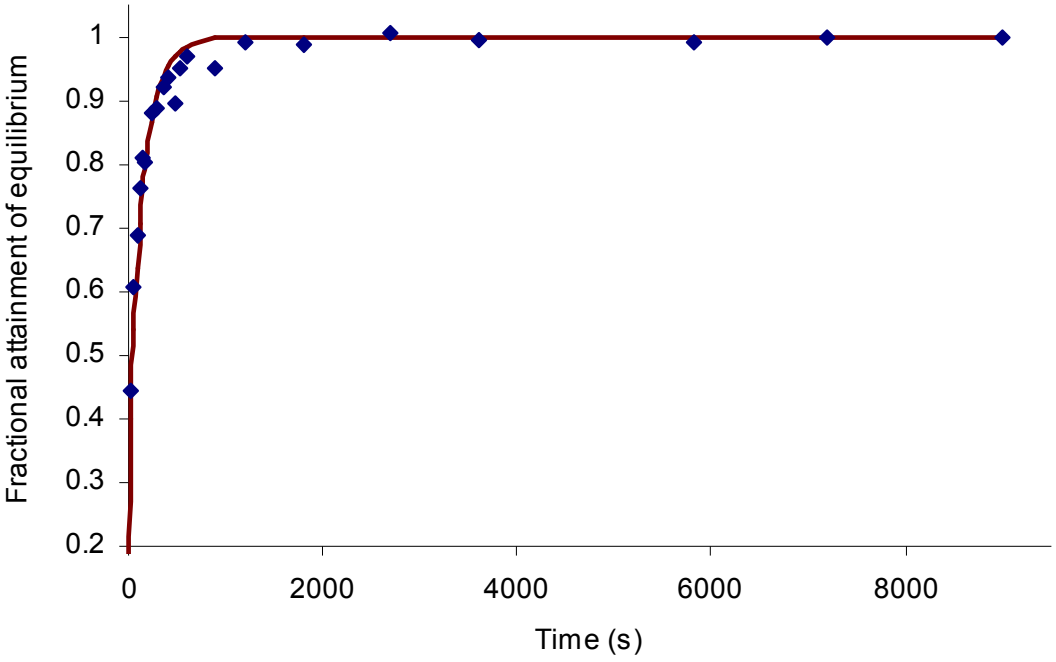

Figure 2.4. Plot of fractional attainment of equilibrium over time for the uptake of ^{86}Rb in $K_2ZrSi_3O_9 \cdot H_2O$. Blue diamonds represent experimental points while the maroon line represents the fit to Vermeulen's approximation.

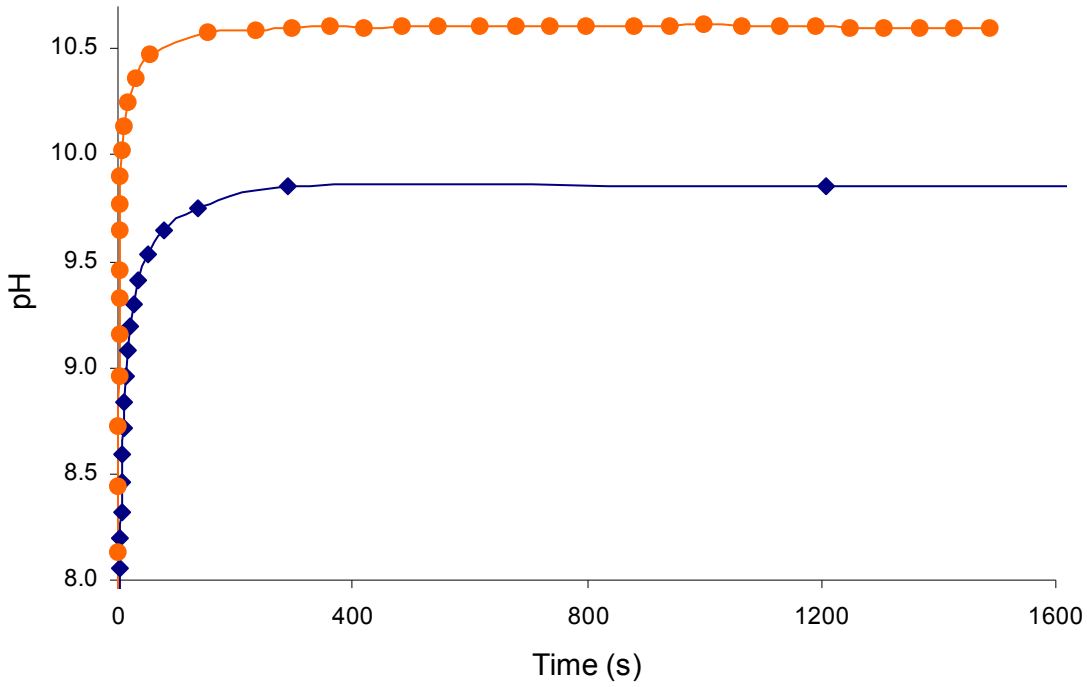

Figure 2.5. Plot of pH versus time for the hydrolysis in water upon addition of ion exchanger. Data in blue diamonds represents addition of $Rb_2ZrSi_3O_9 \cdot H_2O$ to water while the orange spheres represent addition of $K_2ZrSi_3O_9 \cdot H_2O$ to water.

Figure 2.5 shows plots of pH as a function of time for the hydrolysis steps. Diffusion coefficients derived from these plots for Rb ↔ H and K ↔ H were 25.5 and 102.4 $\mu m^2 \cdot s^1$, respectively. A value of 75 μm was used for the particle radius r_o.

2.3.4. Infrared spectrum

The infrared spectrum of compound **1** is shown in Figure 2.6. Bands of lower energy at approximately 740, 700, and 535 cm^{-1} have been reported as Zr-O stretches. Bands at 1040, 970, and 905 are likely the symmetric and asymmetric stretches due to framework Si-O tetrahedra. It has also been reported that stretches in this region extend from those related to Si-O-Zr bonds.[41] The presence of water in Site 1 can be confirmed by the bands located at 1640 cm^{-1} and at higher energy in the region of 3300 cm^{-1}. This is confirmed in the spectra reported for $K_2TiSi_3O_9 \bullet H_2O$.[15] Anomalous in this spectrum is the sharp absorbance at 1380 cm^{-1}. This can be attributed to the O-H bend of methanol, with which the sample was washed thoroughly.[42,43] Other modes for methanol such as the C-O stretch (1033 cm^{-1}) overlap with stronger absorbances of Si-O while weaker C-H modes may also be masked in the areas of 1400-1650 cm^{-1}.

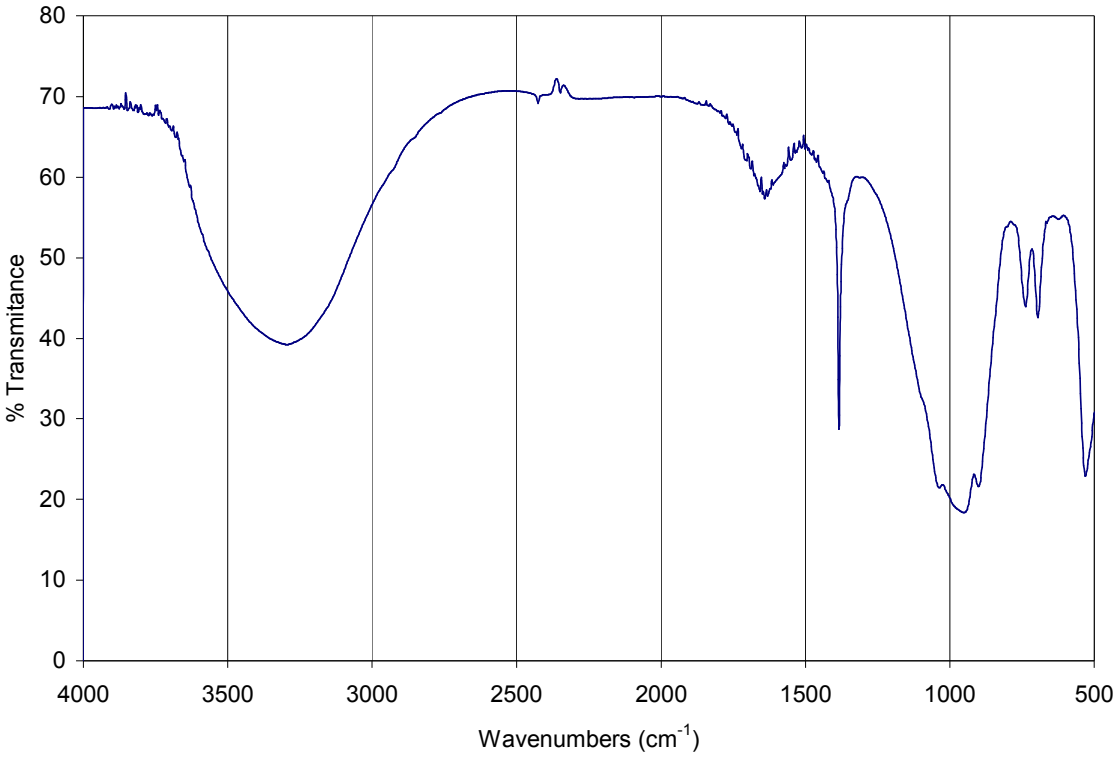

Figure 2.6. Infrared spectrum of compound **1,** $Rb_2ZrSi_3O_9 \bullet H_2O$.

2.3.5. TGA

Thermogravimetric analysis of compound **1** indicated 3.4% weight loss at 125 ^{o}C. This loss is attributed to surface water. A total weight loss of 7.1% at 700 ^{o}C was observed. Therefore 3.7% of the weight loss is due to lattice water. This number is slightly larger than the expected value of 3.54%. The discrepancy can be attributed to the presence of methanol as seen in the IR spectrum.

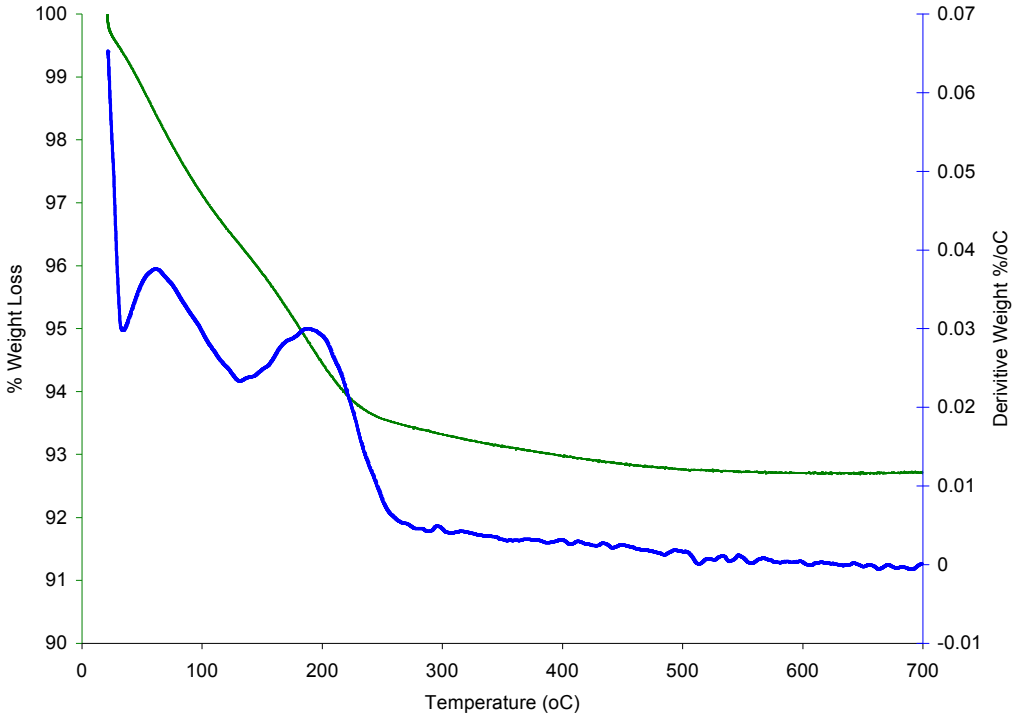

Figure 2.7. Thermal gravimetric curves of compound **1**, $Rb_2ZrSi_3O_9 \bullet H_2O$. The green line represents % weight loss as a function of temperature. The blue line is the differential weight loss. An internal water loss of 3.7% was observed which accounts for 1 mole of water per mole of ion exchanger.

2.4. Discussion

Compounds **1-4** are isostructural with the mineral umbite and all crystallize in the orthorhombic space group $P2_12_12_1$. The increase in unit cell volume for compounds **4-1** is directly related to the extent of exchange. The enlargement of the unit cell takes place mostly along the *a*-axis as the dimension increases from approximately 10.29(1) Å in the parent compound to 10.48(1) Å in compound **1**.

The selectivity of $M_2ZrSi_3O_9 \cdot H_2O$ and $M_2TiSi_3O_9 \cdot H_2O$ for alkali cations has previously been investigated.[32] The ability to collect specific ions is a direct relationship with the size of the channels and cavities they occupy. The affinity of zirconium trisilicate for each particular cation can now be correlated with the coordination environment of the cation. Table 2.6 shows the average M-O distances in Sites 1 and 2 for the K^+, Na^+ and Rb^+ phases of zirconium trisilicate.[44]

Table 2.6. Average cation-oxygen distances related to the sum of their ionic radii at specific coordination number.[31,41]

Cation	Coordination No. (Site 1, Site 2)	Average M-O Distance Site 1 (Å)	Average M-O Distance Site 2 (Å)	Sum of ionic radii (Å)
Na	6, 9	3.04(2)	3.30(3)	2.42, 2.72
K	7, 7	3.05(1)	3.03(1)	2.86
Rb	10, 11	3.210(28)	3.243(25)	3.09

The coordination number of Rb in compound **1** is significantly higher than that for other cations in both ion exchange sites. Rb is 11-coordinate in Site 1 and 11-coordinate in Site 2 however in the parent compound K^+ is only 7-coordinate in both sites. This increase in coordination and the formation of additional M-O contacts can be said to account for the increase in selectivity for Rb. The Rb-O contact distances in **1** are closer to the sum of their ionic radii than that of K-O in the parent compound and Na-O in the sodium exchange phase. The Rb-O contacts in Site 1 are approximately 0.12 Å larger

than their ideal distance, while the disparity between those of K-O and Na-O are +0.19 Å and +0.62 Å, respectively. Rb-O contacts in Site 2 are slightly longer than those of Site 1. Average Rb-O contacts are 3.24 Å for Site 2 in compound **1**, a difference of +0.15 Å from the ideal. For Site 2 the difference between the sum of ionic radii and experimental M-O contacts are +0.19 Å for the K phase and +0.58 Å for the pure Na phase. Again, as the M-O contact distances approach those of the ideal, the affinity for that particular cation grows.

There are additional considerations to address before arriving at a pathway for potassium rubidium exchange. The diffusion coefficients measured for the separate processes occurring during exchange provide insight into the role of hydrolysis in this exchange mechanism. The mass diffusion coefficient given in Table 2.5 for the entire exchange process is 3.4 $\mu m^2 \cdot s^{-1}$. When the K-phase is placed in water an equilibrium pH of approximately 10.65 is observed and the uptake of H^+ has been shown to have a diffusion coefficient of 102.4 $\mu m^2 \cdot s^{-1}$. Furthermore, it has been shown that this quantity, D_{KH}, is independent of Rb concentration (Figure 2.8). This quantity is two orders of magnitude greater than the mass diffusion coefficient and clearly indicates that it is the faster process. We can also see that the exchange of Rb^+ for H^+ is a slower process than exchange of K^+ for H^+. D_{RbH} was measured to be 25.5 $\mu m^2 \cdot s^{-1}$. Therefore the rate determining step in the incorporation of Rb into $K_2ZrSi_3O_9 \bullet H_2O$ is the exchange of H^+ for Rb^+ and not a direct exchange of potassium for rubidium.

The affinity of Sites 1 and 2 for specific cations can also be distinguished on the basis of their coordination environment; however the mobility of ions within the framework is a better method for describing the trends in site occupancy. As discussed in previous work the shape of Site 2 inhibits cation movement through the channel in the *c*-axis direction.[31] The distance between O12 and O13 effectively restricts the movement of cations along this direction, however, this does not prevent diffusion of cations between the two exchange sites. As previously described, a 14-atom channel links Sites 1 and 2 approximately along the $[\bar{1}10]$ plane.[31] Many mechanisms seem plausible, however, any mechanism must begin with loss of K^+ and must also account

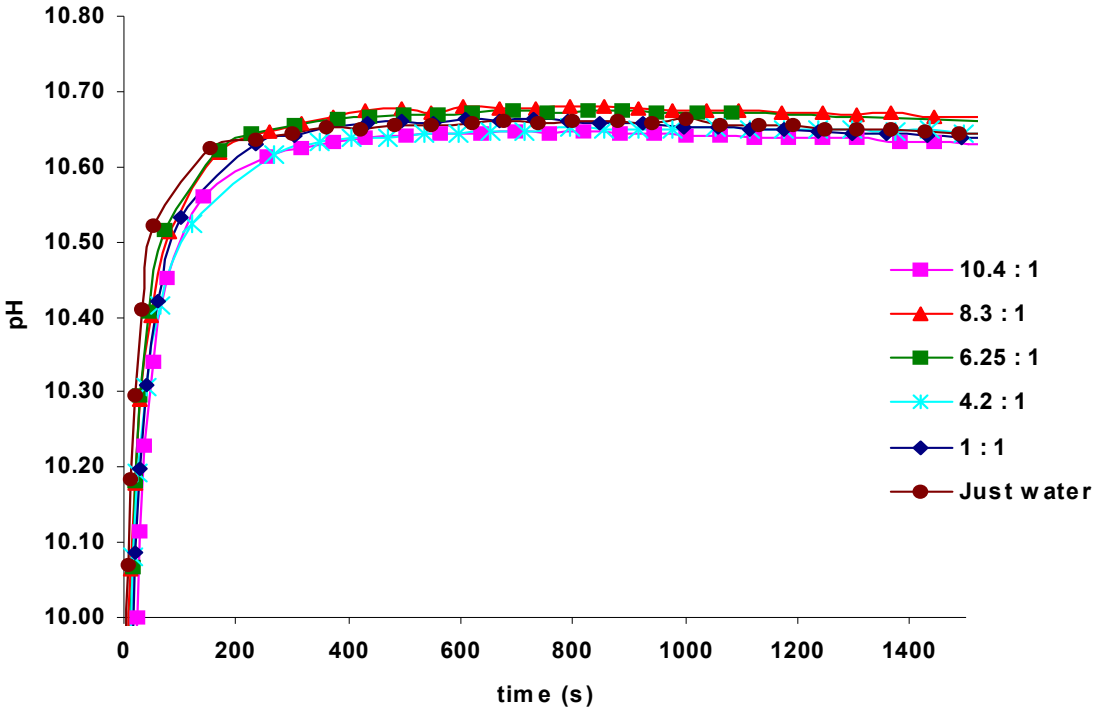

Figure 2.8. Plot of pH versus time for the ion exchange reaction of Rb with $K_2ZrSi_3O_9 \bullet H_2O$. Different Rb:K ratios are shown.

for the observed trends in site occupancy. A detailed description of the ion exchange process must also include the presence of H^+ in the mechanism. A possible pathway is discussed here which fits the experimental observations.

As previously stated, exchange must begin with the loss of K^+. Potassium cations may diffuse out into the solution through either the 14-atom tunnel or through the 16-atom channel along the *c*-axis. If K^+ diffuses out through the large tunnel along the c-axis, a K^+ from Site 2 may now move into Site 1 via the 14-atom tunnel. A proton is then taken up in Site 2 through either the 14-atom channel along the $[\bar{1}10]$ plane or the 12-atom channel in the *c*-direction. As the exodus of K^+ continues through the 16-atom channel, Rb^+ replaces H^+ in Site 2 which can diffuse out back into solution through the 12-atom channel along the *c*-direction. Remember, diffusion along the c-axis through the 12-atom channel is inhibited for larger cations by the encroachment of framework oxygens, however this is not likely to limit the diffusion of H^+ because of its much smaller size. The fact that protons may diffuse through any and all channels makes their replacement by Rb^+ faster than direct K^+ Rb^+ substitution and is in accordance with the kinetic data. Compound **2** shows that Site 1 has been populated with Rb^+. Once Site 2 is approximately 80% populated with Rb^+, diffusion of H^+ through site 2 along the *c*-axis becomes inhibited and the exchange of cations through the framework must now occur almost entirely along the 16-atom channel.

2.5. Conclusions

Four compounds incorporating Rb into $K_2ZrSi_3O_9 \bullet H_2O$ have been synthesized by ion exchange, completing a series of alkali cation substituted zirconium trisilicates. Zirconium trisilicate shows maximum selectivity for Rb throughout the entire pH range. Among the fully substituted trisilicates, compound **1,** $Rb_2ZrSi_3O_9 \bullet H_2O$, shows M-O distances that are closest to their ideal distances, that being the sum of O^{2-} and Rb^+ ionic radii.

It can now be said that, as the M-O distances approach those of the ideal, the affinity of zirconium trisilicate for a particular alkali cation increases. Upon addition of zirconium trisilicate to an aqueous solution, a pH increase is observed indicating that protons are taken up through hydrolysis. Through structural analysis it has been shown that Site 2 is the first to be populated by Rb^+.

CHAPTER III
SYNTHESIS AND CHARACTERIZATION OF PROTONATED ZIRCONIUM TRISILICATE AND ITS EXCHANGE PHASES WITH STRONTIUM

3.1. Introduction

In the continued study of the trisilicate system the push for advanced materials for nuclear waste remediation continues to be basic impulsion for this work. For many years the build up of nuclear waste from power plants and weapons facilities has been a pressing problem for the environment. Disposal strategies have relied on the separation of ^{137}Cs and ^{90}Sr from their constituents in waste streams. These elements are required to be segregated because of their high heat generation stemming from radioactive decay, their environmental threat, and the long half-lives of these elements. Separation of these isotopes also has the effect of reducing the volume of waste after vitrification, a process that solidifies the waste for permanent disposal, typically in borosilicate or phosphate glass. This allows for increased storage space and reduces the need for future disposal facilities. With half-lives of approximately 30 years, separated strontium and cesium waste can be decommissioned and disposed of safely in ten half-lives or 300 years.[45]

The structure and selectivity of zirconium trisilicates for group I cations has been well characterized.[31,32,46] There has been in the zirconium umbite system, however, little work involving cations of higher valence. In order to better understand the mechanism of ion exchange in 3D tunnel framework compounds the partially protonated phase of $K_2ZrSi_3O_9 \bullet H_2O$ has been prepared. It is hoped that this system will serve as a model for ion exchange processes in inorganic framework ion exchangers. In this chapter the protonated phase of zirconium trisilicate and a new study on its exchange phases with group II cations is reported.

3.2. Experimental methods

3.2.1. Analytical procedures and instrumentation

Phase identification and structural data sets were collected using a Bruker-AXS D8 VARIO powder diffractometer. Thermal gravimetric analysis was conducted on a TA Instruments TGA Q 500 unit. A constant temperature ramp of 5 ^{o}C/min was applied while the sample was under 9:1 nitrogen to air volume ratio. Potassium and strontium analysis was performed on a Varian AA 250 atomic absorption spectrometer under an acetylene nitrous oxide flame. Samples for AA analysis were prepared by digestion of the solid in hydrofluoric acid. Measurements of ^{90}Sr uptake were performed on a Wallac 1410 liquid scintillation counter. Titrations and pH measurements were conducted on a TitraLab TIM860 Titration Manager.

3.2.2. Synthesis and ion exchange

Potassium zirconium trisilicate, $K_2ZrSi_3O_9 \bullet H_2O$, was synthesized hydrothermally by modification of methods previously reported by Poojary et al.[31] 7.0 grams of silicic acid was dissolved in 45 mL of 4M KOH and 10 mL of isopropanol. 13.5 mL of a 70% solution of zirconium isopropoxide in isopropanol was diluted with 10 mL of isopropanol and added drop wise to the previous solution. The mixture was divided in two and placed in 100 mL Teflon lined autoclaves. The reaction was carried out at 180^{o}C. After 5 days a white precipitate was isolated and washed with distilled water and dried at 60^{o}C.

Compound **1**, $H_{1.45}K_{0.55}ZrSi_3O_9 \bullet 2H_2O$, was synthesized by shaking $K_2ZrSi_3O_9 \bullet H_2O$ in 0.1M acetic acid at a volume to mass ratio of 500:1 for 24 hours at room temperature. The product was collected by vacuum filtration and washed with distilled water and acetone. The dry product was then shaken in 0.5M acetic acid for 24 hours. The product was again collected by vacuum filtration and rinsed thoroughly with

water and acetone until no odor of acetic acid was detected. Anal. Found: Zr, 23.89; Si, 21.61; K, 5.71. Calcd. for $K_{0.56}H_{1.44}ZrSi_3O_9 \cdot 2H_2O$: Zr, 24.11; Si, 22.28; K, 5.79.

Compound **2**, $K_{0.34}Sr_{0.83}ZrSi_3O_9 \cdot 1.8H_2O$, was synthesized by shaking 1.0 g of **1** in 500 mL of 0.5M $SrCl_2$ for 24 hours at room temperature. The white powder was washed first with water, then acetone, and dried at room temperature. Anal. Found: Zr, 20.70; Si, 19.51; K, 3.31; Sr, 16.58. Calcd. for $K_{0.34}Sr_{0.83}ZrSi_3O_9 \cdot 1.8H_2O$: Zr, 20.62; Si, 19.05; K, 3.00; Sr, 16.43.

Compound **3**, $SrZrSi_3O_9 \cdot 2H_2O$, was synthesized by ion exchange at elevated temperature. 2.0 g of **1** was placed in 250 mL round bottom flask along with 200 mL of 1.0M $SrCl_2$. This mixture was stirred at 90^{o}C for 24 hours. The mixture was allowed to settle and the supernatant liquid was decanted and saved. A fresh 200mL of 1.0M $SrCl_2$ was added and heated again for 24 hours. This process was repeated until the presence of potassium in the supernatant liquid was undetectable by AA spectroscopy. Anal. Found: Zr, 20.76; Si, 19.61; Sr, 20.18. Calcd. for $SrZrSi_3O_9 \cdot 2H_2O$: Zr, 20.61; Si, 19.03; Sr, 19.80.

3.2.3. X-ray data collection and structure refinement

Data sets were collected on a Bruker-AXS D8 VARIO powder diffractometer with standard vertical Bragg-Brentano geometry and a linear PSD detector. The diffractometer was equipped with a Germanium monochromator allowing the use of Cu $K\alpha_1$ radiation only with a wavelength of 1.54056 Å. Powders were loaded on a quartz disc which was spun during data collection to reduce any scattering effects due to preferred orientation. Operating voltage and current were 40kV and 50mA respectively. Data were collected at room temperature with 2θ ranging from 5 to 130 degrees. A step size of 0.016 degrees and a scan time of 15 seconds per step were employed.

Powder patterns were indexed using TREOR, ITO, and DICVOL methods found in the FullProf program suite.47-49 Profile function fitting using the LeBail method and Reitveld refinement were accomplished using the GSAS program suite.[37,38] No

corrections were made for absorption and neutral atom scattering factors were used as stored in GSAS. No attempt was made to model preferred orientation.

Observed and calculated XRD profiles are displayed in Figure 3.1. Compound **1** crystallizes in the monoclinic space group $P2_1/c$ with cell dimensions of a = 7.1002(2), b = 10.1163(3), c = 13.1742(5), and β = 91.181(1)°. The structure of the potassium phase and the partially substituted proton phase are very similar. However, a phase change from an orthorhombic unit cell, space group $P2_12_12_1$, for the K-phase to a monoclinic cell has occurred. To use the potassium phase as a starting model in structural refinement it was necessary to transform the original atomic coordinates by the matrix given in Eqn. 1.

$$\begin{pmatrix} x & & \\ & y & \\ & & z \end{pmatrix} \bullet \begin{pmatrix} z/x & & \\ & \left(\frac{1}{4}y + x/y\right) & \\ & & y/z \end{pmatrix} = \begin{pmatrix} z & & \\ & \left(\frac{1}{4} + x\right) & \\ & & y \end{pmatrix} \qquad [1]$$

Once profile fitting was completed and the framework atomic coordinates were transformed into their new system, bond distance restraints were applied to Si-O and Zr-O contacts. The position of zirconium was refined and subsequently that of each individual trisilicate group. Fourier difference maps were constructed to reveal the position of the missing cations and waters. Once the positions were input, the atomic coordinates of the framework were again refined. Next, the cation and water positions were refined without moving the framework. This see-saw approach was continued until least squares refinement converged rapidly and the shift in atomic coordinates was less than 0.1% of the starting value. The potassium site occupancy for **1** was then refined while isotropic thermal factors were held constant. Once site occupancy was established,

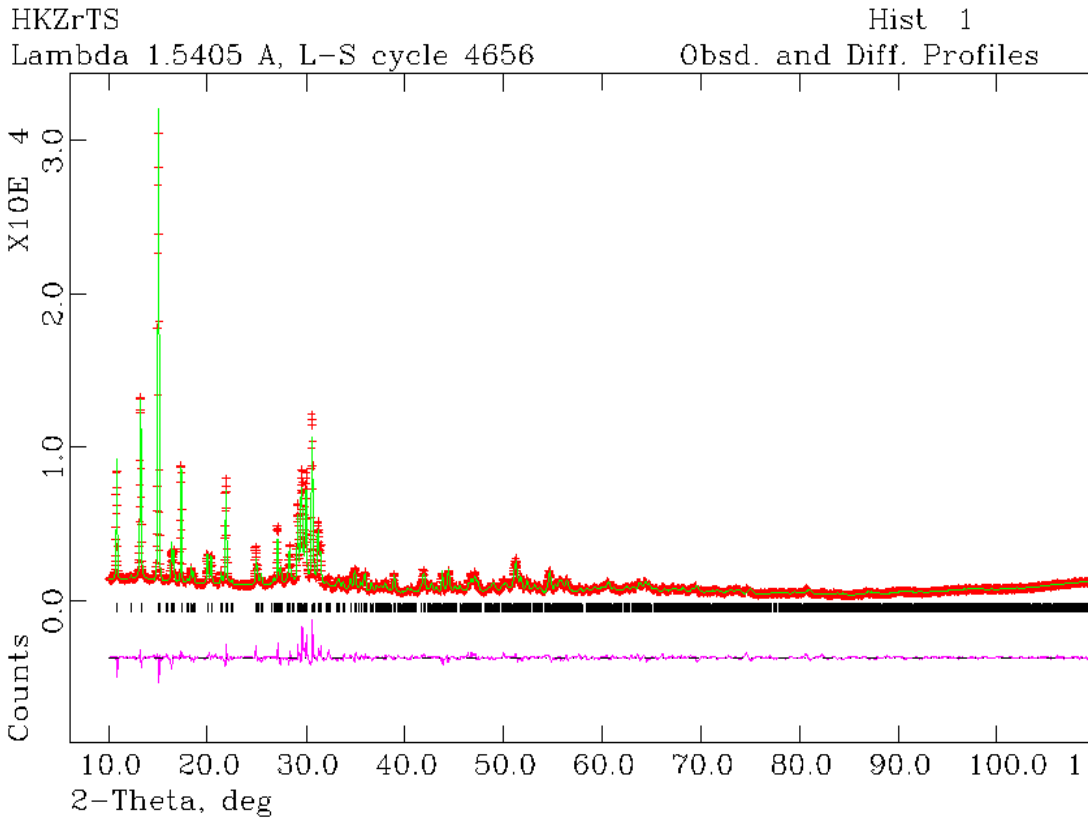

Figure 3.1. Observed (+) and calculated (-) profiles for final Reitveld refinement of **1,** $SrZrSi_3O_9 \bullet H_2O$. Difference plot is shown in the bottom as the pink line. Reflections are marked by the black bars.

isotropic thermal factors for zirconium, potassium, and water oxygens were refined. An attempt to assign hydrogen positions was made, however the result did not make chemical sense and these atoms were not included in the final refinement.

3.2.3. Selectivity and ion exchange kinetics

The rate of strontium uptake was measured under infinite solution volume conditions as specified by Helfferich.[39] Vigorous stirring was employed to ensure particle diffusion controlled kinetics. The rate of Sr^{2+} uptake was measured by tracing a 1.0 equivalent $SrCl_2$ solution with enough ^{90}Sr to yield a count rate of ~60,000 counts per minute. 0.2 grams of ion exchanger was added to 100 mL of this solution under vigorous stirring. 1.0 mL aliquots were taken at designated times and filtered through a Millipore 0.22 μm syringe filter tip. The solution was then shaken with 18 mL of scintillation cocktail and the amount of ^{90}Sr was measured by liquid scintillation counting on a Wallac 1410 liquid scintillation counter.

Mass diffusion coefficients for group II metals were measured using TitraLab TIM860 Titration Manager. To 50 mL of water, adjusted to a pH of 7.0, was added 0.10 grams of **1**. Particles were sieved before addition to achieve an average size of 150 μm. Once an equilibrium pH was achieved, a 62 μL spike containing 1.0 meq of M^{2+} was added and the change in pH over time was recorded.

Ion exchange selectivity series for alkaline earth metals was determined by shaking 0.1g of **1** and 1.0 meq of $M(NO_3)_2$ in 50 mL of deionized water adjusted to the desired pH for 24 hours. The uptake of each cation was measured by determining the concentration of K^+ and M^{2+} by atomic absorption. A suitable sample for AA was prepared by digesting approximately 5mg of the solid exchange phase in 2mL of concentrated HF at room temperature and diluting to 1.000L.

3.3. Results

3.3.1 Structure of $H_{1.45}K_{0.55}ZrSi_3O_9 \bullet 2H_2O$ (1)

Essential crystallographic data are shown in Table 3.1. The structure of **1** is similar to the umbite phase. Linear chains of polymeric silicate groups are linked by zirconium octahedra forming two unique ion exchange sites. These sites are best viewed in a ball and stick representation looking down the a-axis (Figure 3.2). Upon conversion to the acid phase, the unit cell volume decreases approximately 40 $Å^3$ and the space group changes from $P2_12_12_1$ to $P2_1/c$. This is unusual in that the transformation from a noncentrosymmetric space group to a Laue symmetry that contains an inversion center is not often observed.

Table 3.1. Crystallographic data for the zirconium trisilicate phases.[a]

	1	**2**	**3**
fw	378.81	437.87	443.08
space group	$P2_1/c$	$P2_1/c$	$P2_1/c$
a (Å)	7.1000(2)	7.1386(3)	7.1425(5)
b (Å)	10.1169(3)	10.2304(4)	10.2108(8)
c (Å)	13.1742(5)	13.1522(4)	13.0693(6)
β	91.181(1)°	90.222(1)°	90.283(1)°
V ($Å^3$)	946.09(5)	961.25(5)	952.20(17)
Z	4	4	4
D_{calc} (g/cm^3)	2.618	3.003	3.060
No. of reflections	1406	1247	866
R_{wp}	0.0905	0.0789	0.0710
R_p	0.0672	0.0671	0.0543

[a] Formulas: (**1**) $K_{0.56}H_{1.44}ZrSi_3O_9 \bullet 2H_2O$; (**2**) $K_{0.34}Sr_{0.83}ZrSi_3O_9 \bullet 1.8H_2O$; (**3**)$SrZrSi_3O_9 \bullet 2H_2O$

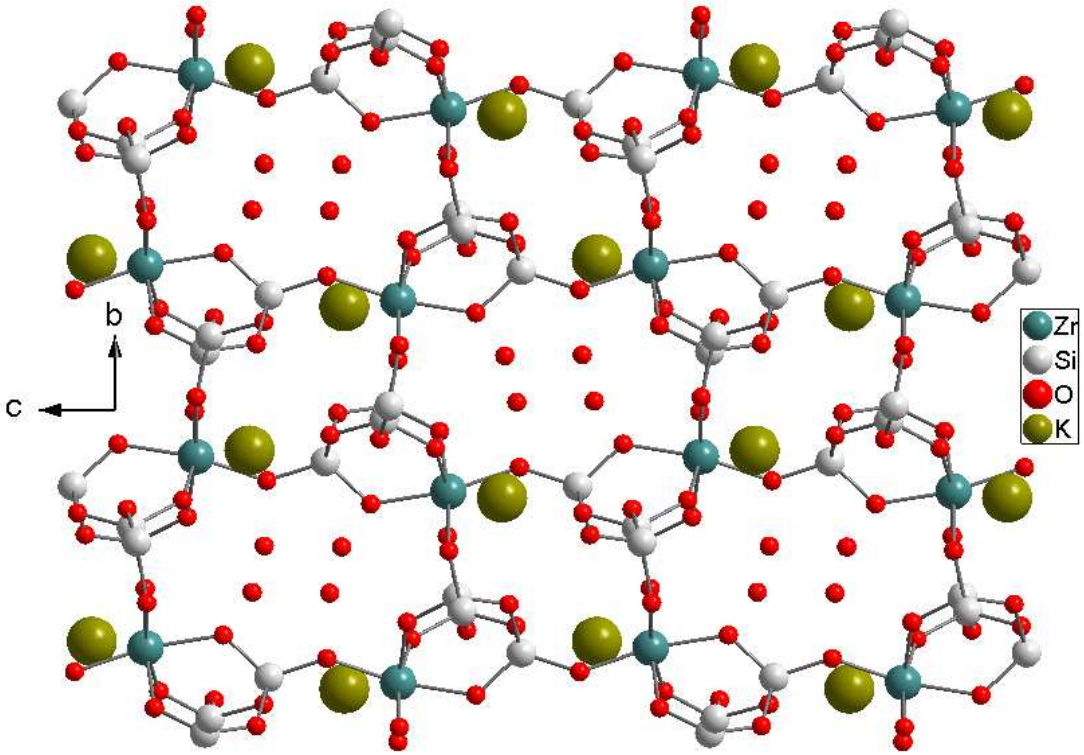

Figure 3.2. Exchange sites 1 in the large ring and 2 containing the K^+ ions as found in $H_{1.45}K_{0.55}ZrSi_3O_9 \bullet 2H_2O$ View is down the *a*-axis.

Positional parameters for **1** are shown in Table 3.2 and selected framework bond distances for all compounds are shown in Table 3.3. Besides the change in space group, the most obvious structural difference between the parent compound, $K_2ZrSi_3O_9 \bullet H_2O$, and compound **1** is the addition of 1 mole of water. The hydrogen bonding of water in Site 2 to framework oxygens was shown by Zou and Dadachov in single crystal x-ray diffraction studies of the potassium titanium trisilicate.[16] In this case a second water resides in Site 2 which was previously occupied by K^+. Selected O-O distances between water molecules and framework oxygens, listed in Table 3.4, suggest the presence of hydrogen bonding between waters in the cavity as most of the distances are approximately 2.8 Å.

Table 3.2. Positional and thermal parameters for $K_{0.56}H_{1.44}ZrSi_3O_9 \bullet 2H_2O$.

	x	**y**	**z**	$\mathbf{U_{iso}}$ [a]
Zr1	0.2589(6)	0.70456(28)	0.20017(26)	0.0380(5)
Si2	0.0112(8)	0.4282(5)	0.1826(4)	0.008
Si3	0.7352(9)	0.2820(5)	0.0557(4)	0.008
Si4	0.5778(8)	0.8903(6)	0.3276(4)	0.008
O5	0.2308(19)	0.6715(7)	0.3541(5)	0.004
O6	0.0390(15)	0.5871(6)	0.2025(10)	0.004
O7	0.2226(20)	0.7674(10)	0.0596(5)	0.004
O8	0.4794(13)	0.8180(8)	0.2264(6)	0.004
O9	0.0960(14)	0.8620(8)	0.2179(6)	0.004
O10	0.4325(17)	0.5491(6)	0.1996(9)	0.004
O11	0.2030(7)	0.3415(8)	0.1637(8)	0.004
O12	0.5247(9)	0.3521(9)	0.0658(5)	0.004
O13	0.878(1)	0.4091(7)	0.0804(5)	0.004
Ow1	-0.0992(24)	0.5592(24)	0.4116(12)	0.155(14)
K15[b]	0.7521(19)	0.6878(10)	0.0938(8)	0.0115(32)
Ow2	0.6344(14)	0.5617(11)	0.5648(8)	0.092(11)

Table 3.3. Selected framework bond distances (Å) for compounds **1-3**.

Bond	1	2	3
Zr1—O5	2.069(8)	2.118(7)	2.116(9)
Zr1—O6	1.963(10)	1.976(10)	2.104(13)
Zr1—O7	1.970(8)	2.075(8)	2.009(9)
Zr1—O8	1.966(10)	2.024(11)	1.977(12)
Zr1—O9	1.985(9)	2.035(10)	2.010(12)
Zr1—O10	1.998(9)	2.067(10)	2.064(13)
Si2—O6	1.640(8)	1.644(9)	1.642(10)
Si2—O9	1.67(1)	1.659(11)	1.649(12)
Si2—O11	1.643(8)	1.651(9)	1.645(9)
Si2—O13	1.641(9)	1.649(10)	1.630(11)
Si3—O5	1.646(9)	1.646(9)	1.646(10)
Si3—O7	1.613(13)	1.663(15)	1.662(17)
Si3—O12	1.662(9)	1.662(10)	1.666(11)
Si3—O13	1.665(9)	1.67(1)	1.662(11)
Si4—O8	1.662(10)	1.658(11)	1.630(12)
Si4—O10	1.647(9)	1.635(9)	1.627(11)
Si4—O11	1.635(8)	1.638(8)	1.637(10)
Si4—O12	1.641(9)	1.65(1)	1.618(11)

[a] $U_{iso} = B_{iso} / 8\pi^2$

[b] Occupancy factor = 0.55

Table 3.5 shows selected cation-oxygen distances of less than 3.6 Å for compounds **1-3**. The coordination environment of the remaining K^+ ion in Site 1 is similar to the parent compound. Potassium cations are 10-coordinate with an average M15-O distance of 3.105(2) Å and have close contacts with O6 and Ow2 of 2.666(16) Å and 2.694(15) Å, respectively. For 10-coordinate potassium ion, the sum of ionic radii

between K^+ and O^{2-} water oxygen can be considered approximately 2.94 Å.[44] There are 4 additional contacts (M15-O8, M15-O10, M15-O12, and M15-O13) within 0.2 Å of this value, hinting that the potassium in this channel is still held tightly.

Table 3.4. Selected O-O distances for $K_{0.56}H_{1.44}ZrSi_3O_9 \cdot 2H_2O$ indicate the presence of hydrogen bonding

Water Oxygen Pair	Distance (Å)
Ow1-Ow2	2.794(21)
Ow2-Ow2′	2.825(16)
Ow1-O9	2.625(33)
Ow2-O8	2.706(14)
Ow1-Ow1′	2.951(26)

3.3.2. Structure of $K_{0.34}Sr_{0.83}ZrSi_3O_9 \cdot 1.8H_2O$ (2)

The incorporation of Sr^{2+} has some interesting consequences; however the space group of the protonic phase and basic structure of the zirconium trisilicate is conserved. The unit cell increases only slightly ~15 $Å^3$ to allow for the exchange of the larger strontium cation for the proton. Analysis of site occupancy shows that Sr^{2+} is almost evenly distributed among Sites 1 and 2, 0.42 and 0.41, respectively. Structural refinement of cation occupancy also shows movement of the K^+, which formerly occupied only exchange Site 1, into Site 2. K^+ occupancy factors for Sites 1 and 2 are 0.20 and 0.14, respectively. The arrangement of the water molecules has shifted within the framework. Ow2 and Ow3 are found in both cation Sites 1 and 2 but unevenly due to the cation distribution. Ow1 remains in its original position and is assigned an occupancy factor of 1.

Table 3.5. Cation-oxygen bonds (Å) for protonated and strontium zirconium trisilicate.

Compound	M14-O	Distance (Å)	M15-O	Distance (Å)
(1)$K_{0.56}H_{1.44}ZrSi_3O_9 \cdot 2H_2O$			K15—O6	2.666(16)
			K15—O7	3.474(19)
			K15—O8	2.946(15)
			K15—O9	3.407(15)
			K15—O10	3.033(16)
			K15—O11	3.560(15)
			K15—O11′	3.428(15)
			K15—O12	2.879(14)
			K15—O13	2.964(13)
			K15—Ow2	2.694(15)
(2)$K_{0.35}Sr_{0.825}ZrSi_3O_9 \cdot H_2O$	M14—O5	2.650(12)	M15—O6	2.767(18)
	M14—O7	3.242(13)	M15—O8	3.049(16)
	M14—O7′	3.204(19)	M15—O9	3.417(16)
	M14—O9	2.950(12)	M15—O10	2.841(18)
	M14—Ow1	2.701(18)	M15—O11	3.577(12)
	M14—Ow1′	3.492(20)	M15—O11′	3.408(12)
			M15—O12	3.090(15)
			M15—O13	3.190(12)
			M15—O13′	3.246(16)
(3)$SrZrSi_3O_9 \cdot H_2O$	Sr14—O5	2.607(16)	Sr15—O6	2.799(30)
	Sr14—O6	3.383(19)	Sr15—O8	3.026(26)
	Sr14—O7	3.176(22)	Sr15—O9	3.286(24)
	Sr14—O9	2.667(17)	Sr15—O10	2.579(27)
	Sr14—Ow1	2.896(18)	Sr15—O12	3.187(23)
			Sr15—O13	3.311(25)
			Sr15—O13′	3.278(20)

The coordination sphere of the cations in sites 1 and 2 are quite different. Cations in Site 1 can be said to be 9-coordiante having average contact distance of 3.176(15) Å with the shortest and longest distances being M15-O6 and M15-O11 at 2.767(18) Å and 3.577(12) Å, respectively. Cations located in Site 2 are 6-coordinate and have a much shorter average contact distance of 3.04(1) Å. This is due to the closer contacts of M14-O5 and M14-Ow1 which are 2.650(12) Å and 2.701(18) Å, respectively.

3.3.3. Structure of $SrZrSi_3O_9 \bullet 2H_2O$ (3)

The fully substituted strontium trisilicate crystallizes in the monoclinic space group $P2_1/c$. The unit cell has decreased in size by 10 $Å^3$ in comparison to compound **2**. Two moles of water are present, one in the larger cavity, and the other split among the ion exchange sites. Strontium is found in both ion exchange sites. The occupancy factors for Sites 1 and 2 are 0.535 and 0.465, respectively.

Strontium cations in Site 1 are more tightly held as the ion exchange site creates a basket or bowl shape to cradle the cation. Sr^{2+} in Site 1 is 7-coordinate with its shortest and longest contacts being Sr15-O10 and Sr15-O13′ which are 2.579(28) Å and 3.278(20) Å, respectively.

Strontium cations in Site 2 are coordinated by only 5 oxygens, four oxygens from the framework and one water molecule. The Sr14-Ow1 distance is longer than predicted being 2.896(18) Å. The closest contact is Sr14-O5 which is 2.607(16) Å. If we consider the ionic radius of Sr^{2+} 6-coordinate as 1.18 Å, then the sum of ionic radii in a Sr-O bond should be approximately 2.6 Å. The Sr14-O9 bond length is 2.667(17) Å and the O5-Sr14-O9 bond angle is 102.6(5)°. A bond angle of 90.3(6)° is observed for O5-Sr14-Ow1.

3.3.4. Selectivity and kinetics of M^{2+} cation exchange and ^{90}Sr uptake

The selectivity of alkali cations in zirconium trisilicate has been probed over the entire pH range. In acidic media the selectivity series is $Rb^+ > Cs^+ > K^+ > Na^+ > Li^+$. In basic media the selectivity series still favors Rb^+ with little difference in uptake of other alkali metals.[15] Uptake of alkaline earth cations for compound **1** is shown in Figure 3.3. There is no selectivity for alkaline earth cations in acidic media. Beyond pH 6 however, the selectivity series is defined as $Ba^{2+} > Sr^{2+} > Ca^{2+} > Mg^{2+}$.

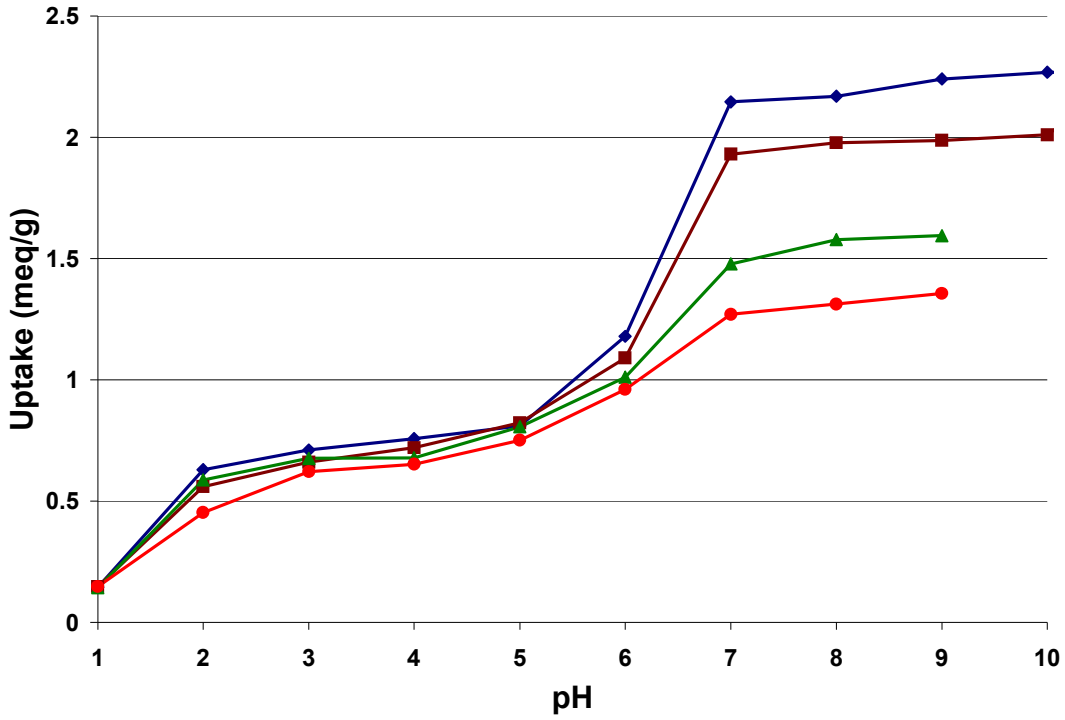

Figure 3.3. Room temperature, pH dependent uptake of alkaline earth cations in $H_{1.45}K_{0.55}ZrSi_3O_9 \bullet 2H_2O$.

Mass diffusion coefficients are listed in Table 3.6. Values were calculated by fitting the fractional attainment of equilibrium over time, U(t), to Vermuelen's approximation, Eqn. 2.

$$\mathrm{U}(t) = \left[1 - \exp\left(-\frac{D_i t \pi^2}{r_o^{\,2}}\right)\right]^{1/2} \qquad [6]$$

D_i is the mass diffusion coefficient, r_o is the average particle radius, in this case 150 μm, and t is time.

Table 3.6. Mass diffusion coefficients for the uptake of M^{2+} by compound **1**.

Cation	Diffusion Coefficient, D ($\mu m^2 \cdot s^{-1}$)	Vermeulen Regression Statistics (R^2, χ^2/DoF)
Mg^{2+}	0.091	0.990, 0.00069
Ca^{2+}	0.205	0.986, 0.00077
Sr^{2+}	0.479	0.991, 0.00075
Ba^{2+}	0.183	0.987, 0.00077

The rate of uptake does not mimic the pattern observed in the selectivity. The absorption of Sr^{2+} by compound **1** is fastest with a mass diffusion coefficient of 0.479 $\mu m^2 \cdot s^{-1}$. The kinetics of uptake for Ba^{2+} and Ca^{2+} are similarly fast, having mass diffusion coefficients of 0.183 and 0.205 $\mu m^2 \cdot s^{-1}$, respectively, while Mg^{2+} shows the slowest uptake. Plots of the experimental and calculated data demonstrating their agreement are shown in Figure 3.4.

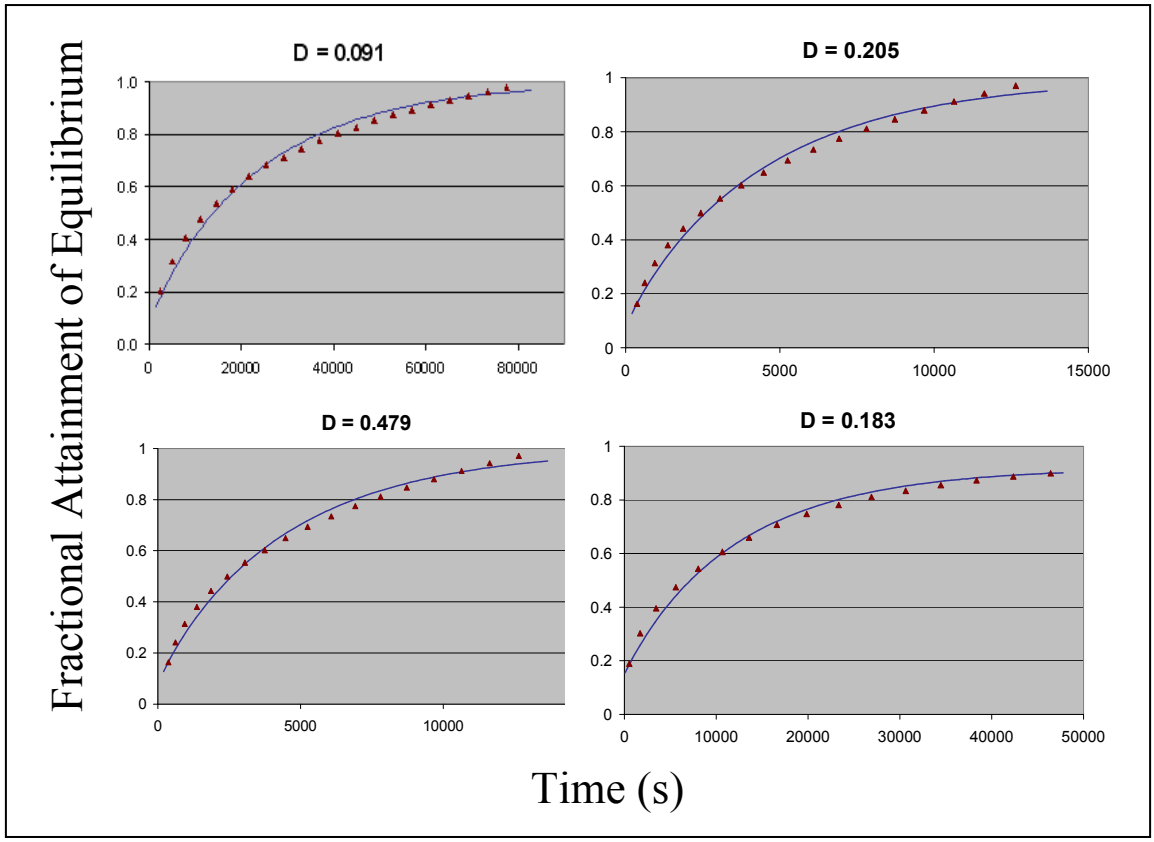

Figure 3.4. Kinetic data for the uptake of alkaline earth metals in $H_{1.45}K_{0.55}ZrSi_3O_9 \bullet 2H_2O$ at neutral pH. Plots fitting Vermeulen's approximation to observed changes in fractional attainment of equilibrium over time. Triangles represent observed data and the solid line represents the Vermeulen model. Mass diffusion coefficients are in units of $\mu m^2 \cdot s^{-1}$.

The kinetic data derived from radio tracer experiments with ^{90}Sr do not support the data found by measuring the change in pH over time. A separate plot of and fit of U versus time is shown in Figure 3.5. The mass diffusion coefficient found for the uptake of ^{90}Sr is 197.2 $\mu m^2 \cdot s^{-1}$. The reason for this disparity is two fold. First, in measuring the change in pH over time, the physical phenomenon being observed is the increase in $[H^+]$ as Sr^{2+} is exchanged in. This method does not include the direct exchange of Sr^{2+} for K^+. Another process that occurs is K^+H^+ exchange. This process is observed simultaneously and has the effect of slowing down the shift to lower pH as the protons liberated by the influx of Sr^{2+} are taken back up and exchanged for K^+. When conducting the radio strontium experiments, the only physical observation is the disappearance of ^{90}Sr over time. In this case, the rate does not depend on the process or mechanism of uptake, only that some of the strontium that was once in solution is now exchanged.

The second and unfortunately inescapable challenge in kinetic studies in this system, is the fact that the starting phase and final phases are not pure, i.e. they contain many different cations, such as K^+, Sr^{2+}, H^+, etc. The reaction is not a simple complete A for B exchange. This contributes to the complications when attempting to describe the mechanism of exchange also, and requires equations with fewer and less descriptive parameters to be utilized.

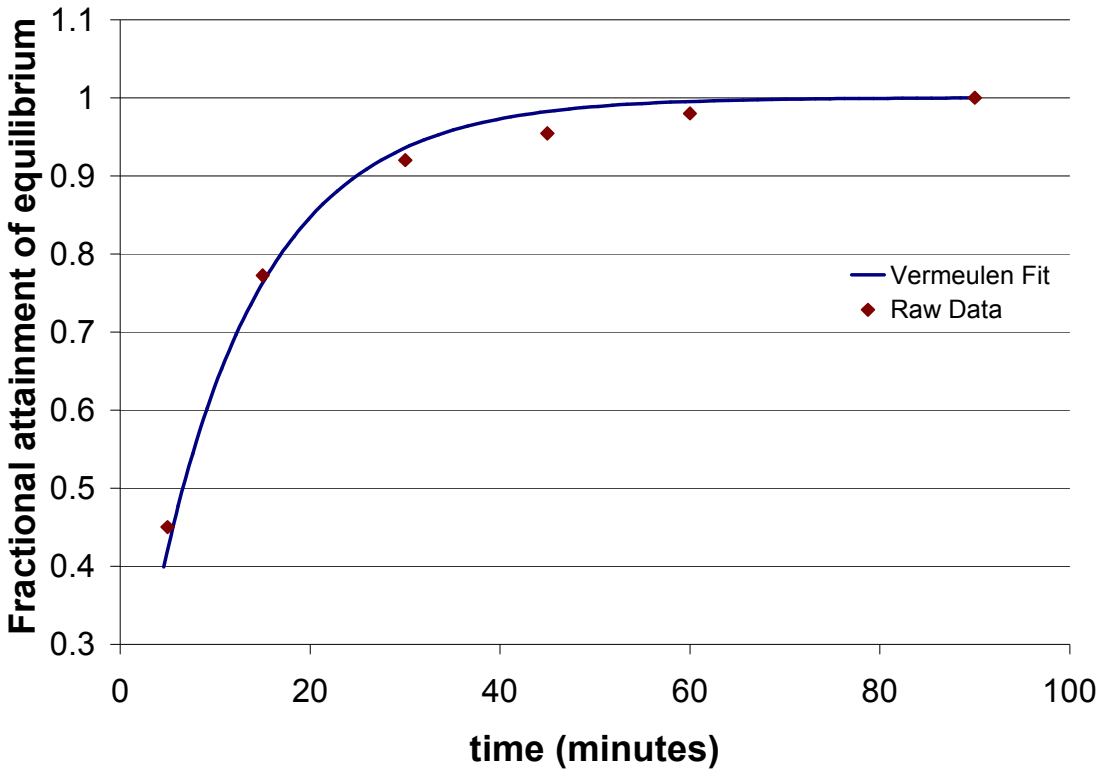

Figure 3.5. Uptake of ^{90}Sr in $H_{1.45}K_{0.55}ZrSi_3O_9 \bullet 2H_2O$ at neutral pH expressed as the fractional attainment of equilibrium over time.

3.3.5. TGA

Thermogravimetric analysis of compound **1** (Figure 3.6) showed a total weight loss of 13.3% at 850°C. The weight loss before 50°C (1.7%) was attributed to surface water. The residue collected after performing TGA was shown to be amorphous. It was then assumed that the final product had the following composition: $K_{0.56}O_{0.28}$: ZrO_2: $3SiO_2$. The calculated total weight loss of interstitial water (9.5%) plus the splitting off of water from protons and silicate oxygens (3.4%) sums to 12.9%.

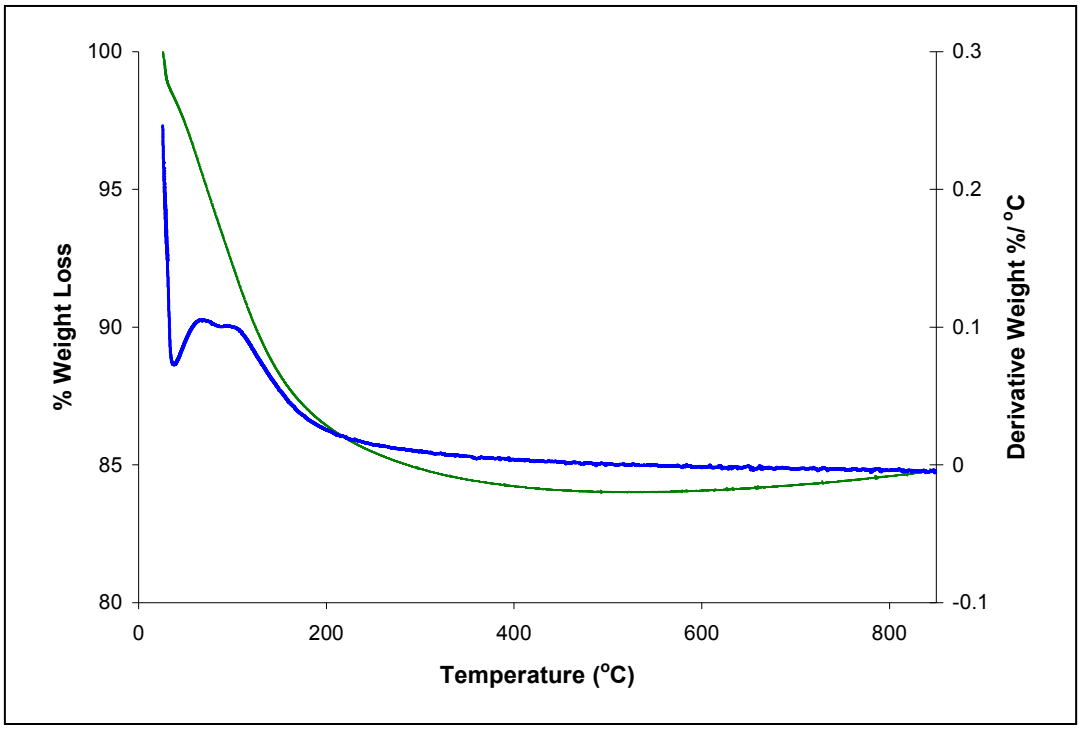

Figure 3.6. Thermal gravimetric curves of compound **1**. The green line represents % weight loss as a function of temperature. The blue line is the differential weight loss. Taking into account 1.7% weight loss due to surface water, an internal water loss of 9.8% was noticed which accounts for 2 moles of water per mole of ion exchanger found in structural refinement.

3.4. Discussion

Previously, Clearfield and coworkers have synthesized and characterized the behavior of $K_2TiSi_3O_9 \bullet H_2O$ and its protonated phases.[15] The conversion from a non-centrosymmetric orthorhombic space group to a monoclinic phase containing a crystallographic inversion center was observed upon conversion of the parent compound to the acid phase. In the zirconium system, the same transformation occurs. The phase change is not unusual and has been documented. Rocha and coworkers have hydrothermally synthesized $Na_{0.2}K_{1.8}ZrSi_3O_9 \bullet H_2O$ which crystallizes in the space group $P2_1/c$.[26] In 2001, Rocha and coworkers also synthesized a sodium tin trisilicate, AV-10 crystallizing in the space group $C222_1$.[25]

Liu and Thomas have also reported the titanium analogue of the mixed sodium potassium trisilicate, UND-1, which crystallizes in the space group $P2_1/c$ and was assigned the formula $Na_{2.7}K_{5.3}Ti_4Si_{12}O_{36} \bullet 4H_2O$.[50] In addition to the phase change, other structural similarities exist between the titanium and zirconium protonated phases. Both phases maintain the same ion exchange cavity structure upon conversion to the acid phase. The monoclinic angle is only slightly larger than 90° in both phases (91.181(1)° in the zirconium phase and 91.447(1)° in the titanium phase). Although the framework building blocks of UND-1, AV-7, and AV-10 are different, their pore structures are closely related, and the ion exchange sites are almost identical. The monoclinic angle in the ion exchange phases is much smaller than the angles reported by Rocha and Liu in their above mentioned work. The space group of UND-1 and Rocha's AV-7 are the same, $P2_1/c$, and their beta angles are 104.366(9)° and 105.0401(8)°, respectively.[25,50] The change in space group upon conversion is unclear but it is not due to any extreme changes in framework linkage that may convert it to an umbite polymorph such as kostylevite. Unpublished data from in situ x-ray diffraction studies point to small shifts in silicon positions and disorder in the cation positions as the cause of the phase change. These shifts destroy the center of symmetry in the $P2_1/c$ space group and must ultimately change the beta angle to 90 once more, reinstituting the orthorhombic phase.

Examination of the pure potassium titanium phase suggested a center of inversion in the orthorhombic cell at 0.25, 0, 0.007. Thus, a small change in atomic positions in the orthorhombic parent compound can generate a center of symmetry creating a monoclinic space group. For the potassium zirconium phase the suggested center of symmetry for the titanium phase fits well and duplicates many atoms in the framework, translating them from x, y, z to –x, -y, -z. This center of symmetry resides in the middle of Site 1 when viewed from the *c*-axis and, neither the cations nor the waters in Site 2 fit to the inversion center as they do not have a mirror image.

The special positions given for the space group $P2_1/c$ in the international tables of crystallography were transformed into positions in $P2_12_12_1$ by using the transformation matrix in Eqn. 1. This did not reproduce the inversion center described by Bortun *et al*. but does fit, although poorly, an inversion center to the waters and cations in Site 2. Because no inversion center can be fit to the cations in Site 2 in the orthorhombic space group that satisfies a point of pseudo symmetry for all atoms in the unit cell, the movement of cations to or from the exchange site likely has no influence on the change in crystal system. The position and occupancy of cations in Site 1 is what determines the space group. The change in framework parameters such as bond lengths and bond angles is subtle and not likely to be entirely responsible for the drop in symmetry.

There are however differences between the titanium acid phase and the zirconium acid phase trisilicates. There are 2 molecules of water in the protonated zirconium trisilicate rather than the 1.8 found in the previously studied titanium analog of similar substitution.[15] In the zirconium phase, these waters are located entirely in Site 2 with the remaining potassium found in Site 1. This is in contrast to the titanium phase which maintains some potassium in Site 1. The disparity demonstrates how the smaller unit cell and therefore the smaller ion exchange cavities in the titanium phase hold the potassium more tightly. The unit cell volumes respond oppositely upon conversion to the acid phase. The cell volume increases ~20 $Å^3$ in the titanium phase, while the corresponding change in the zirconium phase is a decrease of almost 40 $Å^3$. Both

changes demonstrate the flexibility of the breathable framework and its desire to accommodate a smaller or larger guest cation. Further exemplifying this flexibility is the increase in cell volume, upon 75% incorporation of Cs^+ into $K_2ZrSi_3O_9 \cdot H_2O$ the cell volume increases by approximately 70 $Å^3$.

The selectivity series among alkaline earth metals in acidic to neutral pH was shown to be $Ba^{2+} > Sr^{2+} > Ca^{2+} > Mg^{2+}$. According to Eisenman, this type I selectivity behavior is indicative of a system in which the anionic sites are of low field strength.[51] This is true of the trisilicate system where each framework oxygen may be considered to hold a 2/9 e^- charge. For alkali cations, the selectivity of an ion exchanger for two cations in solution depends only on the differences between their free energy of hydration and the energy of binding to the exchange site. The Gibbs free energy of hydration for alkaline earth cations from Ba^{2+} to Mg^{2+} is -1250, -1380, -1505, -1830 $kJ \cdot mol^{-1}$.[52] The energy of binding the cation in the exchange site is unknown. For the titanium trisilicate system Bortun et al. concluded that the free energy of hydration was too large a barrier to overcome and is not compensated for by the free energy change when the cation comes to rest in the exchange site.[15] Because the pores are larger in **1** than in the protonic titanium trisilicate, a more favorable free energy of binding inside the exchanger is possible.

The rates of exchange do not correlate precisely with the selectivity data. Though Ba^{2+} is the most favored cation, the Sr^{2+} cation shows the highest diffusion coefficient. It is important to note that the rates of exchange are defined as mass diffusion, meaning they express the diffusion of all three species involved in the exchange, H^+, K^+, and M^{2+}.

The affinity of the titanium phase for alkaline earth cations is poor and almost no difference in uptake is observed for Ca^{2+}, Sr^{2+}, and Ba^{2+} and there is only a slight improvement in the equilibrium uptake of group II cations for the zirconium phase. Size discrimination should be the deciding difference in the ability to selectively exchange cations but an important change arises when moving from group I to group II cations. The enthalpy of hydration for 2+ cations is at least four times greater than that of a 1+

cation. The change in entropy is however in the reactions favor when exchanging a 1+ cation for a 2+.

From a strictly thermodynamic view, it is obvious that the energy of the product must be lower than the energy of the starting material; however the calculation of a Gibbs energy is not so straight forward concerning ion exchange reactions, especially if a phase change occurs. ΔG can also be an integral value dependent on the level of exchange over time. In their work with alpha zirconium phosphate Clearfield and coworkers also demonstrated that the thermodynamics of exchange were correlated with the extent of hydration.[53] It has been shown however that the entropy term dominates in the Gibbs free energy equation for a variety of ion exchange reactions but are dependent on such factors as the outgoing cation.[54-57] The family of trisilicates would likely show the same trends in entropic driving force, but the question of whether the kinetic data will correlate strongly with thermodynamic data is still unknown.

3.5. Conclusions

A partially protonated phase of zirconium trisilicate has been synthesized by ion exchange and the incorporation of alkaline earth cations has been studied using this new material. Compound **1** is structurally similar to the titanium acid phase and shows the same phase transformation from an orthorhombic to a monoclinic crystal system as the previously studied titanium trisilicate upon conversion to the acid phase.

Two strontium ion exchange phases were derived from the acid phase. Compound **2** is a partially substituted phase in which the strontium cations show no preference for exchange Site 1 or Site 2. The completely strontium substituted compound **3** shows slight preference for strontium in exchange Site 2. Compounds **2** and **3** maintain the monoclinic space group of the parent compound.

The selectivity of **1** for alkaline earth cations follows the order $Ba^{2+} > Sr^{2+} > Ca^{2+} > Mg^{2+}$. The kinetics of exchange does not mimic this pattern as strontium shows the fastest mass diffusion coefficient.

CHAPTER IV
LANTHANIDE ION EXCHANGE IN METAL TRISILICATES

4.1. Introduction

The variety of applications among *f*-block elements makes them a desirable area in which to expand a field of study. Lanthanide chemistry specifically has been extensively investigated and applied in many areas of research. The luminescent properties of many complexes can be tuned simply by changing the Ln^{3+} cation. Silicates and other framework compounds have been used has hosts for lanthanide cations for use as phosphors and other optical devices.[58-67] As good Lewis acids, the rare earths have also contributed to areas of catalysis.[68-72] In the medical arena, the development of gadolinium complexes has revolutionized the field of magnetic imaging.[73] Because of their similar chemistry, however, one problem that still vexes the research community is their efficient separation in complex mixtures, specifically from fission products.

Because the nucleus of an atom splits asymmetrically when it undergoes fission, the yield of daughter nuclei is also asymmetric. A plot of percent yield versus isotopic mass shows that there are peaks and valleys across the periodic table. One of these peaks corresponds to many rare earth isotopes. The literature demonstrates that for years lanthanide fission products have been separated from their actinide counterparts by either a solvent extraction processes such as PUREX combined with a variety of complexing agents or on ubiquitous organic resins such as Dowex or Amberlite.[74-77] The selectivity of these processes has been largely based on the strong Lewis acid character of the lanthanides and the small, but exploitable, covalent character of the actinides which interact more strongly with soft-donor ligands. Separation of rare earths from other rare earths can be accomplished by through acid base chemistry, precipitating hydroxides. This however only achieves separation of the heavier lanthanides from the lighter.

The separations that have been achieved to date are a product of utilizing the small differences in the chemistry of the lanthanides. While the solution chemistry of trivalent rare earths may be similar, their size diminishes across the periodic table with the ionic radii of six coordinate La^{3+} and Lu^{3+} being 1.032 Å and 0.861 Å, respectively.[44] The pores in typical 8% cross-linked resins are approximately 50 Å and cannot take advantage of size discrimination.

This chapter will focus on confirming the size discrimination ability of the trisilicates. Using all classes of trisilicates with isostructural framework substitutions, it is shown that the unit cell dimensions and ergo, the pore size, directly determines which trisilicate is best for sorbing rare earth cations. The complete substitution of Gd^{3+} into $K_2SnSi_3O_9 \bullet H_2O$ has also been achieved via ion exchange and the crystal structure is discussed in detail.

4.2. Experimental methods

4.2.1. Analytical procedures and instrumentation

Phase identification and structural data sets were collected using a Bruker-AXS D8 VARIO powder diffractometer. Thermal gravimetric analysis was conducted on a TA Instruments TGA Q 500 unit. A constant temperature ramp of 5 ^{o}C/min was applied while the sample was under 9:1 nitrogen to air volume ratio. Potassium analysis was performed on a Varian AA 250 atomic absorption spectrometer under an acetylene nitrous oxide flame. Samples for AA analysis were prepared by digestion of the solid in hydrofluoric acid. Titrations and pH measurements were conducted on a TitraLab TIM860 Titration Manager.

4.2.2. Synthesis and ion exchange

Potassium zirconium trisilicate, $K_2ZrSi_3O_9 \cdot H_2O$, was synthesized hydrothermally by modification of methods previously reported by Poojary et al.[31] 7.0 grams of silicic acid was dissolved in 45 mL of 4M KOH and 10 mL of isopropanol. 13.5 mL of a 70% solution of zirconium isopropoxide in isopropanol was diluted with 10 mL of isopropanol and added drop wise to the previous solution. The mixture was divided in two and placed in 100 mL Teflon lined autoclaves. The reaction was carried out at 180°C. After 5 days a white precipitate was isolated and washed with distilled water and dried at 60°C.

Potassium titanium trisilicate, $K_2TiSi_3O_9 \cdot H_2O$, was synthesized according to previously reported methods.[15] 30 mL of a $TiCl_4$ solution, 40 mL of a 30% H_2O_2, 150 mL of distilled water, and 40 mL of a 10 M KOH were combined quickly and with stirring. In a separate container, 12.6 g of SiO_2 dissolved in 200 mL of a 3 M KOH. The two solutions were combined in a 1.0L Teflon lined autoclave and heated at 180°C for 7 days.

Potassium tin trisilicate, $K_2SnSi_3O_9 \cdot H_2O$, was synthesized using a method published by Pertierra et al.[28] 7.2 g of SiO_2 were dissolved in 35 mL of 7M KOH. To this mixture was added drop wise 3.5mL of $SnCl_4$ with stirring. This mixture was sealed in a 100mL Teflon lined autoclave and heated at 190°C for 12 days.

Potassium zirconium trigermanate, $K_2ZrGe_3O_9 \cdot H_2O$, was synthesized by modification of a method published by Yaghi and coworkers.[14] 10.0g of GeO_2 was dissolved in 40 mL of 10M KOH. 13.5 mL of a 70% solution of zirconium isopropoxide in isopropanol was diluted with 10 mL of isopropanol and added drop wise to the previous solution. This mixture was sealed in a Teflon lined autoclave and heated at 200°C for 5 days.

To determine which trisilicate is most selective for gadolinium, 0.05g of exchanger was placed in a 50mL solution of $Gd(NO_3)_3$ with a concentration of 1.0 meq.

After shaking for 5 days, the exchanger was filtered and the solid and supernatant liquid was tested for potassium content by atomic absorption.

Ion exchange selectivity series for rare earth metals was determined by shaking 0.1g of $K_2SnSi_3O_9 \cdot H_2O$ and 1.0 equivalents of Ln^{3+} in 50 mL of deionized water adjusted to the desired pH for 3 days. The uptake of each cation was determined by digesting the recovered exchanger in HF and determining the concentration of K^+ by atomic absorption. The amount of K^+ in the supernatant liquid was determined by AA and added to that found in the solid to determine the total amount of K^+ displaced my the lanthanide cation. Hydrolysis rates were determined by placing 0.05 grams of exchanger in 50mL of deionized water and measuring the pH over time.

4.2.3. Synthesis of compound **1**, $Gd_{0.66}SnSi_3O_9 \cdot H_2O$

$Gd_{0.66}SnSi_3O_9 \cdot H_2O$ was synthesized by exhaustive ion exchange with Gd^{3+}. 1.0g of $K_2SnSi_3O_9 \cdot H_2O$ was added to 100mL of a 0.1M solution of gadolinium chloride. The mixture was shaken for 24 hours and the supernatant liquid was decanted, saved for K^+ analysis, and a fresh solution of Gd^{3+} was added to the wet powder. This process was continued until no K^+ was detectable in the supernatant liquid or in the solid exchanger.

4.2.3. X-ray data collection and structure refinement

Data sets were collected on a Bruker-AXS D8 VARIO powder diffractometer with standard vertical Bragg-Brentano geometry and a linear PSD detector. The diffractometer was equipped with a Germanium monochromator allowing the use of Cu $K\alpha_1$ radiation only with a wavelength of 1.54056 Å. Powders were loaded on a quartz disc which was spun during data collection to partially reduce scattering effects due to preferred orientation. Operating voltage and current were 40kV and 50mA respectively. Data were collected at room temperature with 2θ ranging from 5 to 130 degrees. A step size of 0.016 degrees and a scan time of 15 seconds per step were employed.

Powder patterns were indexed using TREOR, ITO, and DICVOL methods found in the FullProf program suite.[47-49] Profile function fitting using the LeBail method and Reitveld refinement were accomplished using the GSAS program suite.[37,38] No corrections were made for absorption and neutral atom scattering factors were used as stored in GSAS. No attempt was made to model preferred orientation.

For compound **1,** 1004 independent reflections were found in the 2θ range of 10 to 90°. Final refinement statistics show an R_{wp} of 0.0905 and an R_p of 0.0737. Systematic absences were consistent with the orthorhombic space group $P2_12_12_1$. Compound **1** displays unit cell dimensions of a = 10.1274(5) Å, b = 13.1319(5) Å, and c = 7.1775(3) Å. The final refinement difference plot is shown in Figure 4.1. Crystallographic data are given in Table 4.1 and atomic coordinates and isotropic thermal factors for **1** are summarized in Table 4.2.

Table 4.1. Crystallographic data for compound **1**.

	Compound 1, $Gd_{0.66}SnSi_3O_9 \cdot H_2O$
fw	469.77
space group	$P2_12_12_1$
a (Å)	10.1274(5)
b (Å)	13.1319(5)
c (Å)	7.1775(3)
V (Å^3)	954.55(7)
Z	4
D_{calc} (g/cm^3)	3.255
No. of reflections	1006
R_{wp}	0.0905
R_p	0.0735

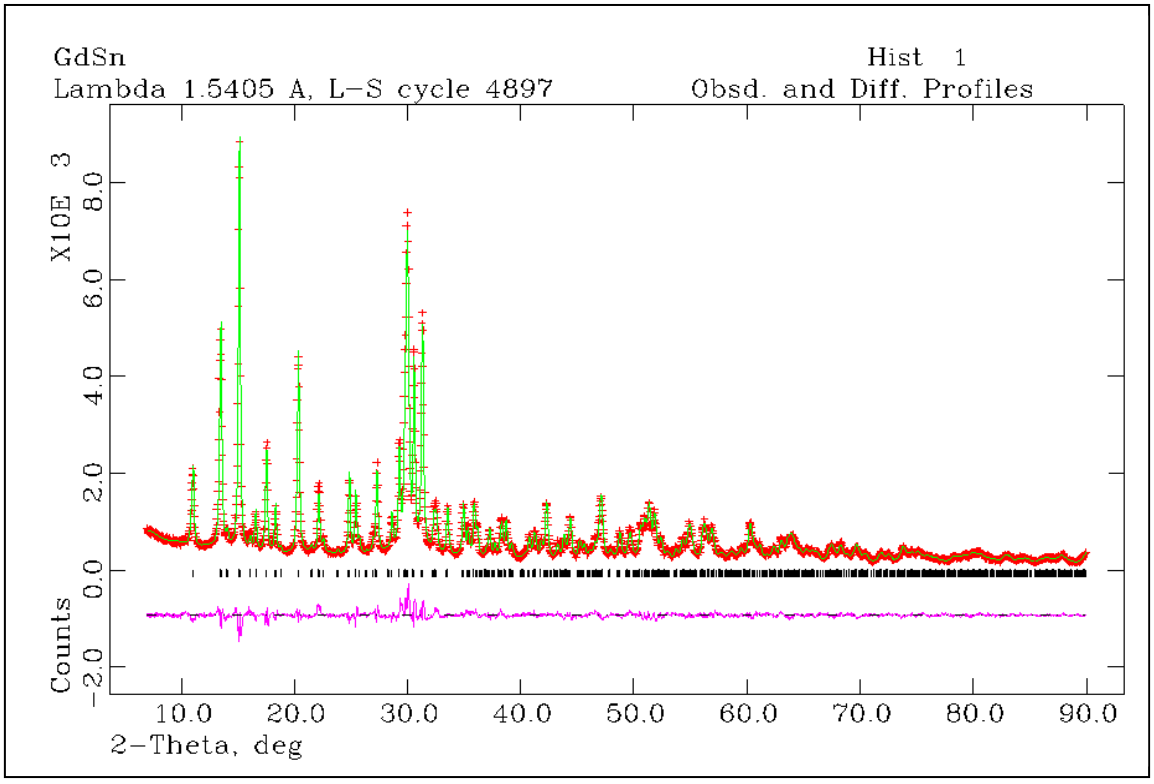

Figure 4.1. Observed (+) and calculated (-) profiles for final Reitveld refinement of $Gd_{0.667}SnSi_3O_9 \bullet H_2O$. Difference plot is shown in the bottom as the pink line. Individual reflections are marked by the black bars.

Table 4.2. Positional and thermal parameters for $Gd_{0.667}SnSi_3O_9 \bullet H_2O$.

	x	y	z	U_{iso} [a]
Sn1	0.45142(28)	0.21094(20)	0.2572(6)	0.0322
Si2	0.1793(5)	0.1791(4)	0.0090(8)	0.008
Si3	0.0394(5)	0.0525(4)	0.7243(8)	0.008
Si4	0.6507(5)	0.3283(4)	0.5734(8)	0.008
O5	0.4153(7)	0.3653(5)	0.2364(21)	0.004
O6	0.3418(5)	0.1912(13)	0.0242(16)	0.004
O7	0.5131(10)	0.0666(4)	0.2502(35)	0.004
O8	0.5755(8)	0.2276(5)	0.4806(12)	0.004
O9	0.6118(7)	0.2190(6)	0.0934(13)	0.004
O10	0.3132(5)	0.1798(11)	0.4465(16)	0.004
O11	0.1029(8)	0.1552(8)	0.2090(6)	0.004
O12	0.0928(9)	0.0608(5)	0.5044(8)	0.004
O13	0.1668(7)	0.0792(6)	0.8679(9)	0.004
Ow1	0.1898(22)	0.4426(16)	0.1381(32)	0.015
Gd1[b]	0.1973(10)	0.6305(6)	0.1635(14)	0.0617
Gd2[c]	0.4455(9)	0.0780(6)	0.7106(14)	0.0562

[a] $U_{iso} = B_{iso} / 8\pi^2$

[b] Occupancy factor = 0.333

[c] Occupancy factor = 0.367

4.3. Results

4.3.1. Selectivity of trisilicates for Gd^{3+}

Because of its selectivity for smaller cations such as K^+ over other alkali cations, the titanium trisilicate was expected to be more highly selective for lanthanide ions than the zirconium or tin phases. To evaluate this hypothesis, two experiments were devised to determine which trisilicate would provide the best separation among complex mixtures of lanthanide ions.

The hydrolysis in water of these materials was examined. In Figure 4.2, it is seen that among the potassium phases, the extent of hydrolysis is as follows, Zr > Sn > Ti > ZrGe. These results demonstrate how tightly held the K^+ ions are in their framework exchange sites and how resistant to hydrolysis each individual compound is. When placed in solutions containing 1.0 meq of Gd^{3+}, the selectivity series among each synthetic umbite did not precisely correspond to the trend in hydrolysis and the affinity for Gd^{3+} was shown to be Sn > Zr > Ti > ZrGe. The content of Gd^{3+} at equilibrium for each umbite mimic is shown in Table 4.3. The potassium tin trisilicate showed the greatest affinity for Gd^{3+} over all other synthetic umbites. Because of its level of hydrolysis and because of its greater affinity for gadolinium ion, the tin trisilicate was chosen for further studies in lanthanide separations and structural characterization.

Table 4.3. Gadolinium uptake at equilibrium for each potassium umbite.

Gd uptake in meq/g	Proposed molecular formula
1.300	$K_{0.47}Gd_{0.51}SnSi_3O_9 \bullet H_2O$
1.053	$K_{0.761}Gd_{0.413}ZrSi_3O_9 \bullet H_2O$
0.9409	$K_{0.893}Gd_{0.369}TiSi_3O_9 \bullet H_2O$
0.5992	$K_{1.295}Gd_{0.35}ZrGe_3O_9 \bullet H_2O$

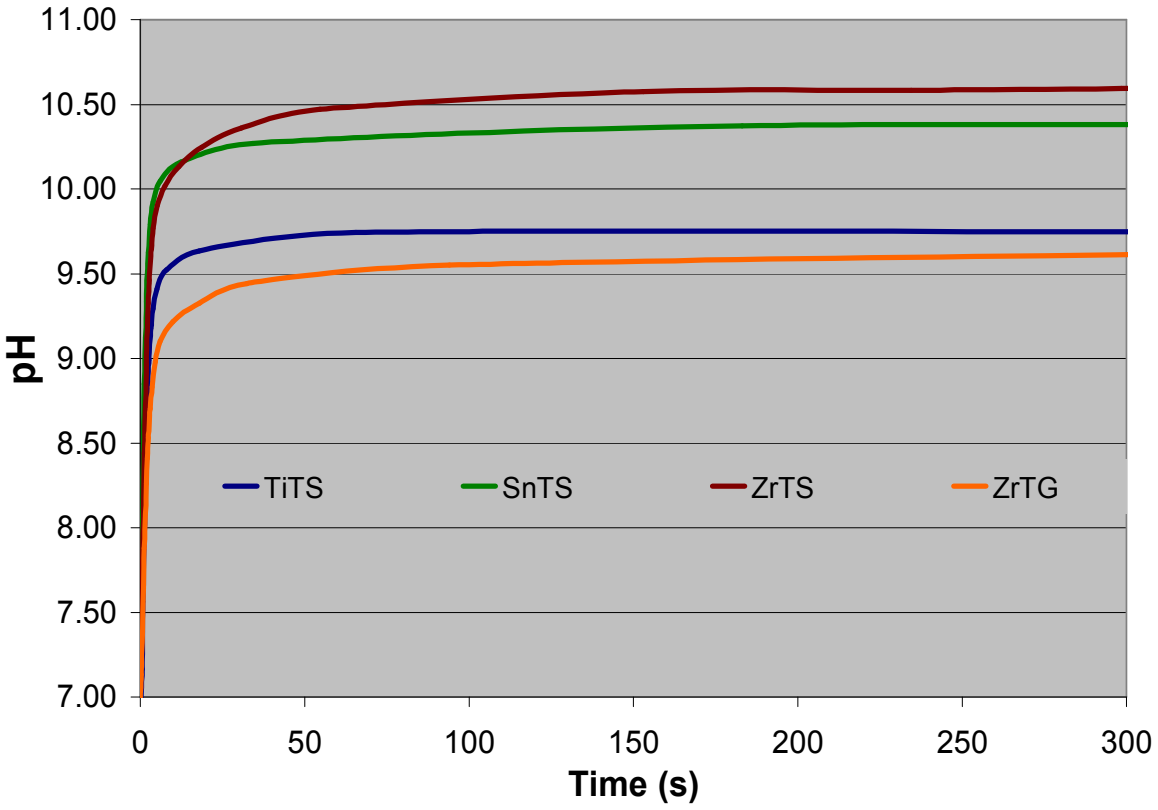

Figure 4.2. Extent of hydrolysis for individual potassium umbites shown as a function of pH over time.

4.3.2. Lanthanide separation and size selectivity

The affinity of $K_2SnSi_3O_9 \cdot H_2O$ for selected lanthanide cations was tested over a pH range of 1-10. The affinity of the tin trisilicate for individual lanthanides is greatest in alkaline media as shown in Figure 4.3. The trend clearly demonstrates size selectivity as the largest lanthanide ion, La^{3+}, is preferred over the smallest, Er^{3+}. The complete selectivity series under basic conditions is La > Pr > Sm > Gd > Er.

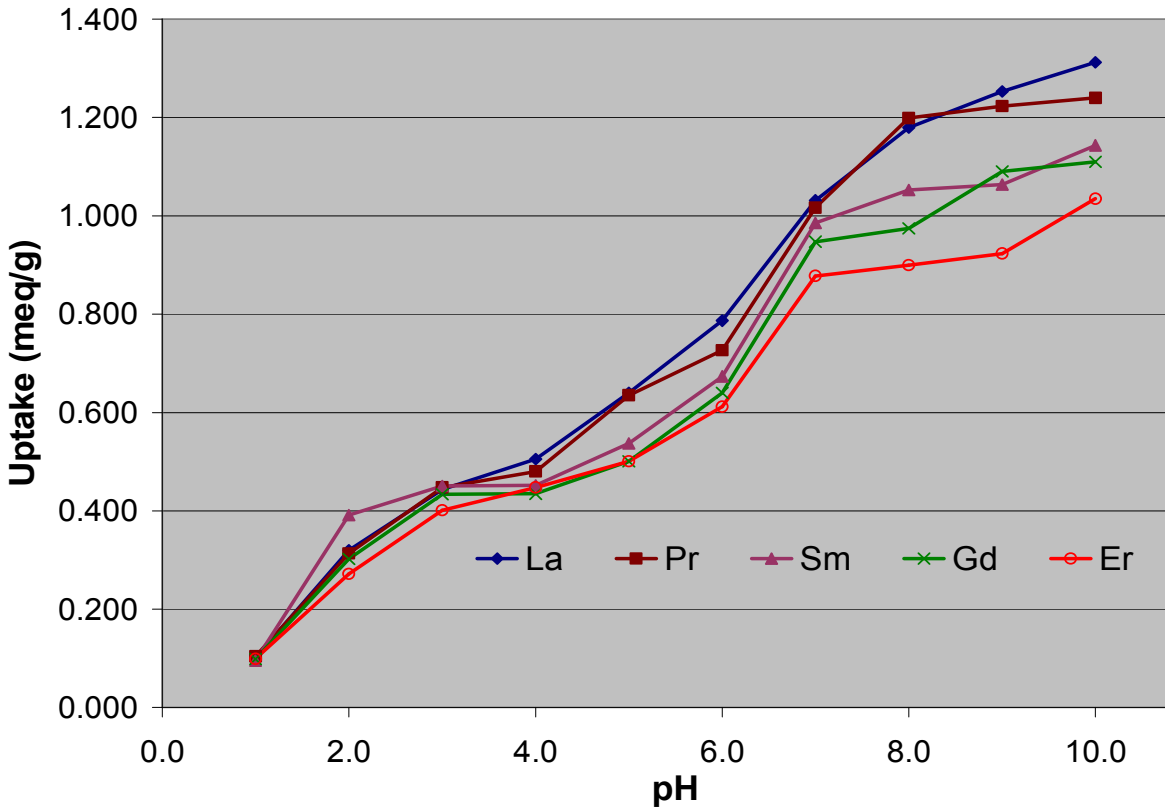

Figure 4.3. pH dependent uptake of selected lanthanides in $K_2SnSi_3O_9 \cdot H_2O$.

4.3.3. Structure of $Gd_{0.667}SnSi_3O_9 \bullet H_2O$ (1)

The final Reitveld refinement difference plot of compound **1** is shown in Figure 4.1 and a ball and stick representation of compound **1** is presented in Figure 4.4. Again, the compound maintains the umbite framework structure and consists of infinite silicate chains linked by tin octahedra. The orthorhombic space group $P2_12_12_1$ is also conserved. Selected bond distances are shown in Table 4.4. Contact distances between framework oxygens and Gd^{3+} are shown in Table 4.5. The closest contact is that of Ow1—Gd1, with a distance of 2.474(22) Å. All other contacts are greater than the sum of ionic radii for Gd^{3+} and O^{2-}, the shortest among those being Gd2—O12, with a distance of 2.679(15) Å. These distances are similar to those identified in the sodium tin trisilicate and this commonality will be discussed further in Chapter V.

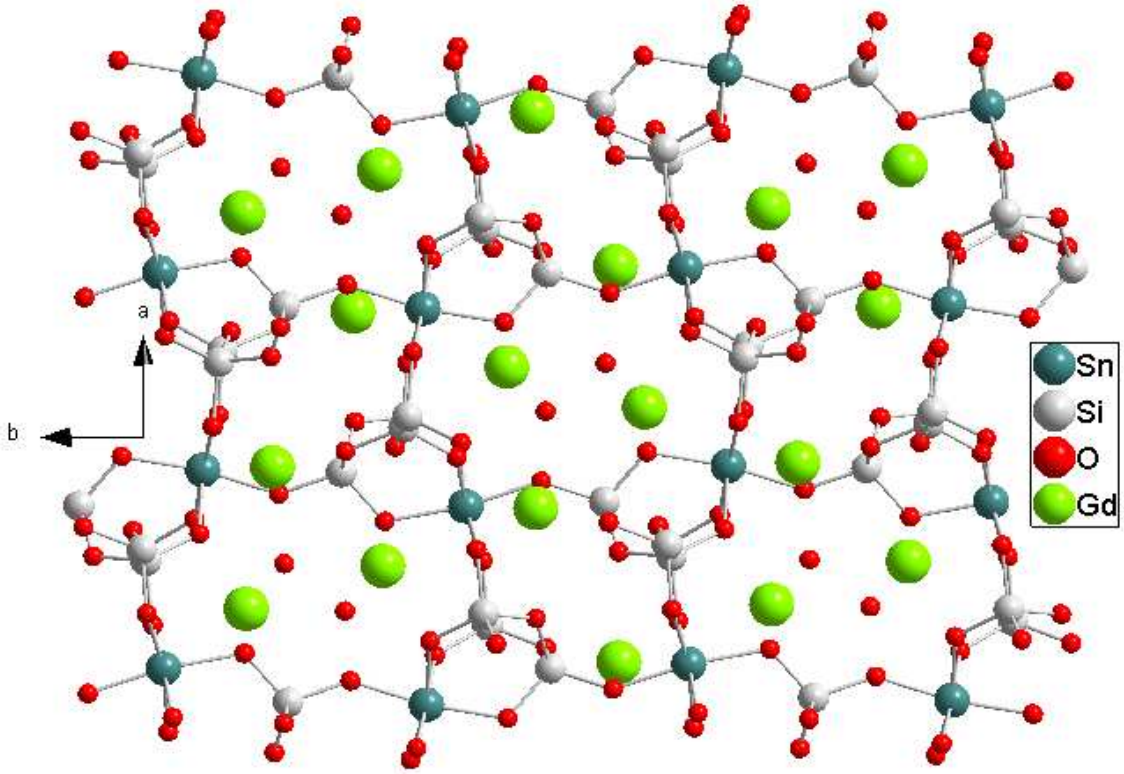

Figure 4.4. Ball and stick cartoon of compound **1** viewed down the *c*-axis.

Table 4.4. Selected framework bond distances (Å) for compound **1**.

Bond	$Gd_{0.667}SnSi_3O_9 \cdot H_2O$ (1)
Zr1-O5	2.065(7)
Zr1-O6	2.024(11)
Zr1-O7	1.996(7)
Zr1-O8	2.049(9)
Zr1-O9	2.008(9)
Zr1-O10	1.993(10)
Si2-O6	1.657(7)
Si2-O9	1.673(10)
Si2-O11	1.661(8)
Si2-O13	1.662(9)
Si3-O5	1.681(9)
Si3-O7	1.662(8)
Si3-O12	1.672(8)
Si3-O13	1.688(9)
Si4-O8	1.665(9)
Si4-O10	1.655(7)
Si4-O11	1.649(8)
Si4-O12	1.666(9)

Table 4.5. Cation-oxygen bond distances (Å) for compounds **1**.

Gd1-O	Distance	Gd2-O	Distance
Gd1—O6	2.895(16)	Gd2—O8	2.828(13)
Gd1—O8	2.884(12)	Gd2—O9	2.854(13)
Gd1—O10	2.679(15)	Gd2—O10	2.940(16)
Gd1—O12	2.814(11)	Gd2—Ow1	2.474(22)
Gd1—O13	3.040(12)		
Gd1—Ow1	2.715(24)		

4.4. Discussion

The affinity for Gd^{3+} has been examined in all metal trisilicates and the tin trisilicate takes up more Gd^{3+} than any other trisilicate. The reason for this affinity is two fold.

First, the extent of hydrolysis in the zirconium and tin phases is similar reaching a maximum pH of 10.60 and 10.37, respectively. This indicates that the K^+ in the exchange sites is more loosely held than in the titanium or the trigermanate phases. If this was the only reason for the selectivity then the zirconium phase would be expected to show the greatest affinity for Gd^{3+}. It is however, not the only factor at play in this system.

The second reason for selectivity is the size of the exchange cavity. Unit cell volumes for the zirconium and tin phases are 987 $Å^3$ and 949 $Å^3$, respectively, and as the size of the cell volume decreases so does the size of the pores and therefore the size of the exchange cavity. When compared to other trisilicates, the rate and extent of hydrolysis combined with a more comfortable and tighter fitting exchange cavity, make the tin trisilicate a better ion exchanger for Gd^{3+} sorption.

Because the size of the cavity is of key importance the crystal structure of the completely substituted gadolinium tin trisilicate was closely inspected. The compound crystallizes in the space group $P2_12_12_1$ and has unit cell dimensions of a = 10.1274(5) Å, b = 13.1319(5) Å, and c = 7.1775(3) Å. This corresponds to a cell volume of approximately 954 $Å^3$. This is only 5 $Å^3$ larger than the parent compound. It was suspected that the cell size would decrease due to the smaller ionic radius of the Gd^{3+} compared to the K^+ ion which are, for six coordinate species, 0.94 Å and 1.37 Å, respectively.

Another anomaly observed in the crystal structure is the lack of preference for either exchange site. Gd^{3+} cations are equally distributed in both exchange sites having site occupancies of 0.33 and 0.336 for Gd1 and Gd2, respectively.

4.5. Conclusions

The affinity for Gd^{3+} has been examined in all metal trisilicates. The potassium tin trisilicate shows the greatest affinity for Gd^{3+} and has demonstrated its tendency towards size segregation among rare earth cations. The greater affinity for Gd^{3+} can be attributed to the fact that the level of hydrolysis is higher than the zirconium trisilicate, indicating that the K^+ is not held as tightly as in the titanium phase and is freer to exchange. Although the K^+ is more tightly held in the tin phase than the zirconium phase, the size of the exchange sites are smaller due to the smaller ionic radius of the Sn^{4+}. This provides a smaller unit cell and therefore a smaller exchange cavity that that of the zirconium trisilicate, which better accommodates the Gd^{3+} ion. The selectivity series in basic media for a group of select lanthanides is as follows, La > Pr > Sm > Gd > Er.

The completely substituted gadolinium tin trisilicate has been synthesized through ion exchange. Having the molecular formula $Gd_{0.667}SnSi_3O_9 \bullet H_2O$, it crystallizes in the orthorhombic space group $P2_12_12_1$. There is no preference for either exchange site and the Gd^{3+} cations are equally distributed.

CHAPTER V
INCORPORATION OF THORIUM IN POTASSIUM TIN TRISILICATE

5.1. Introduction

The size discrimination among metal trisilicates has been demonstrated. Depending on the substituted framework octahedral metal and therefore, the size of the unit cell, an umbite mimic can be synthesized to better separate a specific ion from complex solutions. The reasons for the size selectivity revolve around the size of the incoming ion and how tightly held the outgoing is in the parent exchanger.

The affinity for 4^+ cations has not however been evaluated and represents an important aspect of this work in terms of nuclear waste remediation. Thorium is often used as a surrogate for plutonium because of its similar ionic radius and stable 4+ oxidation state. The use of thorium ion in exchange experiments involving synthetic umbites also provides a unique opportunity to examine the impact on valence of the exchange species while keeping the ionic radius relatively constant.

In this chapter, the incorporation of Th^{4+} will be discussed. The structure of the fully exchanged thorium tin trisilicate is analogous to the sodium, calcium, and gadolinium phases discussed in earlier chapters. In binary mixtures of Th^{4+} and cations of like ionic radius but lower valence, Th^{4+} is exchanged preferentially.

5.2. Experimental methods

5.2.1. Analytical procedures and instrumentation

Phase identification and structural data sets were collected using a Bruker-AXS D8 VARIO powder diffractometer. Thermal gravimetric analysis was conducted on a TA Instruments TGA Q 500 unit. A constant temperature ramp of 5 ^{o}C/min was applied while the sample was under 9:1 nitrogen to air volume ratio. Potassium, Sodium, and Calcium analysis was performed on a Varian AA 250 atomic absorption spectrometer under an acetylene nitrous oxide flame. Samples for AA analysis were prepared by digestion of the solid in hydrofluoric acid. Measurement of ^{232}Th uptake was performed on a Wallac 1410 liquid scintillation counter. Titrations and pH measurements were conducted on a TitraLab TIM860 Titration Manager.

5.2.2. Synthesis and ion exchange

Potassium tin trisilicate, $K_2SnSi_3O_9 \bullet H_2O$, was synthesized using a method published by Pertierra et al.[28] 7.2 g of SiO_2 were dissolved in 35 mL of 7M KOH. To this mixture was added drop wise 3.5mL of $SnCl_4$ with stirring. This mixture was sealed in a 100mL Teflon lined autoclave and heated at 190^{o}C for 12 days.

Fully exchanged thorium tin trisilicate, compound **1** was synthesized by exhaustive ion exchange. 1.0g of $K_2SnSi_3O_9 \bullet H_2O$ was stirred for 24 hours at room temperature in a solution of 0.1M $Th(NO_3)_3$. The supernatant liquid was decanted and measured for potassium content. A fresh solution of thorium nitrate was added to the exchanger and shaken again for 24 hours. This process was repeated until no potassium was detected in the supernatant liquid or in the solid exchanger. The potassium content of the solid was determined by AA, dissolving a 5mg sample of the dry solid exchanger in 2mL of concentrated HF at room temperature and diluting to 1.000L. Synthesis of

$CaSnSi_3O_9•H_2O$ and $Na_2SnSi_3O_9•H_2O$ were accomplished by exhaustive ion exchange in the same fashion using their respective nitrate salts.

5.2.3. X-ray data collection and structure refinement

Data sets were collected on a Bruker-AXS D8 VARIO powder diffractometer with standard vertical Bragg-Brentano geometry and a linear PSD detector. The diffractometer was equipped with a Germanium monochromator allowing the use of Cu $K\alpha_1$ radiation only with a wavelength of 1.54056 Å. Powders were loaded on a quartz disc which was spun during data collection to reduce any scattering effects due to preferred orientation. Operating voltage and current were 40kV and 50mA respectively. Data were collected at room temperature with 2θ ranging from 5 to 130 degrees. A step size of 0.016 degrees and a scan time of 15 seconds per step were employed.

Powder patterns were indexed using TREOR, ITO, and DICVOL methods found in the FullProf program suite.[47-49] Profile function fitting using the LeBail method and Reitveld refinement were accomplished using the GSAS program suite.[37,38] No corrections were made for absorption and neutral atom scattering factors were used as stored in GSAS. No attempt was made to model preferred orientation.

Observed and calculated XRD profiles are displayed in Figure 5.1. Compound **1**, $Th_{0.5}SnSi_3O_9•H_2O$, crystallizes in the orthorhombic space group $P2_12_12_1$ with cell dimensions of a = 10.1013(7), b = 12.9815(9), c = 7.0479(5) and a unit cell volume of 924.20(14) $Å^3$.

Once profile fitting was completed and the framework atomic coordinates were transformed into their new system, bond distance restraints were applied to Si-O and Zr-O contacts. The position of zirconium was refined and subsequently that of each individual trisilicate group. Fourier difference maps were constructed to reveal the position of the missing cations and waters. Once the positions were input, the atomic coordinates of the framework were again refined. Next, the cation and water positions were refined without moving the framework. This see-saw approach was continued until

least squares refinement converged rapidly and the shift in atomic coordinates was less than 0.1% of the starting value. The potassium site occupancy was then refined while isotropic thermal factors were held constant. Once site occupancy was established, isotropic thermal factors for tin, potassium, and water oxygens were refined. No attempt was made to assign water hydrogen positions.

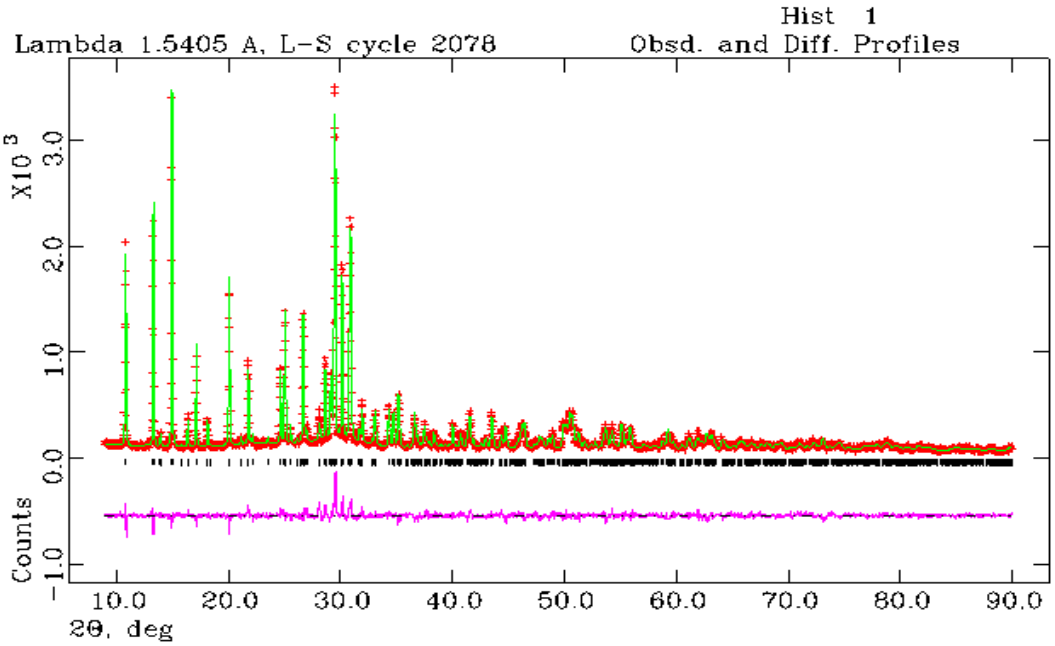

Figure 5.1. Observed (+) and calculated (-) profiles for final Reitveld refinement of $Th_{0.5}SnSi_3O_9 \bullet H_2O$. Difference plot is shown in the bottom as the pink line. Individual reflections are marked by the black bars.

Competitive studies between cations with an ionic radius near 1.0 Å were performed by placing 0.1 grams of ion exchanger into a solution of two different cations. The total concentration of each cation was held at 1.0 meq. The concentration of each cation in the solid at equilibrium and the concentration in the exchange solution were determined by atomic absorption. The concentration of Th was determined by LSC.

5.3. Results

5.3.1. Ion exchange in competitive solutions

The results of the competitive binary solution study are presented in Table 5.1. In all cases, the cation of greater valence was taken up preferentially. The selectivity series among cations of like ionic radius (~1.0 Å) is therefore, $Th^{4+} > Gd^{3+} > Ca^{2+} > Na^{+}$. A selectivity quotient is also presented in Table 5.1 and simply represents the equivalent uptake of the preferred cation divided by the equivalent uptake of the lesser preferred cation. This quotient shows how the selectivity is greater for the higher valence cation in the competitive environments. For example, in the Na/Th solution, 8 times more Th^{4+} is taken up. The most competitive solution is the Ca/Gd system in which almost twice as much Gd^{3+} is taken up.

Table 5.1. Uptake of individual cations in binary solutions expressed in terms of equivalents. The selectivity quotient is calculated by dividing the equivalent uptake of the most preferred cation by that of the least preferred cation.

	K	Na	Ca	Gd	Th	Selectivity quotient
Na/Ca	0.35	0.38	1.27			3.34
Na/Gd	0.42	0.24		1.338		5.58
Na/Th	0.37	0.18			1.45	8.06
Ca/Gd	0.41		0.56	1.029		1.84
Ca/Th	0.27		0.42		1.31	3.12
Gd/Th	0.31			0.45	1.24	2.76

5.3.2. Structure of $Th_{0.5}SnSi_3O_9 \bullet H_2O$.

The fully substituted thorium tin trisilicate crystallizes in the space group $P2_12_12_1$. Its unit cell dimensions are a = 10.1013(7), b = 12.9815(9), c = 7.0479(5) with a unit cell volume of 924.20(14) Å^3. Crystallographic data for compound **1** and the Na, Ca, and Gd tin trisilicate phases are shown in Table 5.2. Atomic positions and thermal parameters are shown in Table 5.3.

Table 5.2. Crystallographic data for Th, Gd, Ca, and Na phases of tin trisilicate.

	Na	**Ca**	**Gd**	**Th**
fw	410.92	405.02	469.77	480.96
space group	$P2_12_12_1$	$P2_12_12_1$	$P2_12_12_1$	$P2_12_12_1$
a (Å)	10.4381(5)	10.1479(8)	10.1274(5)	10.1013(7)
b (Å)	13.2656(4)	13.1621(9)	13.1319(5)	12.9815(9)
c (Å)	7.2440(3)	7.1942(5)	7.1775(3)	7.0479(5)
V (Å^3)	1003.06(6)	960.91(12)	954.55(7)	924.19(14)
Z	4	4	4	4
D_{calc} (g/cm^3)	2.708	2.786	3.255	3.442
No. of reflections	791	1026	1006	1172
R_{wp}	0.0642	0.0683	0.0905	0.1365
R_p	0.0436	0.0456	0.0735	0.1072

Selected bond lengths are shown in Table 5.4 and cation oxygen distances for all four substituted tin compounds are summarized in Table 5.5. The thorium tin trisilicate shows two close contacts with framework oxygens in the smaller cavity, Th1—O8 and Th1—O10 which have bond lengths of 2.462(22) Å and 2.440(24) Å, respectively. The water contact, Th1—Ow1 is 2.667(66) Å, which is surprisingly 0.2 Å shorter than the previously mentioned framework contacts.

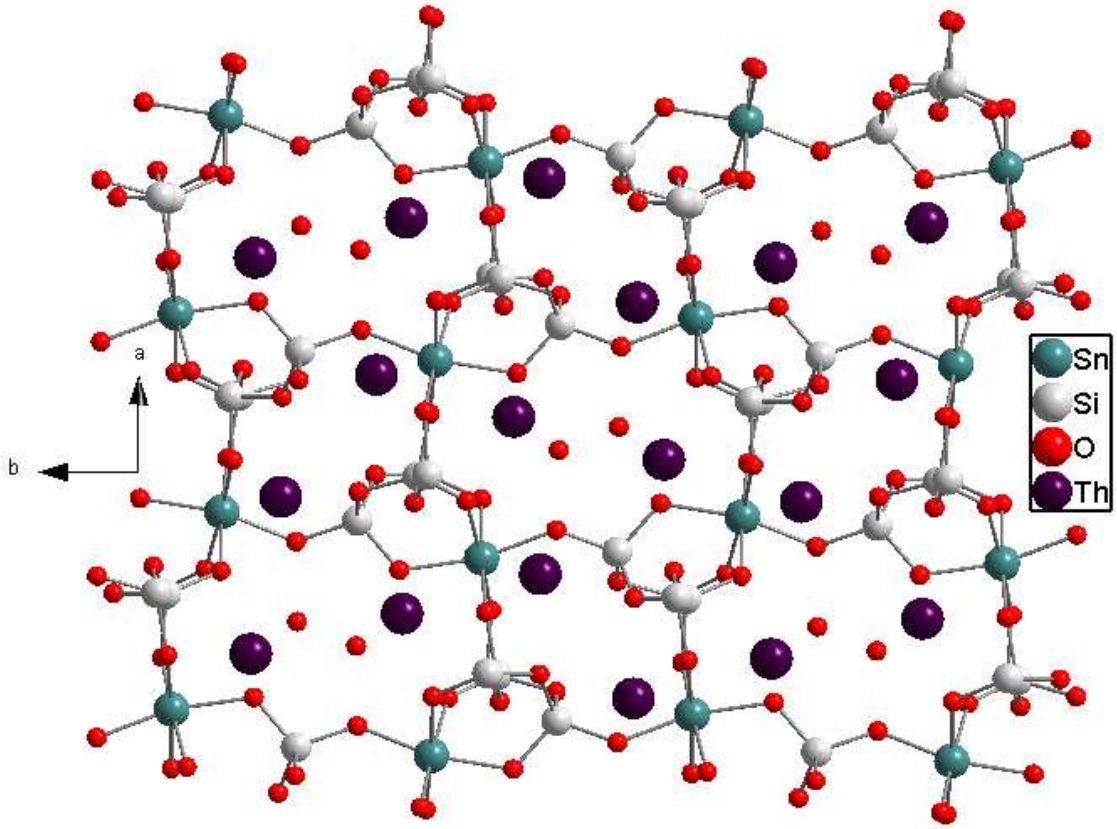

Figure 5.2. Ball and stick cartoon of $Th_{0.5}SnSi_3O_9 \bullet H_2O$ viewed down the *c*-axis.

Table 5.3. Positional and thermal parameters for $Th_{0.5}SnSi_3O_9 \bullet H_2O$.

	x	y	z	U_{iso} [a]
Sn1	0.4444(6)	0.2037(5)	0.2431(15)	0.034
Si2	0.1536(15)	0.1903(14)	0.0306(26)	0.008
Si3	0.0365(14)	0.0565(9)	0.7336(29)	0.008
Si4	0.6500(14)	0.3276(12)	0.5521(23)	0.008
O5	0.4125(16)	0.3612(10)	0.259(6)	0.004
O6	0.3141(15)	0.1841(19)	0.0353(27)	0.004
O7	0.5178(22)	0.0607(9)	0.275(4)	0.004
O8	0.5897(13)	0.2337(18)	0.4257(35)	0.004
O9	0.5940(17)	0.2047(17)	0.0666(35)	0.004
O10	0.3084(14)	0.1943(15)	0.4450(28)	0.004
O11	0.0836(18)	0.1659(17)	0.2370(26)	0.004
O12	0.1093(25)	0.0582(14)	0.5225(29)	0.004
O13	0.1529(21)	0.0900(18)	0.8898(31)	0.004
Th1[b]	0.1978(15)	0.6449(11)	0.1240(22)	0.1675
Th2[c]	0.4056(14)	0.0906(10)	0.7578(31)	0.1257
Ow1	0.220(6)	0.443(5)	0.062(8)	0.015

[a] $U_{iso} = B_{iso} / 8\pi^2$

[b] Occupancy factor = 0.257

[c] Occupancy factor = 0.243

Table 5.4. Selected framework bond distances (Å) for compound **1**.

Bond	$Th_{0.5}SnSi_3O_9 \cdot H_2O$ (1)
Sn1—O5	2.073(15)
Sn1—O6	1.985(20)
Sn1—O7	2.012(15)
Sn1—O8	1.991(21)
Sn1—O9	1.957(22)
Sn1—O10	1.982(19)
Si2—O6	1.624(21)
Si2—O9	1.640(28)
Si2—O11	1.648(26)
Si2—O13	1.637(29)
Si3—O5	1.647(20)
Si3—O7	1.643(19)
Si3—O12	1.660(29)
Si3—O13	1.668(28)
Si4—O8	1.628(27)
Si4—O10	1.625(20)
Si4—O11	1.633(24)
Si4—O12	1.626(25)

Table 5.5. Cation-oxygen bond distances (Å) for Th, Gd, Ca, and Na phases of tin trisilicate.

Compound	Site 1	Distance	Site 2	Distance
	Th1—O5	2.805(42)	Th2—O6	2.480(28)
	Th1—O8	2.462(22)	Th2—O10	2.763(27)
$Th_{0.5}SnSi_3O_9•H_2O$	Th1—O10	2.440(24)	Th2—O12	2.690(26)
	Th1—O11	3.019(24)	Th2—O13	2.717(26)
	Th1—Ow1	2.667(66)		
	Gd1—O6	2.895(16)	Gd2—O8	2.828(13)
	Gd1—O8	2.884(12)	Gd2—O9	2.854(13)
$Gd_{0.667}SnSi_3O_9•H_2O$	Gd1—O10	2.679(15)	Gd2—O10	2.940(16)
	Gd1—O12	2.814(11)	Gd2—Ow1	2.474(22)
	Gd1—O13	3.040(12)		
	Gd1—Ow1	2.715(24)		
	Ca1—O6	2.899(37)	Ca2—O8	3.059(30)
	Ca1—O8	2.937(31)	Ca2—O9	2.746(29)
$CaSnSi_3O_9•H_2O$	Ca1—O10	2.978(35)	Ca2—O10	2.917(31)
	Ca1—O11	2.981(29)	Ca21—O11	2.899(30)
	Ca1—O12	2.707(33)	Ca2—Ow1	2.459(26)
	Ca1—O13	2.936(24)		
	Ca1—Ow1	2.452(31)		
	Na2—O6	2.802(46)	Na1—O6	3.048(63)
	Na2—O8	3.058(40)	Na1—O10	2.945(66)
$Na_2SnSi_3O_9•H_2O$	Na2—O10	3.017(44)	Na1—O11	2.402(18)
	Na2—O12	3.097(43)	Na1—Ow1	3.174(40)
	Na2—Ow1	3.049(32)	Na1—Ow1’	3.132(66)

5.4. Discussion

A study of competitive ion exchange in binary solutions of cations of like size was conducted in the potassium tin trisilicate system. When ionic radius is held constant, it was discovered that the selectivity depends on the charge of the cation. The selectivity among ions with an ionic radius of ~1.0 Å was shown to be $Th^{4+} > Gd^{3+} > Ca^{2+} > Na^{+}$. The reason for the trisilicates to desire higher valence cations is unclear. In the absence of counter ions, the framework has a net charge of 2^{-}. When distributed among the framework oxygens this charge becomes soft and diffuse with each oxygen having a charge of -2/9. In terms of hard-soft interactions, the softness of the framework and the hardness of the thorium cation make this interaction counter intuitive.[78-80]

The crystal structure of the thorium tin trisilicate does however indicate that the bonding is tighter as the Th^{4+} moves closer to the frame work than other cations of smaller charge. Two Th-O contacts are below 2.5 Å, which closely approaches the sum of their ionic radii. The water contact is, however, longer than expected, with the Th-Ow1 distance being approximately 2.67 Å. The water carries no residual charge and even though it is free to move inside the cavity, it technically has little ability to satisfy the naked 4+ charge of the thorium ion. Other close contacts with framework oxygens in the Gd, Ca, and Na phase are longer than those of the Th phase. The M-Ow1 contacts for Gd and Ca are, however, closer than 2.5 Å. Gd-Ow1 has a single water contact of 2.474(22), while Ca has two water contacts with Ca1-Ow1 and Ca2-Ow1 distances of with bond distances of 2.452(31) Å and 2.459(26) Å, respectfully.

In every tin trisilicate in this study the cations in Site 1 have more contacts under 3.0 Å than those located in Site 2. As the charge of the cation increases however, the cations become equally distributed among both sites.

5.5. Conclusions

A completely substituted thorium tin trisilicate, $Th_{0.5}SnSi_3O_9 \bullet H_2O$ (**1**) has been synthesized by ion exchange with potassium tin trisilicate. The crystal structure of **1** shows that the composition of the framework is identical to that of the parent compound. Thorium occupies both exchange sites with no preference. There are two Th-O contacts in the small cavity that are shorter than the water contact which, given the water's translational freedom to move closer to the high valence cation, is very unique.

When compared to the crystal structures of other completely substituted compounds with ions of the same size the thorium structure is remarkably similar. The largest difference is the volume of the unit cell. The Th^{4+} tin phase has almost the same cell volume as the potassium titanium trisilicate with cell volumes of approximately 924 $Å^3$ and 915 $Å^3$ respectively.

Another factor in the selectivity of the trisilicates for certain cations has been discovered. When cations of like size are combined in solution with the trisilicate exchanger, the cation of higher valence is exchanged in preferentially. Among cations of ionic radius close to 1.0 Å, the selectivity series was shown to be $Th^{4+} > Gd^{3+} > Ca^{2+} > Na^{+}$.

CHAPTER VI
IN SITU X-RAY DIFFRACTION STUDY OF CESIUM EXCHANGE IN PROTONATED ZIRCONIUM TRISILICATE

6.1. Introduction

For decades, knowledge about the mechanism of ion exchange and intercalation has been justly derived from kinetic measurements coupled with studies of thermodynamic equilibrium quantities such as entropy, enthalpy, and energy of activation. In order to arrive at these quantities, certain principles about ion exchange have been granted a priori since the early 1900's. Most notably, that the rate-determining step of an exchange reaction is a diffusion limited process, therefore it may be erroneous to think of it as an actual chemical exchange.[39] Other meaningful mechanistic information such as diffusion coefficients can be derived from time resolved uptake data by fitting uptake curves to a variety of models given by G.E. Boyd and others.[81,82] Application of Nernst-Planck equations can allow for formal definition of rate expressions, however Helfferich warns against the physical interpretation of these values in the same manner as actual chemical reactions. [39]

While the theory and experimental observations previously mentioned provide insight into the mechanism of ion exchange they do little to describe the paths of the cations through 3D extended framework structures. Coupling the information given by theory and kinetic observations with structural data provides a clearer picture of what the ions are doing inside the exchanger. Monitoring the exchange reaction in situ by X-ray diffraction provides numerous advantages to ex situ ion exchange studies. Any structural change in the framework can be monitored as the host and guest ions change places. The path of the ions to the exchange site can also be tracked. Structural refinement of the ex situ exchange products show only the average position of the ion around the exchange site, however while monitoring ion exchange as it occurs the role of solvent can be assessed. Work of this nature has already been performed on inorganic

framework materials with zeolite type pores.[83-85] Celestian and coworkers were able to describe the Na/K exchange behavior of the germanium analog of the mineral gismondine using data gathered from in situ ion exchange time resolved x-ray diffraction studies. O'Hare and coworkers have studied the intercalation and exchange mechanism of $[LiAl_2(OH)_6]Cl•H_2O$ extensively by a variety methods including in situ X-ray diffraction.[86-88]

6.2. Experimental methods

6.2.1. Synthesis of starting materials

Potassium zirconium trisilicate, $K_2ZrSi_3O_9•H_2O$, was synthesized hydrothermally by modification of methods previously reported by Poojary et al.[31] 7.0 grams of silicic acid was dissolved in 45 mL of 4M KOH and 10 mL of isopropanol. 13.5 mL of a 70% solution of zirconium isopropoxide in isopropanol was diluted with 10 mL of isopropanol and added drop wise to the previous solution. The mixture was divided in two and placed in 100 mL Teflon lined autoclaves. The reaction was carried out at 180°C. After 5 days a white precipitate was isolated and washed with distilled water and dried at 60°C.

Compound **1**, $H_{1.22}K_{0.84}ZrSi_3O_9•2.16H_2O$, was synthesized by shaking $K_2ZrSi_3O_9•H_2O$ in 0.1M acetic acid at a volume to mass ratio of 500:1, in mL/g, for 24 hours. The product was collected by vacuum filtration and washed with distilled water and acetone. The dry product was then shaken in 0.5M acetic acid for 24 hours. The product was again collected by vacuum filtration and rinsed thoroughly with water and acetone until no odor of acetic acid was detected.

6.2.2 In situ ion exchange study

The apparatus used for the time resolved ion exchange studies was a modification of the one described by Parise and coworkers and is shown in Figure 6.1.[89] Time resolved studies were performed at Brookhaven National Laboratories. X-rays from the National Synchrotron Light Source beam line X7B were used with a wavelength of 0.9221(1) Å. Diffraction data were collected on a MAR 345 imaging plate detector. Data collection time was 60 seconds. The goniometer was rotated 1^{o} per second with respect to φ with a fixed χ of 90^{o}. Imaging of the plate detector and dumping of the data lasted 80s bringing the total time resolution to 140s. Diffractometer constants such as wavelength, beam center, and detector distance were calculated from a LaB_6 standard frame.

Approximately 0.01g of **1** was ground and passed through a 75 μm sieve before being loaded into the capillary. A dry frame of **1** was captured and then a wet frame with only distilled water flowing through the capillary. The initial ion exchange solution was prepared by adding 0.011g of CsCl to 200 mL of distilled water. This solution was allowed to flow over the sample for approximately 40 frames with no detectable change in the diffraction pattern. An additional 0.1g of CsCl was added bringing the total concentration of Cs^{+} to 3.3mM. Frames were collected consecutively for approximately 1 hour at the end of which the exposure time was increased to 10 minutes and φ was rotated thru 60^{o} at 0.1^{o} per second to collect a final frame.

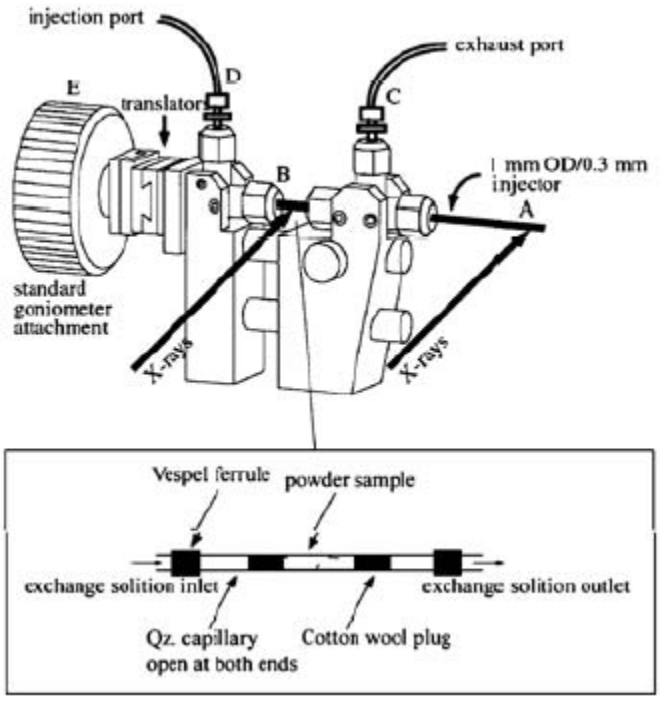

Figure 6.1. In situ ion exchange x-ray diffraction cell.

Data from the imaging plate were integrated using the Fit2D software package.[90-93] The integrated intensities were transformed into CPI file format with the Program ConvX.[35] Powder patterns were indexed using TREOR, ITO, and DICVOL methods found in the FullProf program suite.[47-49] Profile function fitting using the LeBail method and Reitveld refinement were accomplished using the GSAS program suite.[37,38]

Structure determination from the powder data was begun by using the framework atomic coordinates found for the protonated phase as a starting model.[94] Later, for the orthorhombic phases beginning at frame 231 and beyond, the framework atomic parameters derived from the pure potassium phase were employed as a starting model.[31] Contact distance constraints were applied for Si-O, Zr-O and O-O contacts. Isotropic thermal factors for all atoms were fixed. The zirconium position was first refined and subsequently each trisilicate group. Once least squares refinement converged Fourier difference maps were constructed to reveal the positions of the cations and water oxygen. Since no analytical data was available, starting occupancies were estimated. Fourier difference maps were again constructed and the site occupancies were adjusted until the largest value of rho was less than 2 e^- per $Å^2$. Cation positions were then refined while holding framework positions constant. Once the positions of the cations stabilized, the framework atoms were refined while holding the cation positions fixed. This back and forth approach was continued until all atom positions could be refined together and the shift in atomic position was less than 0.001Å.

Once the positional parameters were stable the occupancy of the cations was refined. The initial refinement returned unsatisfactory results that did not make chemical sense. It was assumed the degree of disorder was extreme and a much more accurate starting point was necessary for GSAS to refine each occupancy. To model this disorder, Cs, K, and O atoms were placed at each extra framework site and their atomic coordinates were constrained such that any refinement of position moved each atom to the same point in space.

A similar method was used by Poojary and coworkers to model the disorder encountered while solving the ion exchange structures of the potassium phase.[31] Sites M1, M2, and M3 correspond to exchange Site 1 in the small channel, exchange Site 2 in the large channel, and the water site in the large channel, respectively. The sum of individual occupancies was constrained to 1 and initial occupancy values were set to 1/3 for each atom in sites M1, M2, and M3. From there site occupancies were again refined, this time allowing a result that made chemical sense. Once the site occupancies and positional parameters were refined and stable, the isotropic thermal factors for each cation and zirconium atom were refined. Thermal factors for silicon and framework oxygens were held constant and no attempt to describe the water hydrogens was made.

6.2.3. Solid state NMR

^{133}Cs MAS MNR experiments were performed on a Bruker Avance-400 equipped with standard 4 and 7mm MAS and wide line probe heads. An external standard of solid CsCl dried at 60^{o}C for 3 days was used. Two samples of **(1)** were loaded to a Cs^{+} content of 5% and 75%. Samples were spun between 6-10 kHz depending on the shifts of the sidebands.

6.3. Results

6.3.1. Structure of $H_{1.22}K_{0.84}ZrSi_3O_9 \bullet 2H_2O$ (**1**)

Unit cell parameters and refinement statistics are found in Table 6.1. Selected bond distances for the framework atoms in compounds **1** and **2** are listed in Table 6.2. The final refinement difference plot for compounds **1** and **2** are shown in Figure 6.2. The structure of **1** was derived from Reitveld refinement of the first wet frame 01. The structure of the partially protonated phase has been discussed in previous work.[94] The framework consists of polymeric chains of silicate groups linked by zirconium atoms. Identical to the channel network in the parent compound, this arrangement gives rise to two unique channels and ion exchange sites which run parallel to each other and contain the cations and interstitial water. The first tunnel, denoted Site 1, is a 12-atom ring containing two cations. Site 2 is a 16-atom ring containing two cations and two water molecules. A 14-atom channel runs perpendicular to these channels linking them to one another.

Table 6.1. Crystallographic data for compounds **1** and **2**.[a]

	1	**2**
fw	389.05	536.17
space group	$P2_1/c$	$P2_12_12_1$
a (Å)	7.2814(3)	7.3946(6)
b (Å)	10.4201(4)	10.6668(8)
c (Å)	13.4529(7)	13.5821(11)
β	90.53(1)°	-
V (Å^3)	1020.67(8)	1071.31(15)
Z	2	4
D_{calc} (g/cm^3)	2.517	3.318
No. of reflections	238	174
R_{wp}	0.0377	0.0204
R_p	0.0280	0.0144

[a] (**1**) $H_{1.22}K_{0.84}ZrSi_3O_9 \bullet 2.16H_2O$;
(**2**) $H_{0.18}K_{0.45}Cs_{1.37}ZrSi_3O_9 \bullet 0.98H_2O$

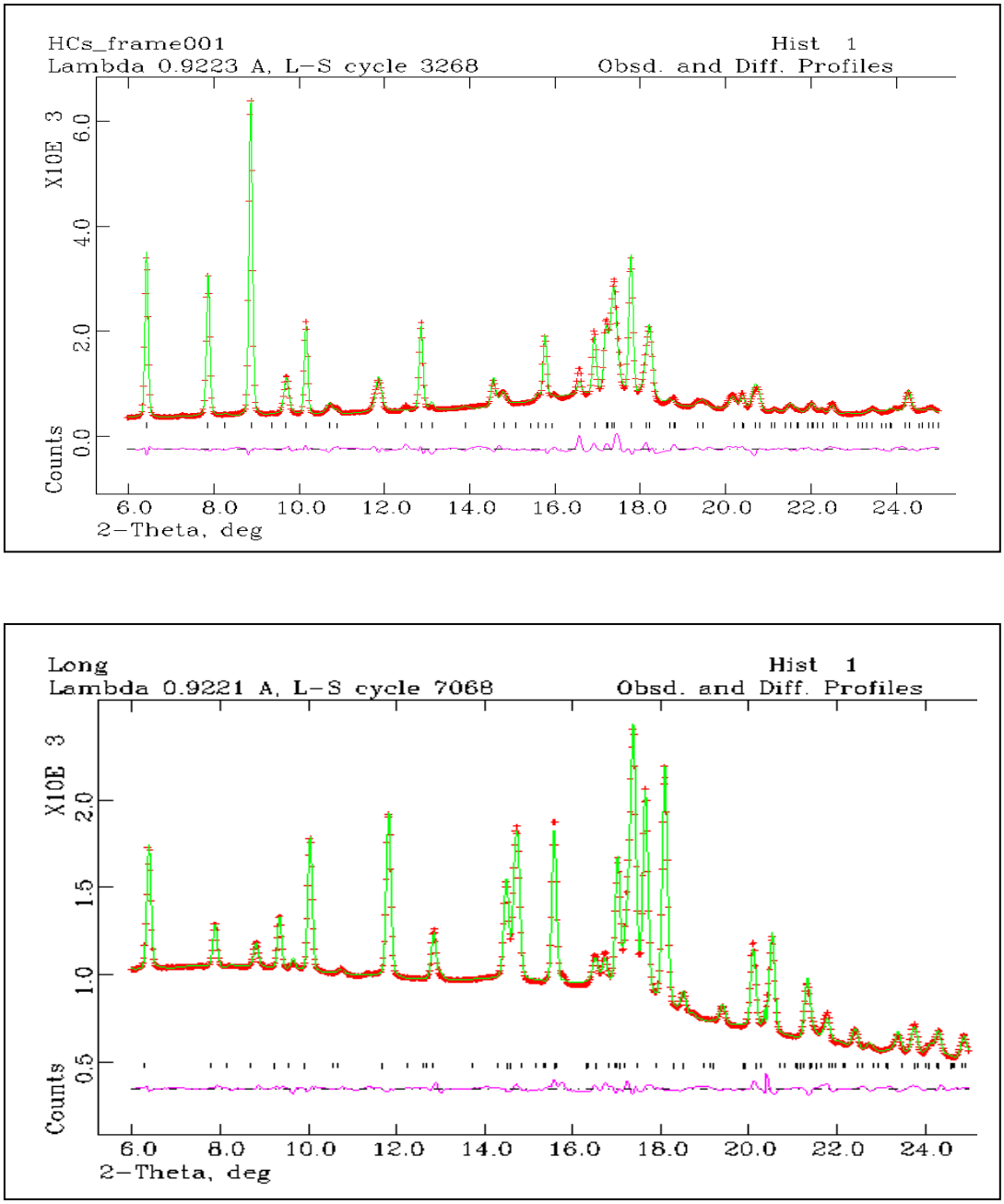

Figure 6.2. Reitveld refinement difference plots for $H_{1.22}K_{0.84}ZrSi_3O_9 \cdot 2.16H_2O$ and $H_{0.18}K_{0.45}Cs_{1.37}ZrSi_3O_9 \cdot 0.98H_2O$

Table 6.2. Selected framework bond distances (Å) for compounds **1** and **2**.

Bond	1	2
Zr1—O5	2.161(13)	2.118(7)
Zr1—O6	2.067(16)	1.976(10)
Zr1—O7	1.982(13)	2.075(8)
Zr1—O8	1.978(16)	2.024(11)
Zr1—O9	1.986(17)	2.035(10)
Zr1—O10	2.015(17)	2.067(10)
Si2—O6	1.676(15)	1.644(9)
Si2—O9	1.652(19)	1.659(11)
Si2—O11	1.640(15)	1.651(9)
Si2—O13	1.655(17)	1.649(10)
Si3—O5	1.667(16)	1.646(9)
Si3—O7	1.626(17)	1.663(15)
Si3—O12	1.659(17)	1.662(10)
Si3—O13	1.665(17)	1.67(1)
Si4—O8	1.664(18)	1.658(11)
Si4—O10	1.661(15)	1.635(9)
Si4—O11	1.625(15)	1.638(8)
Si4—O12	1.627(16)	1.65(1)

The major difference is the space group in which the parent compound and the protonated phase crystallize. Compound **1** crystallizes in the monoclinic space group $P2_1/c$ with unit cell dimensions of a = 7.2814(3) Å, b = 10.4201(4) Å, c = 13.4529(7) Å, and β = 90.53(1)°. The parent compound, $K_2ZrSi_3O_9 \cdot H_2O$, crystallizes in the orthorhombic space group of $P2_12_12_1$ and has cell dimensions of a = 10.2977(2) Å, b =

13.3207(3) Å, c = 7.1956(1) Å.[31] After conversion to the protonated phase, all of the remaining K^+ cations are located in Site 1. The cation positions in Site 2 are now occupied by water molecules. This arrangement of cations represents the dry sample described by Clearfield and Fewox in previous work.[94] In this case the division of remaining K^+ ions is different in the sample with water flowing through it. The majority of K^+ ions remain in Site 1 showing an occupancy factor of 0.64 for M1. The remainder of the cations are found in Site 2 with occupancy factor of 0.2 for M2.

6.3.2. Time-resolved exchange of Cs^+ in compound **1**

Time resolved in situ X-ray diffraction patterns are shown in Figure 6.3. 32 frames were collected over the space of approximately 1 hour. Frames were automatically numbered beginning with 1 and increasing in steps of 5 such that the next frame after 001 would be named 006. Frames 201 thru 346, including the final data set collected over 10 minutes, were indexed and their unit cell dimensions and space group are listed in Table 6.3. The unit cell volume increases steadily from 1019 $Å^3$ in frame 201 to 1061 $Å^3$ in frame 346. The transition from the monoclinic to the orthorhombic crystal system occurs between frames 226 and 231.

Table 6.3. Unit cell dimensions for selected frames.

Frame	*a*	*b*	*c*	*β*	Volume
346	10.695(3)	13.501(1)	7.3465(9)		1060.79
341	10.697(2)	13.498(1)	7.3453(8)		1060.72
336	10.696(3)	13.499(1)	7.3464(9)		1060.74
331	10.627(3)	13.504(1)	7.3465(8)		1054.35
326	10.621(3)	13.512(2)	7.3415(10)		1053.64
321	10.594(3)	13.497(1)	7.3442(9)		1050.22
316	10.634(2)	13.498(3)	7.3439(9)		1054.00
311	10.592(3)	13.504(3)	7.3447(8)		1050.65
306	10.619(2)	13.500(3)	7.3431(7)		1052.80
301	10.592(3)	13.501(3)	7.3449(9)		1050.36
296	10.592(3)	13.506(3)	7.3447(9)		1050.84
291	10.590(2)	13.504(2)	7.3438(9)		1050.27
286	10.591(2)	13.503(3)	7.3443(8)		1050.33
281	10.590(2)	13.508(2)	7.3437(8)		1050.62
276	10.588(3)	13.507(1)	7.3424(7)		1050.09
271	10.587(3)	13.508(1)	7.3427(10)		1050.15
261	10.587(2)	13.510(2)	7.3419(8)		1050.16
256	10.584(2)	13.506(1)	7.3398(9)		1049.31
251	10.585(3)	13.509(3)	7.3398(8)		1049.60
246	10.582(3)	13.505(2)	7.3391(9)		1048.85
241	10.579(2)	13.504(3)	7.3370(8)		1048.24
236	10.578(2)	13.505(2)	7.3364(8)		1048.09
231	10.574(3)	13.510(1)	7.3357(8)		1048.07
226	13.492(3)	10.566(3)	7.3248(8)	90.227	1044.26
221	13.478(1)	10.560(2)	7.3195(7)	90.194	1041.88
216	13.435(1)	10.439(3)	7.2881(8)	90.329	1022.29
211	13.406(1)	10.436(3)	7.2756(8)	90.268	1017.98
206	13.424(4)	10.430(6)	7.2814(11)	90.309	1019.56
201	13.426(2)	10.426(3)	7.2789(9)	90.222	1018.96

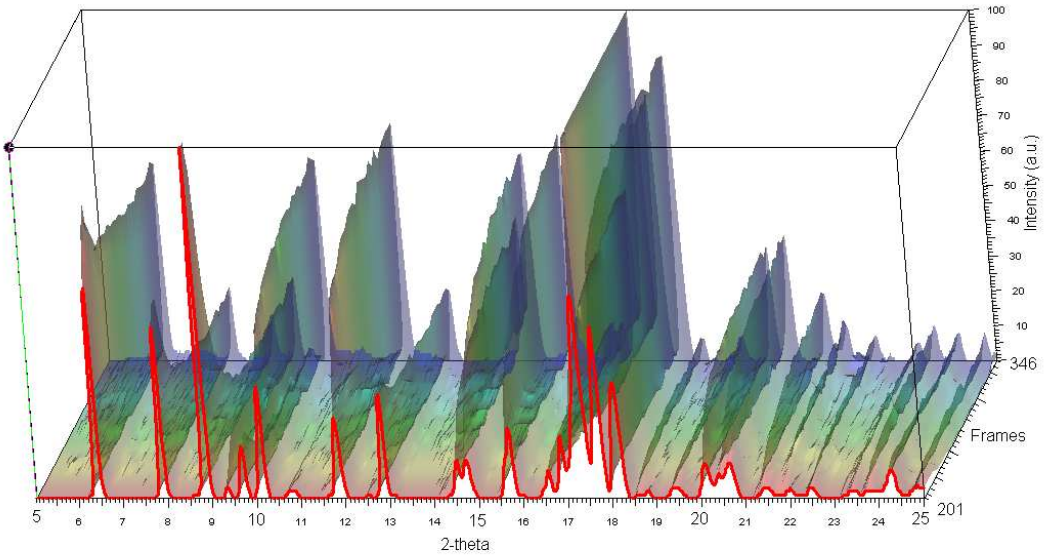

Figure 6.3. Time resolved x-ray diffraction patterns for the ion exchange of Cs^+ in to $H_{1.22}K_{0.84}ZrSi_3O_9 \bullet 2.16H_2O$.

6.3.3 Structure of $H_{0.18}K_{0.45}Cs_{1.37}ZrSi_3O_9 \bullet 0.98H_2O$ (2)

Data for the final frame were collected over 10 minutes. Reitveld refinement of this data showed that the unit cell had swollen to approximately 1071 $Å^3$. **2** crystallizes in the orthorhombic space group $P2_12_12_1$ with cell dimension of a = 10.6668(8) Å, b = 13.5821(11) Å, c = 7.3946(6) Å. Site 1 is completely occupied by Cs^+ and the remainder of the K^+ cations are found in the large channel distributed among M2 and M3 with occupancy factors being 0.35 and 0.1 respectively. Water molecules are found in the large channel with occupancies in M2 and M3 of 0.26 and 0.8, respectively. Cation oxygen distances for M1-O, M2-O, and M3-O are shown in Table 6.4. Average Cs-O contact distance in Site 1 is 3.434(43) Å.

6.3.4. NMR

The ^{133}Cs MAS NMR spectra of a 5% and 75% Cs^+ loaded sample of compound 1 are seen in Figure 6.4. At 5% Cs^+ loading the chemical shift from the CsCl standard was -165 ppm. In the 75% Cs^+ loaded sample the chemical shift was found to be -172 ppm.

6.3.5. Valence bond sums

Valence bond calculations were performed using equation 3. Values of R_o and b are 2.417 and 0.370, respectively. 14 Cs-O contacts are reported with bond lengths shorter than 4.0Å. Values of S_{ij} for these 14 Cs-O contacts in Site 1 are listed in Table 6.5. The valence bond sum, ΣS_{ij}, is 1.003, completely accounting for a charge of +1 on Site 1 cesium cations.

$$s_{ij} = e^{\left(\frac{R_o - R_{ij}}{b}\right)} \qquad [7]$$

Table 6.4. Cation oxygen distances for compounds **1** and **2**.

Compound	M1—O	Distance (Å)	M2—O	Distance (Å)	M3-O	Distance (Å)
(1)$H_{1.22}K_{0.84}ZrSi_3O_9$•2.16$H_2O$	M1—O6	2.967(27)	M2—O5	3.026(36)		
	M1—O8	3.420(25)	M2—O7	3.152(32)		
	M1—O9	3.135(25)	M2—O8	2.648(27)		
	M1—O10	2.757(27)	M2—O10	2.882(29)		
	M1—O11	3.669(19)	M2—O11	3.342(29)		
	M1—O12	3.454(20)	M2—Ow1	2.734(39)		
	M1—O13	3.454(20)				
	M1—Ow1	2.821(30)				
(2)$H_{0.18}K_{0.45}Cs_{1.37}ZrSi_3O_9$•0.98$H_2O$	M1—O6	3.407(41)	M2—O6	3.200(32)	M3—O5	3.653(34)
	M1—O7	3.789(57)	M2—O8	3.129(21)	M3—O5′	3.080(41)
	M1—O7′	3.657(57)	M2—O9	3.437(21)	M3—O7	3.348(46)
	M1—O8	3.405(35)	M2—O10	2.980(24)	M3—O8	3.112(30)
	M1—O9	3.240(34)	M2—O1	2.964(17)	M3—O10	3.512(28)
	M1—O10	3.211(36)	M2—Ow1	2.921(24)		
	M1—O11	3.845(22)	M2—Ow1′	2.731(30)		
	M1—O11′	3.320(23)				
	M1—O12	3.375(23)				
	M1—O12′	3.387(34)				
	M1—O13	3.499(25)				
	M1—O13′	3.265(33)				
	M1—Ow1	3.240(44)				
	M1—Ow3	3.878(14)				

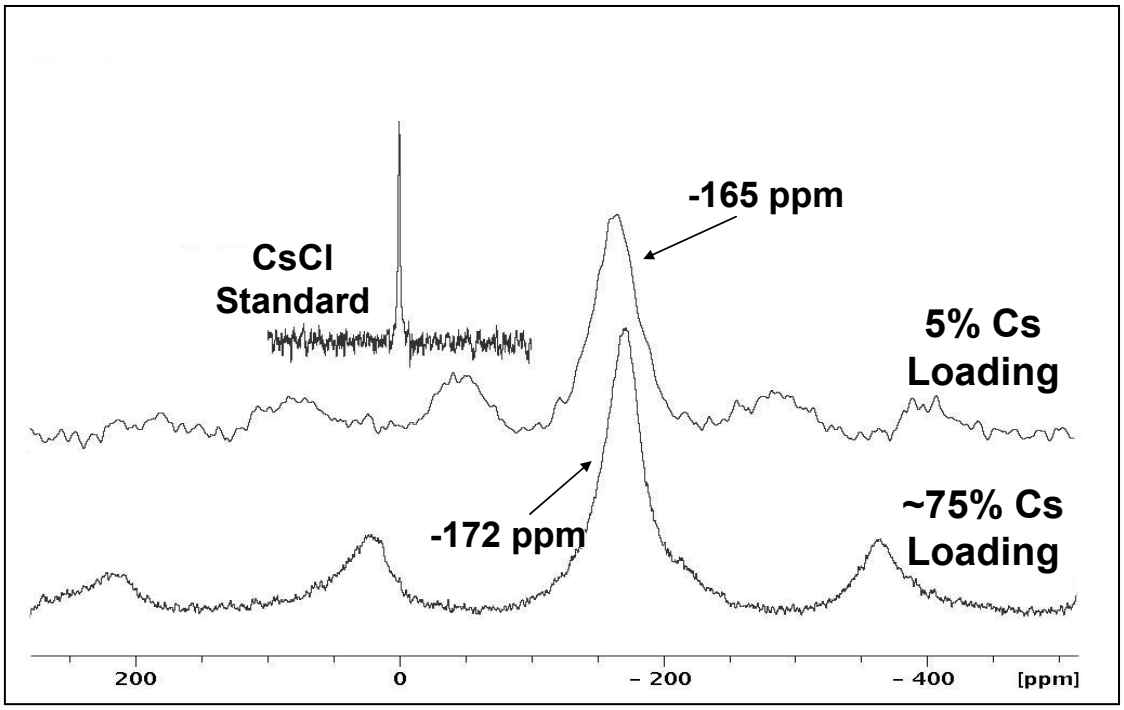

Figure 6.4. ^{133}Cs MAS NMR.

Table 6.5. Bond valence sums for Cs14—O contacts shorter than 4.0 Å.

Bond	Length	S_{ij}
Cs14—O6	3.407(41)	0.072
Cs14—O7	3.789(57)	0.026
Cs14—O7'	3.657(57)	0.037
Cs14—O8	3.405(35)	0.072
Cs14—O9	3.240(34)	0.113
Cs14—O10	3.211(36)	0.122
Cs14—O11	3.845(22)	0.022
Cs14—O11'	3.320(23)	0.091
Cs14—O12	3.375(23)	0.078
Cs14—O12'	3.387(34)	0.076
Cs14—O13	3.499(25)	0.056
Cs14—O13'	3.265(33)	0.105
Cs14—Ow1	3.240(44)	0.113
Cs14—Ow3	3.878(14)	0.020
Valence Bond Sum		1.003

6.4. Discussion

Reitveld refinements of selected frames from 201 through 346 clearly show the paths of the cations as they travel to and from the exchange sites. Cation site occupancies for refined frames are listed in Table 6.6. Before the incorporation of Cs^+ begins, the K^+ in site 1 migrates into exchange site 2. Once the K^+ occupancy in site 1 has been reduced to approximately 0.35, Cs^+ cation begins to diffuse in from the large cavity. As exchange continues K^+ diffuses into the large tunnel to make room for more Cs^+ in the smaller channel. The level of K^+ in the large channel increases from an occupancy of 0.25 to 0.35 as K^+ diffuses in from the smaller channel and out to solution.

Changes in interstitial water content also occur with increasing Cs^+ incorporation. The amount of water in exchange site 1 decreases to nil as Cs^+ moves into the small cavity. Water in the M3 cation position moves to the M2 position and eventually an entire mole of water per mole of exchanger is returned to solution. Cation sites M2 and M3 in the large channel are now populated by water, K^+, and Cs^+.

The reason for the phase change from a monoclinic to an orthorhombic crystal system is clear in compound **2**. Illustrated by Figure 6.5, if the special positions in the $P2_1/c$ space group are transformed to the $P2_12_12_1$, the inversion centers are found in site 1, the small cavity. If one measures the distance between this point of pseudosymmetry and for example a Zr atom, the corresponding atom, Zr′, should be equidistant if reflected through the center of symmetry. Cations and waters in site 2 (M2, M3) are not reflected thru the inversion center. This destroys the center of symmetry in the monoclinic phase and causes a shift to a non centrosymmetric space group. Framework atoms Si2 and Si4 are also not reflected through the center of symmetry. Apart from the afore mentioned atoms, all other framework atoms and the Cs^+ in site 1 conform to the inversion center. Strangely, there is no noticeable shift in framework bond angles or bond distances. To accommodate the larger Cs^+ cations, the Zr-O distances have increased slightly. The exchange of Cs^+ for H^+ and K^+ is incomplete. Charge balance dictates that some protons must remain in the exchanger.

Table 6.6. Refined fractional occupancies of Cs^+, K^+ and water O for selected frames.

Frame	Cs (M1)	Cs (M2)	Cs (M3)	K (M1)	K (M2)	Water (M1)	Water (M2)	Water (M3)
201	0.112	0.012	0.008	0.355	0.254	0.505	0.544	0.992
211	0.162	0.048	0.002	0.341	0.264	0.490	0.462	0.991
216	0.180	0.028	0.012	0.324	0.286	0.496	0.518	0.924
221	0.220	0.052	0.010	0.298	0.304	0.470	0.475	0.883
226	0.334	0.078	0.050	0.282	0.304	0.320	0.511	0.904
231	0.555	0.238	0.048	0.253	0.310	0.183	0.420	0.902
241	0.642	0.219	0.070	0.182	0.340	0.176	0.419	0.869
251	0.663	0.201	0.094	0.134	0.341	0.183	0.360	0.842
261	0.662	0.204	0.100	0.129	0.343	0.209	0.338	0.830
281	0.718	0.195	0.173	0.060	0.345	0.221	0.292	0.757
291	0.741	0.249	0.184	0.061	0.347	0.214	0.275	0.751
301	0.751	0.214	0.181	0.060	0.344	0.204	0.262	0.744
311	0.752	0.233	0.171	0.059	0.343	0.195	0.228	0.747
326	0.754	0.237	0.173	0.059	0.348	0.191	0.227	0.719
336	0.778	0.231	0.171	0.056	0.352	0.168	0.229	0.712
346	0.784	0.251	0.173	0.066	0.363	0.158	0.223	0.721
long	1.000	0.230	0.143	0.000	0.353	0.000	0.299	0.760

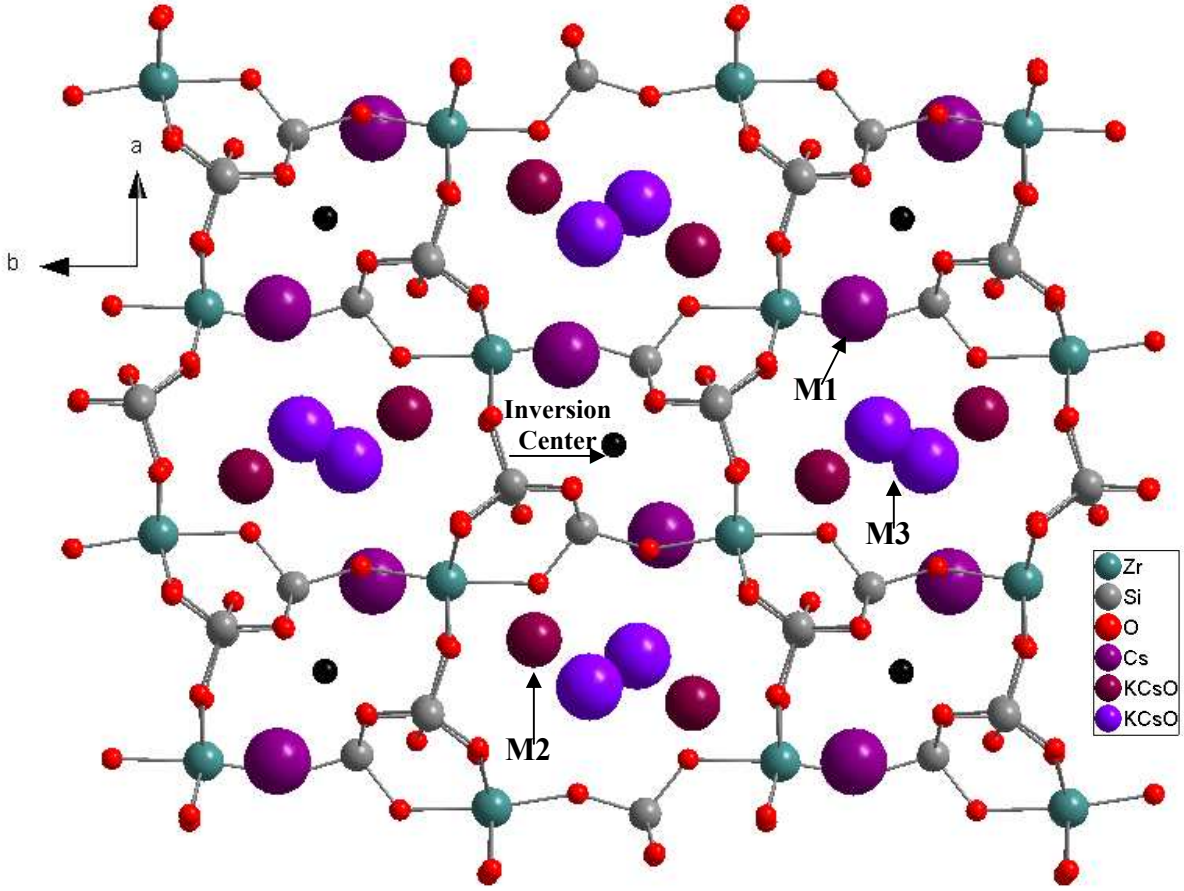

Figure 6.5. Ball and stick representation of compound 2. The inversion center (black sphere) at ½, 0, 0 represents a site of pseudosymmetry.

6.5. Conclusions

The path of Cs^+ as it is incorporated into a partially protonated form of potassium zirconium trisilicate was followed in situ by x-ray diffraction. A rearrangement of the potassium cations must occur first for the incoming Cs^+ cations to reach their preferred exchange site of the two unique cavities. This rearrangement leads to great disorder in Site 2 and is likely the reason for the phase change. Cations in Site 2 (M2, M3) do not fit the inversion center present when the space group is $P2_1/c$, therefore the space group cannot stay centrosymmetric. The change in phase is not accompanied by any noticeable framework rearrangement as the bond angles and bond distances do not change significantly.

CHAPTER VII
SUMMARY AND SUGGESTIONS FOR FUTURE WORK

It was the goal of this work to further our understanding of the origins of selectivity in framework inorganic ion exchangers. This work was given consideration in the context of radioactive waste and the work presented in this dissertation is part of an ongoing search for better methods of remediating low-level and high-level nuclear waste. In order to develop new materials that can assist in this problem, the properties of inorganic ion exchangers have been closely examined. As a model system for understanding three-dimensional tunnel type inorganic materials, the ion exchange properties of the synthetic form of the mineral umbite the have been rigorously probed.

The afore mentioned synthetic umbite has the ideal formula $K_2ZrSi_3O_9 \bullet H_2O$ and crystallizes in the orthorhombic space group $P2_12_12_1$. The framework is composed of polymeric chains of trisilicate groups linked by zirconium atoms resulting in zeolite type channels. The exchangeable cations are found in two unique tunnels along the *c*-axis. Site 1 is marked by a 12-atom ring and contains two cations. Site 2, a 16-atom ring, contains two cations and two water molecules. Linking these tunnels is a 14-atom channel which runs perpendicular to the two main exchange sites approximately along the -110 plane. Isostructural substitution of the zirconium octahedral metal for Sn^{4+} or Ti^{4+} decreases the size of the unit cell and has been shown to alter the selectivity of the compound by changing the size of the exchange cavity.

To understand the selectivity of this compound for specific ions a two pronged approach was employed. Of principal importance was the structure of the substituted umbite. By examining in detail the ion exchange environment and the coordination of the cation in its final exchange position, correlations were made between the size of the cavity and the selectivity of the material. Experimentally, whenever possible, a pure phase was synthesized via ion exchange so that the cation oxygen distance was discernable and not an average of the distances for cations of different ionic radius.

The second task in understanding the origins of selectivity in metal trisilicates was to examine the kinetics and identify a mechanism of exchange. This was accomplished in two ways. First, measurements of hydrolysis rates and exchange rates combined with the identification of the equilibrium ion exchange product provided an excellent but incomplete picture of the mechanism of exchange. These data were gathered by measuring the change in pH over time as a sample of ion exchanger was contacted with an equivalent of exchangeable cation. Another method used for elucidating the mechanism of ion exchange was to conduct in situ x-ray diffraction experiments using a synchrotron radiation source. While passing a dilute solution of exchangeable cations through a fixed bed of exchanger, an x-ray diffraction pattern was taken. This effectively takes a "snap shot" of the changes inside the framework and by solving the crystal structure provides a picture of how the cations move during ion exchange.

While the crystal structure of the mineral umbite is well known, the structure of the exchange phases and selectivity for individual cations had not been thoroughly studied. The first step in understanding the origins of selectivity in these compounds was to identify the alkali cation for which $K_2ZrSi_3O_9 \cdot H_2O$ is most selective and then study the structure of its exchange phases with that cation. The selectivity series for potassium zirconium trisilicate in basic media was found to be Rb > Cs, K, Na > Li. The structural characteristics of the K and Na phases, including partially substituted Cs exchange forms were previously studied; however structural examination of the Rb phase had not yet been performed.

A fully substituted rubidium exchange form has been made and the structure of its partially and fully exchange forms has been examined. $Rb_2ZrSi_3O_9 \cdot H_2O$, shows M-O distances that are closest to their ideal distances, that being the sum of O^{2-} and Rb^+ ionic radii. It can now be said that, as the M-O distances approach those of the ideal, the affinity of zirconium trisilicate for a particular alkali cation increases. The crystal structures of the partially substituted Rb/K phase show that the smaller cavity is preferentially occupied by the incoming Rb.

In an effort to simplify titration data and to characterize a new exchange phase, the protonated form of potassium zirconium trisilicate was synthesized. Previously a challenge due to drastic decreases in crystallinity, a partially protonated form was synthesized by ion exchange in dilute acetic acid. Having the molecular formula $H_{1.45}K_{0.55}ZrSi_3O_9 \cdot 2H_2O$, this phase crystallizes in the monoclinic space group $P2_1/c$, yet maintains an extended framework and pore shape identical to the orthorhombic parent phase. This behavior was previously observed in the titanium phase as it to shifts from an orthorhombic to a monoclinic crystal system. Besides the phase change, another important discovery was made in the structure of the protonated phase. A second water of hydration is present and occupies the position vacated by the cations in the large tunnel. The remaining cations are held in the smaller tunnel further confirming that the "grip" on these cations is tighter than in the larger cavity.

The ion exchange behavior of trisilicates towards group II alkaline earth cations was also studied in the protonated phase. The selectivity series was found to be Ba > Sr > Ca > Mg. This trend did not coincide with the observed kinetics of exchange in which Sr was taken up faster than Ba.

The crystal structure of the partially and fully substituted strontium phases was also examined closely. Upon exchange, the space group is conserved and remains monoclinic. The water content is nearly the same in both compounds; however, in the partially substituted K/Sr phase, $K_{0.34}Sr_{0.83}ZrSi_3O_9 \cdot 1.8H_2O$, the position of the residual K^+ has shifted. Potassium cations now occupy both the smaller and larger exchange sites where, in the parent compound before Sr^{2+} exchange, it was only found in the smaller cavity. In the partially substituted phase, the distribution of Sr^{2+} in the cavities is almost identical and strontium shows no preference for either site.

In the fully substituted strontium zirconium trisilicate, $SrZrSi_3O_9 \cdot 2H_2O$, the crystal system is also conserved. Retaining the space group $P2_1/c$, the framework of this compound is identical to that of the starting acid phase. Strontium cations show slight preference for the smaller cavity and occupancies for Sites 1 and 2 are 0.535 and 0.465, respectively.

Work with lanthanide exchange was also of interest in this study as rare earths are notoriously difficult to separate due to their similar ionic radii and solution chemistry. Ion exchange experiments were conducted using all forms of synthetic umbites to further bolster the hypothesis that the size of the unit cell and therefore the pore size is one factor in determining the selectivity of the individual trisilicate. The potassium phases of four synthetic umbites with complete framework substitutions of Ti, Sn, Zr, and Ge for Si were tested for Gd^{3+} uptake. It was found that, at equilibrium, the tin trisilicate took up more gadolinium than all other umbites tested. The affinity for selected lanthanides was then tested in the potassium tin trisilicate. The selectivity series in basic media was as predicted, La > Pr > Sm > Gd > Er. This trend follows from the largest to the smallest lanthanide tested, with ionic radii beginning at the largest 1.032 Å for La^{3+} and 0.890 Å for Er^{3+}.

A fully substituted gadolinium tin trisilicate was made by ion exchange with the potassium phase. The structure of this phase is similar to the sodium zirconium trisilicate. The framework and space group remain unchanged. It was thought that the extra void space brought about by introducing a 3+ cation would increase the water content yet surprisingly the water content also remained the same. It was suspected that the cations also played a role in the structural integrity of the framework and for this reason it was difficult to achieve a pure proton phase. This was not so however, and one can conclude that the cations are not responsible for holding up the integrity or crystallinity of the framework.

Increasing the valence of the cation one final time, the incorporation of thorium and uranium was studied in the potassium tin trisilicate. Encouraged by the ease at which Gd^{3+} was completely substituted for K^{+} it was thought that the charge of the cation might play a role in the selectivity of the trisilicate. Because Th^{4+} has an ionic radius of approximately 1.0 Å, three other cations were chosen because of their similar size. Binary solutions of Na, Ca, Gd, and Th were made and then contacted with the tin trisilicate until equilibrium was reached. In all cases, though the cations were of like ionic radius, the cation of higher valence was taken up preferentially.

To demonstrate that charge is indeed a dominant force in the selectivity a fully substituted thorium tin trisilicate was synthesized by ion exchange along with completely exchanged Na, Ca, and Gd phases. When the coordination of cations is compared, the contact distances between framework oxygens are similar and the number of close contacts is almost identical.

The greatest tool employed in the search for a possible mechanism of ion exchange was the use of in situ time resolved x-ray diffraction facilities at beam line X7B at Brookhaven National Laboratories. The path of Cs^+ as it enters the cavities of a partially protonated zirconium trisilicate was followed using Reitveld refinement techniques to solve the structures of each pattern as ion exchange occurred. As the Cs^+ content increased the monoclinic acid phase was converted back to the orthorhombic phase. The material changes phases because the center of symmetry is destroyed by shifting cation positions and small changes in the framework. The proposed mechanism of exchange follows the previously postulated mechanism whereby cations enter the large tunnel and migrate to the smaller exchange site. This forces a rearrangement of the cations in the smaller Site 1 which is evident in the final structure. The great disorder and multiple site occupancies in Site 2 indicate that much of the exchange takes place either through that avenue or through the 14-atom ring connecting the two main tunnels.

In continuing this research, several goals remain unrealized, and though the mechanism and reasons for selectivity in these synthetic umbites is better understood, more work is needed to fully describe this system.

In order to determine the mechanism completely, and accurately conduct titrations using $M^{n+}(OH)_n$ a complete proton form of each trisilicate must be made. One proposed pathway to this goal is to first synthesize the partially protonated forms using acetic acid as described in Chapter III. To complete the exchange without destroying the integrity of the framework it may be possible to use a flux of low melting organic acid, heating the compound gently or using higher temperature solvothermal methods.

With this fully protonated umbite in hand and the continued improvements in time resolution, in situ ion exchange studies will be able to capture the movements of the

cations more precisely and the exact path of the ions as they travel to their final exchange sites will be elucidated.

It is suspected that there is a modestly complex hydrogen bonding scheme between the waters of hydration and the framework. With a completely deuterated proton phase, neutron diffraction experiments can be performed to locate the water hydrogens and the positions of the protons. Will the protons be present as hydronium ions or will they be bonded to the framework is a question that can be answered using this technique.

Practical application of the trisilicates can also be studied. Ion exchange behavior towards toxic metals such as arsenic and mercury could lead to pragmatic uses of the trisilicates in contaminated ground water or soil remediation. Experiments testing the separation capabilities of the trisilicates will be performed. It has been shown that the tin trisilicate has unique affinities for rare earths and it may be possible to separate complex mixtures of lanthanides in a typical fixed bed or column elution method.

Finally, the question of whether or not the trisilicates can be applied to nuclear waste remediation still remains. Testing of the trisilicate compounds in waste simulants and actual waste at Savannah River National Laboratories is in progress.

REFERENCES

(1) Crowley, K. D.; Ahearne, J. F. *American Scientist*, **2002**, *90*, 514.

(2) Roy Cahill Ph. D. Dissertation, 1996.

(3) Yates, S. F.; Sylvester, P. *Sep. Sci. Technol.* **2001**, *36*, 867.

(4) Behrens, E. A.; Sylvester, P.; Clearfield, A., *Environ. Sci. Technol.* **1998**, *32*, 101.

(5) Poojary, D. M.; Cahill R. A.; Clearfield, A., *Chem. Mater.* **1994**, *6*, 2364.

(6) Poojary, D. M.; Bortun, A. I.; Bortun, L. N.; Clearfield, A., *Inorg. Chem.*, **1996**, *35*, 6131.

(7) Tripathi, A.; Medvedev, D.; Nyman, M.; Clearfield, A. *Solid State Chem.*, **2003**, *175*, 72.

(8) Tripathi, A.; Medvedev, D.; Delgado, J.; Clearfield, A. *J. Solid State Chem.*, **2004**, *177*, 2903.

(9) Beherns, E. A.; Poojary, D. M.; Clearfield, A. *Chem. Mater.* **1997**, *8*, 1236.

(10) Clearfield, A. *Solid State Sciences*, **2001**, *3*, 103.

(11) Harrison, W. T. A.; Gier, T. E.; Stucky, G. D., *Zeolites*, **1995**, *15*, 408.

(12) Henshaw, D. E. *Mineral*. *Mag*. **1955**, *30*, 585.

(13) G. D. Ilyushin, *Inorg. Mater.* **1993**, *29*, 853.

(14) Plevert, J; Sanchez-Smith, R.; Gentz, T. M.; Li, H.; Groy, T. L.; Yaghi, O. M.; O'Keeffe, M. *Inorg. Chem.* **2003**, *42*, 5954.

(15) Bortun, A. I.; Bortun, L. N.; Poojary, D. M.; Xiang, O; Clearfield, A. *Chem. Mater.* **2000**, *12*, 294.

(16) Zou, X.; Dadachov, M. S. *Acta. Cryst.* **2000**. *C56*, 738.

(17) Valtchev, V.; Paillaud, J. L.; Mintova, S.; Kessler, H. *Microporous Mesoporous Mater*. **1999,** *32*, 287.

(18) Dobelin, N.; Armbruster, T. *Microporous Mesoporous Mater*. **2007,** 99, 279.

(19) Sebastian, V.; Lin, Z.; Rocha, J.; Tellez, C; Santamaria, J.; Coronas, J. *Chem*. *Commun*. **2005**, *24*, 3036.

(20) Sebastian, V.; Lin, Z.; Rocha, J.; Tellez, C; Santamaria, J.; Coronas, J. *Chem. Mater.* **2006,** *18,* 2472.

(21) Corcoran, E. W., Jr.; Vaughan, D. E. W. *Solid State Ionics* **1989**, *32/33*, 423.

(22) Dyer, A.; Jafar, J. J. *J. Chem. Soc., Dalton Trans*. **1990**, *11*, 3239.

(23) Dyer, A.; Jafar, *J. Chem. Soc., Dalton Trans*. **1991**, *10*, 2639.

(24) Lin, Z.; Rocha, J.; Valente A. *Chem. Commun.*, **1999**, *24*, 2489.

(25) Lin, Z.; Rocha, J.; Pedrosa de Jesus, J. D.; Ferreira, A. *J. Mater. Chem.* **2000**, *10*, 1353.

(26) Ferreira, A.; Zhi Lin, Z.; Joao Rocha, J.; Morais, C. M.; Lopes, M.; Fernandez, C. *Inorg. Chem.* **2001**, *40,* 3330.

(27) Pertierra, P.; Salvado, M. A.; Garcia-Granda, S.; Bortun, A. I.; Khainakov, S. A.; Garcia, J. R. *Inorg. Chem. Commun.* **2002**, *5*, 824.

(28) Pertierra, P; Salvado M. A.; Garcia-Granda, S.; Khainakov, S. A.; Garcia, J. R. *Thermochimica Acta.* **2004**, *423*, 113.

(29) Loa, F.-R.; Lii, K.-H. *J. Sol. St. Chem.* **2005**, *178*, 1017.

(30) Choisnet, J.; Deschanvres, A.; Raveau, B. *J. Sol. St. Chem.* **1973**, *7*, 408.

(31) Poojary, D. M., Bortun, A. I., Bortun, L. N., Clearfield, A., *Inorg. Chem*., **1997**, *36*, 3072.

(32) Clearfield, A.; Bortun, A. I.; Bortun, L. N.; Poojary, D. M.; Khainakov, S. A. *J. Molec. Struc.* **1998**, *470*, 207.

(33) Ilyushin, G. D.; Dem'yanets, L. N. *Inorg. Mater.* **2002,** *38*, 739.

(34) Ilyushin, G. D. *Inorg. Mater.* **2002**, *38*, 1102.

(35) Plevert, J; Sanchez-Smith, R; Gentz, T. M.; Li, H.; Groy, T. L.; Yaghi, O. M.; O'Keeffe, M. *Inorg. Chem.* **2003**, *42*, 5954.

(36) Dong, C. *J. Appl. Crystallogr.* **1999**, *32*, 838.

(37) Larson, A.; Dreele, R. B. *GSAS: Generalized Structure Analysis System*; LANSCE, Los Alamos National Laboratory, Los Alamos, NM; Copyright 1985-88 by the Regents of the University of California.

(38) Le Bail, A.; Duroy, H.; Fourquet, J. L. *Mater. Res. Bull*. **1988**, *23*, 4467.

(39) Helfferich, F. *Ion Exchange*; McGraw-Hill: New York, 1962.

(40) Inglezakis, V. J.; Grigoropoulou, H. P. *J. Col. Inter. Sci.* **2001,** *234***,** 434.

(41) Dang, Z.; Anderson, B. G.; Amenomiya, Y.; Morrow, B. A. *J. Phys. Chem.* **1995**, *99*, 14437.

(42) Predoi-Cross, A.; Lees, R. M.; Johns, J. W. C. *J. Mol. Spect.* **1998**, *191*, 348.

(43) Haase, F.; Sauer, J. *J. Am. Chem. Soc.* **1995**, *117*, 3780.

(44) Shannon, R. D.; Prewitt, C. T. *Acta Cryst.* **1969**, *B25*, 925.

(45) Schultz, W. W.; Lombardo, N. J. *Separation Science and Technology for Disposal of Radioactive Tank Waste*, Plenum Press, New York, 1998.

(46) Fewox, C. S.; Kirumakki, S.; Clearfield, A. *Chem. Mater.* **2007**, *19*, 384.

(47) Rodríguez-Carvajal, J. Abstracts of the Satellite Meeting on Powder Diffraction of the XV Congress of the IUCr, Toulouse, France 1990, 127.

(48) Roisnel, T.; J. Rodríguez-Carvajal, J. Science Forum, Proceedings of the Seventh European Powder Diffraction Conference 2000, (*EPDIC 7*), 118.

(49) Rodríguez-Carvajal, J.; Roisnel, T. Commission for Powder Diffraction, International Union for Crystallography, *Newletter (May-August) Summer* **1998**.

(50) Liu, X.; Shang, M.; Thomas, J. K. *Microporous Mater.* **1997**, *10*, 273.

(51) Eisenman, G. *Biophys. J.* **1962**, *2*, 259.

(52) Marcus, Y. *J. Chem. Soc. Faraday Trans.* **1991**, *87*, 2995.

(53) Kullberg, L; Clearfield, A. *J. Phys. Chem.* **1981**, *85*, 1585.

(54) Roca, S.; Airoldi, C. *Thermochimica Acta* **1996**, *1*, 289.

(55) Chen, S.; Chao, K.; Leet, T. *Ind. Eng. Chem. Res.* **1990**, *29*, 2020.

(56) Keane, M. A. *Microporous Mater.* **1995**, *3*, 394.

(57) Tarasevich, Y. I.; Krysenko, D. A.; Polyakov, V. E. *Theor. Exp. Chem.* **2006***, 42,* 320.

(58) Riello, P.; Bucella, S.; Krsmanovic, R.; Meneghetti, S.; Pietrantoni, S.; Francini, R. *J. Phys. Chem. B.* **2005**, *109*, 13424.

(59) Xie, R.-J.; Hirosaki, N.; Suehiro, T.; Xu, F.-F.; Mitomo, M. *Chem. Mater.* **2006**, *18*, 5578.

(60) Setlur, A. A.; Heward, W. J.; Gao, Y.; Srivastava, A. M.; Chandran, R. G.; Shankar, M. V. *Chem. Mater.* **2006**, *18*, 3314.

(61) Aitasalo, T.; Holsa, J.; Jungner, H.; Lastusaari, M.; Niittykoski, J. *J. Phys. Chem. B.* **2006**, *110*, 4589.

(62) Choi, H.-J.; Shin, J. H.; Suh, K.; Seong, H.-K.; Han, H.-C.; Lee, J.-C. *Nano Lett.* **2005**, *5*, 2432.

(63) de Lill, D. T.; de Bettencourt-Dias, A.; Cahill, C. L. *Inorg. Chem.* **2007**, *46*, 3960.

(64) Hidayat, R.; Sugihara, O.; Tsuchimori, M.; Kagami, M.; Nishikubo, T.; Kaino, T. *Nonlin. Opt. Quant. Opt.* **2005**, *34*, 91.

(65) Dias Filho, F. A.; Ribeiro, S. J. L.; Goncalves, R. R.; Messaddeq, Y.; Carlos, L. D.; De Zea Bermudez, V.; Rocha, J. *J. Alloys Compd.* **2004**, *374*, 74.

(66) Rambabu, U.; Munirathnam, N. R.; Prakash, T. L.; Buddhudu, S. *Mat. Chem. Phys.* **2002**, *78*, 160.

(67) Lina, Z.; Dominguesa, J. P.; Rocha, J.; Carlos, L. D. *J. Lumin.* **2007**, *122–123*, 902.

(68) Bambirra, S.; van Leusen, D.; Tazelaar, C. G. J.; Meetsma, A.; Hessen, B. *Organometallics,* **2007**, *26*, 1014.

(69) Bambirra, S., Bouwkamp, M. W.; Meetsma, A.; Hessen, B. *J. Am. Chem. Soc.* **2004**, *126*, 9182.

(70) Gschneidner, K. A., Jr.; Eyring, L.; Editors. *Handbook on the Physics and Chemistry of Rare Earths, Volume 29: The Role of Rare Earths in Catalysis*: North Holland, Oxford, UK, 2000.

(71)Dominique, R.; Alexander A. T.; Voth,, P; Okuda, J. *J. Organomet. Chem.* **2006**, *21*, 691.

(72) Yu, L.; Chen, D; Li, J.; Wang, P. G. *J. Org. Chem.* **1997,** *62,* 3575.

(73) Caravan, P.; Ellison, J. J.; McMurry, T. J.; Lauffer, R. B. *Chem. Rev.* **1999**, *99*, 2293.

(74) Nash, K. *Solvent Extr. Ion Exch.* **1993**, *11*, 729.

(75) Nilsson, M.; Ekberg, C. *Solvent Extr. Ion Exch.* **2006**, *24*, 823.

(76) Kaur, H.; Agrawal Y. K. *React. Funct. Polym.* **2005**, *65*, 277.

(77) Sasaki, Y.; Choppin, G. R. *J. Radioanal. Nucl. Chem.* **1997**, *222*, 271.

(78) Pearson, R. *J. Chem. Educ.* **1968**, *45*, 643.

(79) Pearson, R. *Chem. Brit.* **1967**, *3*, 103.

(80) Ionova, G.; Ionov, S.; Hill, C. R.; Madic, C.; Guillaumont, R. C.; Modolo, G.; Krupa, J. C. *New J. Chem.* **2001**, *25*, 491.

(81) Boyd, G.E.; Adamson, A. W.; Myers, L. S. *J. Am. Chem. Soc*. **1947**, *69*, 2836.

(82) Vermeulen, T. *Ind. Eng. Chem.* **1953**, *45*, 1664.

(83) Celestian, A. J.; Parise, J. B.; Goodell, C.; Tripathi, A.; Hanson, *J. Chem. Mat.* **2004**, *16*, 2244.

(84) Celestian, A. J.; Medvedev, D. G.; Tripathi, A.; Parise, J. B.; Clearfield, A. *Nucl. Instrum. Methods.* **2005,** *B238*, 61.

(85) Ciraolo, M. F.; Hanson, J. C.; Grey, C. P. *Microporous Mater.* **2001**, *49*, 111.

(86) Fogg, A. M; Dunn, J. S.; O'Hare, D. *Chem. Mater.* **1998,** *10,* 356.

(87) Ragavan, A.; Khan A. I.; O'Hare, D. *J. Mater. Chem.* **2006**, *16*, 602.

(88) Ragavan, A.; Khan A. I.; O'Hare, D. *J. Mater. Chem.*, **2006**, *16*, 4155.

(89) Norby, P.; Cahill, C.; Koleda, C.; Parise, J. B. *J. Appl. Cryst.* **1998**, *31*, 481.

(90) Hammersley, A. P. *FIT2D: V9.129 Reference Manual V3.1*; ESRF: Grenoble, France, 1998.

(91) Hammersley, A. P.; Svensson, S. O.; Thompson, A. *Nucl. Instrum. Methods* **1994**, *A346*, 312.

(92) Hammersley, A. P.; Svensson, S. O.; Thompson, A.; Graafsma, H.; Kvick, A.; Moy, J. P. *Rev. Sci. Instrum.* **1995**, *66*, 2729.

(93) Hammersley, A. P.; Svensson, S. O.; Hanfland, M.; Finch, A. N.; Hausermann, D. *High-Pressure Res.* **1996**, *14*, 235.

(94) Fewox, C. S.; Clearfield, A. *J. Phys. Chem. A*. **2008**, *112,* 2589.

VITA

Christopher Sean Fewox

Department of Chemistry, Texas A&M University
Mail Stop 3255
College Station, TX 77843

EDUCATION
Ph.D. / Chemistry
Texas A&M University, College Station, TX
Dissertation: Ion Exchange Behavior Among Metal Trisilicates: Probing Selectivity, Structure, And Mechanism
(Advisor: Prof. Abraham Clearfield)
B. S. / Chemistry
North Carolina State University, Raleigh, NC; May 2002

PROFESSIONAL EXPERIENCE
January 2003 – Present
Department of Chemistry Texas A&M University, College Station, TX
Graduate Research Assistant

- Synthesized and developed ion exchange materials for applications directed towards separations and nuclear waste remediation
- Evaluated ion exchange materials in simulated radioactive waste streams using radiochemical methods
- Conducted in situ x-ray diffraction experiments at the Brookhaven National Synchrotron Light Source to elucidate ion exchange mechanism
- Collaborated with research scientist at Savannah River National Labs and Sandia National Labs to develop ion exchange materials for nuclear waste remediation
- Utilized traditional air sensitive techniques to synthesize metal-metal bonded complexes
- Mentored undergraduate and REU students, teaching proper laboratory techniques and fostering enthusiasm in learning chemistry

June 1998 – 2002
Radiation safety technician with North Carolina State University Department of Environmental Health and Safety

- Collected and Disposed of radioactive waste generated from campus research laboratories
- Developed quench curves for accurate determination of radioactive activity in complex waste streams for shipping manifests and ultimate disposal

HONORS AND AWARDS

Tucker Award Scholar 1999
Student Graduation Commencement Speaker, North Carolina State University, 2000